

2014

I. FUNCTIONALIZATION OF CRYTPOHANE CAGES FOR XENON  
MRI II. VANADIUM CATALYZED OXIDATIVE COUPLING OF SP<sup>3</sup> C –  
H BONDS TO HETEROARENES

Marissa Simone  
University of Rhode Island, msimone@chm.uri.edu

Follow this and additional works at: <https://digitalcommons.uri.edu/theses>

Terms of Use

All rights reserved under copyright.

---

**Recommended Citation**

Simone, Marissa, "I. FUNCTIONALIZATION OF CRYTPOHANE CAGES FOR XENON MRI II. VANADIUM CATALYZED OXIDATIVE COUPLING OF SP<sup>3</sup> C – H BONDS TO HETEROARENES" (2014). *Open Access Master's Theses*. Paper 468.  
<https://digitalcommons.uri.edu/theses/468>

This Thesis is brought to you by the University of Rhode Island. It has been accepted for inclusion in Open Access Master's Theses by an authorized administrator of DigitalCommons@URI. For more information, please contact [digitalcommons-group@uri.edu](mailto:digitalcommons-group@uri.edu). For permission to reuse copyrighted content, contact the author directly.

I. FUNCTIONALIZATION OF CRYPTOPHANE  
CAGES FOR XENON MRI

II. VANADIUM CATALYZED OXIDATIVE  
COUPLING OF SP<sup>3</sup> C – H BONDS TO  
HETEROARENES

BY

MARISSA SIMONE

A THESIS SUBMITTED IN PARTIAL FULFILLMENT OF THE  
REQUIREMENTS FOR THE DEGREE OF

MASTER OF SCIENCE

IN

CHEMISTRY

UNIVERSITY OF RHODE ISLAND  
2014

MASTER OF CHEMISTRY THESIS

OF

MARISSA C. SIMONE

APPROVED:

Thesis Committee:

Major Professor

Brenton DeBoef

Mindy Levine

Al Bach

Nasser H. Zawia

DEAN OF THE GRADUATE SCHOOL

UNIVERSITY OF RHODE ISLAND

2014

## ABSTRACT

The lack of resolution and selectivity in current imaging techniques such as x-ray, optical, and magnetic resonance imaging (MRI) has spurred the development of new biosensor technologies. Cryptophane A, a molecular cage composed of two cyclotrimeratrylene (CTV) units connected by alkoxy bonds, can be turned into biosensors by attaching a target moiety capable of binding to a particular analyte. Cryptophanes can encapsulate xenon making it an attractive biosensor candidate for detection by hyperpolarized xenon-129 ( $HP\text{-}^{129}\text{Xe}$ ) MRI. Further detection enhancement is achieved by using a technique called hyperpolarized chemical exchange saturation transfer (HYPER-CEST). One of the key challenges in developing Xe-biosensors is the need for water soluble cryptophanes and their attachment to biomolecules that specifically bind physiological targets.

The first manuscript entitled “Functionalization of Cryptophane cages for Xenon MRI” discusses the synthesis of cryptophane cages and their potential to be further functionalized. The manuscript centers on synthesizing cryptophanes that are water soluble functionalized with gold nanoparticles, which can eventually be further modified for imaging molecular events in vivo.

The second manuscript, “Vanadium Catalyzed Oxidative Coupling of  $sp^3$  C-H Bonds to Heteroarenes” discusses oxidative aminomethylation of imidazolpyridines. This manuscript proposes a vanadium catalyzed oxidative coupling of imidazolpyridines with *N*-methylmorpholine oxide which serves as both  $sp^3$  hybridized coupling partner and the oxidant. The reaction was optimized and performed with a variety of substrates

to yield on a library of aminomethylated products. We investigated the mechanism and propose that a Mannich-type mechanism is responsible for the formation of the product.

## ACKNOWLEDGMENTS

I would like to thank my advisor **Dr. Brenton DeBoef** for his encouragement, advice, guidance, and help in developing my skills as a chemist throughout the years. I could not have accomplished any of this without my parents, Karen and Greg Simone, whose unfaltering love, encouragement, and support has been a vital component in achieving my goals. Most importantly, my grandfather Eustace Fotiu, who initiated by love for chemistry and whose memory I carry with me every day, and to my grandmother Mary Fotiu whose comfort and support I could never imagine being without. Additionally, I would also like to thank my friends and labmates.

## PREFACE

The following work is presented in manuscript format according to the guidelines presented by the University of Rhode Island Graduate School. This thesis will consist of two manuscripts that are currently in the process of publication.

Manuscript 1 entitled, “Functionalization of Cryptophane Cages for  $^{129}\text{Xe}$  MRI” will be submitted to *Bioorganic and Medicinal Chemistry Letters* in December 2014.

Manuscript 2 entitled, “Vanadium Catalyzed Oxidative Coupling of  $\text{sp}^3$  C–H Bonds to Heteroarenes” will be submitted to *Organic Letters* for publication in November 2014.

## TABLE OF CONTENTS

<b>ABSTRACT</b> .....	<b>ii</b>
<b>ACKNOWLEDGMENTS</b> .....	<b>iv</b>
<b>PREFACE</b> .....	<b>v</b>
<b>TABLE OF CONTENTS</b> .....	<b>vi</b>
<b>LIST OF TABLES</b> .....	<b>viii</b>
<b>LIST OF FIGURES</b> .....	<b>ix</b>
<b>LIST OF SCHEMES</b> .....	<b>x</b>
<b>LIST OF SPECTRA</b> .....	<b>xi</b>
<b>INTRODUCTION</b> .....	<b>1</b>
<b>Hyperpolarized Xenon</b> .....	<b>2</b>
<b>Cryptophanes</b> .....	<b>5</b>
<b>Hyper-CEST</b> .....	<b>8</b>
<b>References</b> .....	<b>11</b>
<b>MANUSCRIPT 1</b>	
<b>Efforts Towards Cryptophanes Functionalized with AuNPs</b> .....	<b>15</b>
<b>Abstract</b> .....	<b>15</b>
<b>General Introduction</b> .....	<b>15</b>
<b>Cryptophanes and Gold Nanoparticles</b> .....	<b>18</b>
<b>Conclusion</b> .....	<b>26</b>
<b>References</b> .....	<b>27</b>



<b>Experimental Section .....</b>	<b>30</b>
<b>References.....</b>	<b>54</b>
<b>MANUSCRIPT 2</b>	
<b>Vanadium Catalyzed Oxidative Coupling of sp<sup>3</sup> C-H Bonds to Heteroarenes. 57</b>	
<b>Abstract .....</b>	<b>57</b>
<b>Introduction .....</b>	<b>57</b>
<b>Results and Discussion .....</b>	<b>59</b>
<b>Conclusions.....</b>	<b>64</b>
<b>References.....</b>	<b>65</b>
<b>Experimental Section .....</b>	<b>67</b>

## LIST OF TABLES

TABLE	PAGE
<b>Introduction</b>	
Table 1. Characteristics of different imaging techniques.....	1
Table 2. Properties of Cryptophanes .....	6
<b>Manuscript 1</b>	
Table 1. Optimization of Click Conditions .....	25
<b>Manuscript 2</b>	
Table 1. Optimization of Vanadium Catalyzed Coupling.....	61
Table 2. Scope of the Cyclization of N-Benzylbenzimidazoles .....	63

## LIST OF FIGURES

FIGURE	PAGE
<b>Introduction</b>	
Figure 1: SEOP set up.....	3
Figure 2: MRIs of a subject with COPD and asthma.....	4
Figure 3: Cryptophane A, cryptophane 3,3,3, cryptophane 1,1,1, cryptophane TAAC, and TTPC .....	5
Figure 4: $^{129}\text{Xe}$ NMR spectra of water soluble cryptophanes .....	7
Figure 5: Depiction of Hyper-CEST .....	9
Figure 6: Hyper-CEST process .....	10
<b>Manuscript 1</b>	
Experimental Section	
Figure 1: TEM of 1.20 .....	54
Figure 2: TEM of 1.20 .....	55
<b>Manuscript 2</b>	
Figure 1: Pharmaceuticals with imidazo[1,2-a]pyridines backbones .....	60

## LIST OF SCHEMES

SCHEME	PAGE
<b>Manuscript I</b>	
Scheme 1. Click reaction of Cryptophane A to gold nanoparticles .....	17
Scheme 2. Synthesis of Cage Top.....	19
Scheme 3. Synthesis of Propargyl Linker .....	21
Scheme 4. Synthesis of Tri-Propargyl Cryptophane 2,2,2.....	21
Scheme 5: Synthesis of Protected Thiol Azide Linkers.....	23
Scheme 6. Click Pathways to Sulfur Functionalized Cages .....	25
<b>Manuscript 2</b>	
Scheme 1. Amination vs aminomethylation .....	59
Scheme 2. Synthesis of starting material .....	60
Scheme 3. Pure mannich conditions .....	63
Scheme 4. Proposed mechanism of product and impurity.....	64

## LIST OF SPECTRA

SPECTRUM	PAGE
<b>Manuscript 1</b>	
Spectrum 1. $^1\text{H}$ NMR of Compound 1.13.....	44
Spectrum 2. $^{13}\text{C}$ NMR of Compound 1.13.....	45
Spectrum 3. $^1\text{H}$ NMR of Compound 1.16.....	46
Spectrum 4. $^{13}\text{C}$ NMR of Compound 1.16.....	47
Spectrum 5. $^1\text{H}$ NMR of Compound 1.18.....	48
Spectrum 6. $^{13}\text{C}$ NMR of Compound 1.18.....	49
Spectrum 7. COSY of Compound 1.18.....	50
Spectrum 8. HMQC of Compound 1.18.....	51
Spectrum 9. $^1\text{H}$ NMR of Compound 1.19.....	52
Spectrum 10. $^{13}\text{C}$ NMR of Compound 1.19.....	53
<b>Manuscript 2</b>	
Spectrum 1. $^1\text{H}$ NMR of Compound 2.....	70
Spectrum 2. $^{13}\text{C}$ NMR of Compound 2.....	71
Spectrum 3. $^1\text{H}$ NMR of Compound 4.....	72
Spectrum 4. $^{13}\text{C}$ NMR of Compound 4.....	73
Spectrum 5. $^1\text{H}$ NMR of Compound 5.....	74
Spectrum 6. $^{13}\text{C}$ NMR of Compound 5.....	75
Spectrum 7. $^1\text{H}$ NMR of Compound 6.....	76
Spectrum 8. $^{13}\text{C}$ NMR of Compound 6.....	77

Spectrum 9. $^1\text{H}$ NMR of Compound 7 .....	78
Spectrum 10. $^{13}\text{C}$ NMR of Compound 7 .....	79
Spectrum 11. $^1\text{H}$ NMR of Compound 8.....	80
Spectrum 12. $^{13}\text{C}$ NMR of Compound 8.....	81
Spectrum 13. $^1\text{H}$ NMR of Compound 9.....	82
Spectrum 14. $^{13}\text{C}$ NMR of Compound 9.....	83
Spectrum 15. $^1\text{H}$ NMR of Compound 10.....	84
Spectrum 16. $^{13}\text{C}$ NMR of Compound 10.....	85
Spectrum 17. $^1\text{H}$ NMR of Compound 11 .....	86
Spectrum 18. $^{13}\text{C}$ NMR of Compound 11 .....	87
Spectrum 19. $^1\text{H}$ NMR of Compound 12.....	88
Spectrum 20. $^{13}\text{C}$ NMR of Compound 12.....	89
Spectrum 21. $^1\text{H}$ NMR of Compound 13.....	90
Spectrum 22. $^{13}\text{C}$ NMR of Compound 13.....	91
Spectrum 23. $^1\text{H}$ NMR of Compound 14.....	92
Spectrum 24. $^{13}\text{C}$ NMR of Compound 14.....	93
Spectrum 25. $^1\text{H}$ NMR of Compound 15.....	94
Spectrum 26. $^{13}\text{C}$ NMR of Compound 15.....	95
Spectrum 27. $^1\text{H}$ NMR of Compound 16.....	96
Spectrum 28. $^{13}\text{C}$ NMR of Compound 16.....	97
Spectrum 28. $^1\text{H}$ NMR of Compound 17.....	98
Spectrum 30. $^{13}\text{C}$ NMR of Compound 17.....	99
Spectrum 31. $^1\text{H}$ NMR of Compound 18.....	100

Spectrum 32. $^{13}\text{C}$ NMR of Compound 18.....	101
Spectrum 33. $^1\text{H}$ NMR of Compound 19.....	102
Spectrum 34. $^{13}\text{C}$ NMR of Compound 19.....	103
Spectrum 35. $^1\text{H}$ NMR of Compound 21.....	104
Spectrum 36. $^{13}\text{C}$ NMR of Compound 21.....	105
Spectrum 37. $^1\text{H}$ NMR of Compound 22.....	106
Spectrum 38. $^{13}\text{C}$ NMR of Compound 22.....	107

## INTRODUCTION

The ability to make a definitive medical diagnosis and follow the onset of certain diseases is vital in treating patients. Current imaging techniques, such as CT, PET, and MRI, possess different limitations that lower their overall effectiveness (**Table 1**).<sup>1</sup> Computed tomography, a non-invasive imaging method, generates an image by using X-rays that are absorbed by tissues.<sup>2</sup> Though inexpensive, CT is incapable of molecular imaging and exposure to hazardous X-ray radiation renders CT a less attractive method for imaging. Positron emission tomography (PET) and single photon emission computed tomography (SPECT) are capable of anatomical and molecular imaging. These techniques are advantageous as there are no depth detection limits, short temporal resolutions, no perturbation of biological systems, and they require very low doses of the probe molecules. However, both techniques lack spatial resolution, require exposure to harmful radiation and are very costly.<sup>1</sup>

<b>Imaging Technique</b>	<b>Image generation</b>	<b>Spatial Resolution</b>	<b>Temporal resolution</b>	<b>Type of probe used</b>	<b>Principal Use</b>
<b>CT</b>	X-rays	50-200 mm	10 secs to mins	N.A.	Anatomical
<b>PET</b>	$\gamma$ -rays	1-2 mm	Minutes	Radio labeled	Gene expression
<b>SPECT</b>	$\gamma$ -rays	1-2 mm	Minutes	Radio labeled	Gene expression
<b>MRI</b>	radiowaves	50-500 mm	Minutes to hours	Paramagnetic	Physiological, anatomical

**Table 1:** Characteristics of different imaging techniques<sup>1</sup>

Magnetic resonance imaging (MRI) is widely used for scanning deep tissue in the diagnosis of human diseases. Though this technique allows for high spatial resolution, only a small percentage of hydrogen nuclei align with the magnetic field, rendering this technique inherently insensitive. To increase signal intensity, contrast



agents, such as gadolinium or iron oxide-based particles are often employed. These contrast agents work by changing the  $T_1$  and  $T_2$  relaxation times of water, thereby enhancing signal intensity.<sup>3</sup> However, recent findings suggest that development of nephrogenic systemic fibrosis (NSF) in patients can be triggered by the administration of gadolinium agents.<sup>4</sup> Other MRI contrast agents such as manganese and lanthanides, are toxic even at low concentrations and interfere with neuronal functions by blocking ion-channels.<sup>5</sup> As a result, the need for non-toxic and non-proton MRI contrast agents needs to be explored. These issues may be circumvented by incorporating the inert noble gas xenon-129 ( $^{129}\text{Xe}$ ) as a molecular probe, since it is not present in the body, it is non-toxic, and it can be hyperpolarized to enhance its sensitivity. Herein, the use of xenon-129 in MRI, its ability to be hyperpolarized, Hyper-CEST techniques that allow for better detection, and the utilization of water soluble cryptophanes as hosts for Xe will be discussed.

### **Hyperpolarized Xenon**

Xe exists as two NMR active isotopes, a spin-1/2 nucleus  $^{129}\text{Xe}$  and spin-3/2 nucleus  $^{131}\text{Xe}$ . Only the former is capable of being hyperpolarized.<sup>6</sup> The ability to hyperpolarize  $^{129}\text{Xe}$  is advantageous, as it allows for a 10,000-times signal enhancement as a result of the alignment of more nuclear spins with the magnetic field. Where typical proton MRI has only a 15 ppm chemical shift range,  $^{129}\text{Xe}$  has range over 200 ppm, which allows for chemical shift imaging.<sup>7</sup> Solubility of xenon in lipid-rich tissue and blood allows for imaging of brain, lung and other regions.<sup>8</sup>

Spin exchange optical pumping (SEOP) is a three-step process used to hyperpolarize  $^{129}\text{Xe}$ . The first step involves the generation of circular polarized light by

a Ti:sapphire laser (**Figure 2**). In the second step, a droplet of Rb is heated in a glass cell, while exposed to a magnetic field, to produce a vapor, which then absorbs circular polarized light, driving the selective excitation of the D<sub>1</sub> transition state. The third step produces hyperpolarized <sup>129</sup>Xe. When polarized Rb collides with <sup>129</sup>Xe, it transfers the spin of its valence electron to the <sup>129</sup>Xe nucleus. As a result of this dipole interaction, xenon is now predominately in the state that is aligned with the external magnetic field.<sup>9</sup> Once hyperpolarized (HP) <sup>129</sup>Xe is achieved, it can be delivered in vivo to be imaged.

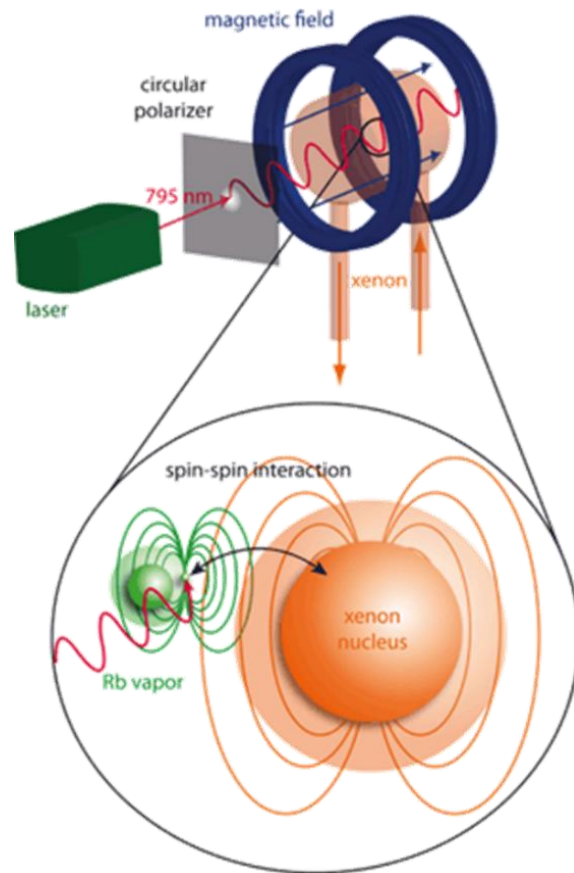


**Figure 1:** SEOP set up<sup>9</sup>

The delivery of HP <sup>129</sup>Xe to the body can be achieved through inhalation or injection. Inhalation of hyperpolarized <sup>129</sup>Xe permeates through lung tissue and blood, allowing for exploration of certain high concentration of characteristics of lung

function.<sup>10</sup> Studies have shown that inhalation of HP-<sup>129</sup>Xe results in highly spatially resolved images (**Figure 2**). Typical <sup>1</sup>H MRI is not a viable option for evaluation of patients with chronic obstructive lung disease (COPD) or asthma as it is not capable of imaging lungs, due to their low proton density (Figure 2 left). While using HP-<sup>129</sup>Xe in MRI yields an image that allows for distinction between lung airspaces in patients with COPD and asthma, rendering HP-<sup>129</sup>Xe superior to <sup>1</sup>H MRI.<sup>11</sup>

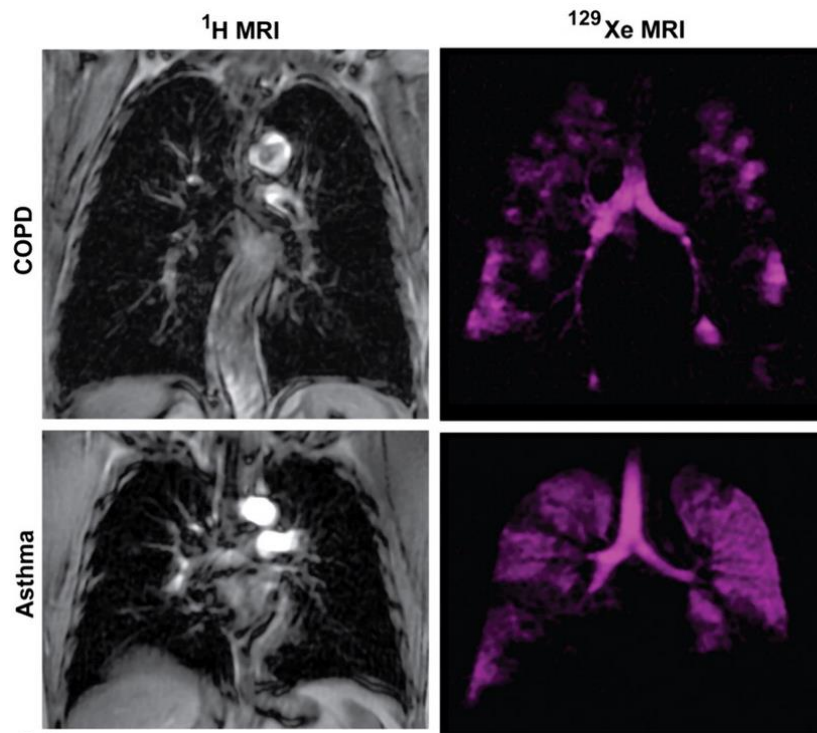


**Figure 2:** MRIs of a subject with COPD and asthma, left: <sup>1</sup>H MRI, right: HP-<sup>129</sup>Xe MRI.<sup>11</sup>

The polarization lifetime of <sup>129</sup>Xe is dependent on its molecular environment. In oxygenated blood  $T_1 = 13$  s, deoxygenated blood  $T_1 = 4$  s, and  $T_1 \approx 100$  s in deuterated saline solution.<sup>6</sup> While long polarization lifetimes are advantageous, they require longer time for imaging, which still does not result in optimal detection. Use of a host for <sup>129</sup>Xe allows for targeted imaging of molecular events. Such targeted molecular imaging via

$^{129}\text{Xe}$  MRI is usually accomplished by employing molecular probes that contain cage-shaped structures that are capable of encapsulating xenon atoms. The most common molecular cage that is used for this task is called cryptophane A.

### Cryptophanes

Cryptophanes are molecular cages composed of two cyclotrimeratrylenes (CTVs) that are connected by alkoxy linkers (**Figure 3**).<sup>12</sup> The lipophilic character of cryptophane's cavity allows for reversible binding of small, non-polar molecules, like xenon.

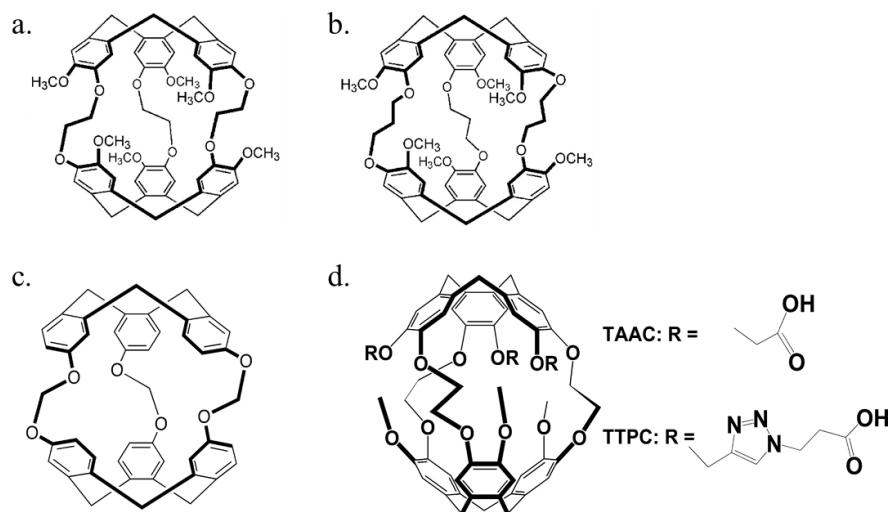


**Figure 3:** a) Cryptophane A, b) cryptophane 3,3,3, c) cryptophane 1,1,1, d) cryptophane TAAC, and TTPC.<sup>11,13, 14</sup>

The affinity and exchange rate of xenon depends on the cavity size of the cryptophane, which is varied by changing the number of carbons in the alkoxy linkers that join the two CTVs (**Table 2**). As the cavity size of cryptophanes decreases, there is an increase in the xenon binding constant.<sup>15</sup> While large binding constants are advantageous, the development of new detection techniques require the in and out exchange to be fast, and therefore,  $^{129}\text{Xe}$  should not be so tightly bound.<sup>9</sup>

<b>Cryptophane</b>	<b>Cavity Size (Å<sup>3</sup>)</b>	<b>Binding constant (M<sup>-1</sup>)</b>	<b>k<sub>in</sub> (s<sup>-1</sup>)</b>	<b>k<sub>out</sub> (s<sup>-1</sup>)</b>
(1.1.1)	81	10,000	n.d	2.4
A (2,2,2)	95	3900	50	25
E (3,3,3)	121	10	n.d	n.d
TAAC A (2.2.2)	95	17,300	n.d	n.d
TTPC	n.d	33,000	n.d	n.d

**Table 2:** Properties of cryptophanes<sup>11,12,13</sup>

When <sup>129</sup>Xe is bound in the cavity of a cryptophane cage, it produces a unique chemical shift distinct from free <sup>129</sup>Xe in the <sup>129</sup>Xe NMR spectra. The typical chemical shift of Xe@cryptophane complexes is demonstrated in **Figure 4**, where the larger the cavity size, the more the peak corresponding to encapsulated <sup>129</sup>Xe is shifted up-field.<sup>6</sup> This trend is broken by Xe@cryptophane-1,1,1 with a chemical shift of 31.1 ppm, whereas cryptophane A is at 65 ppm. It has been postulated this anomalous result is derived from the absence of methoxy groups, which suggests that modifying cages with electron withdrawing or donating groups can alter the chemical shift of Xe@cryptophanes.<sup>6</sup> Functionalizing cryptophanes with water solublizing groups, which are necessary for use in vivo, results in a higher binding affinity of <sup>129</sup>Xe (**Table 2**).<sup>13,15</sup>

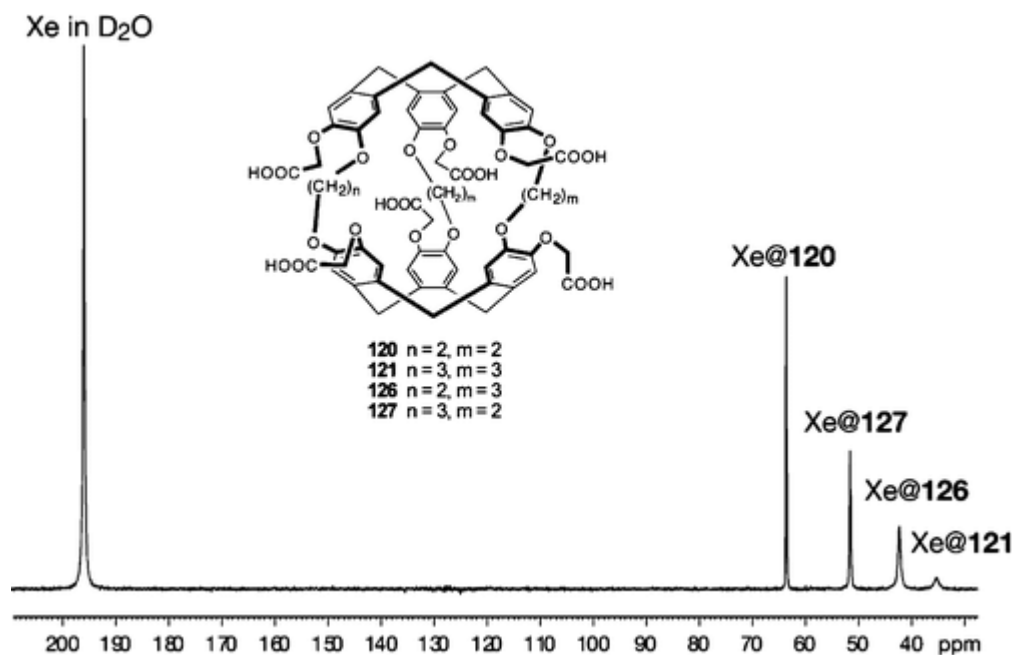


**Figure 4:**  $^{129}\text{Xe}$  NMR spectra of water soluble cryptophanes <sup>16</sup>

One of the most promising applications of cryptophanes that encapsulate xenon is their ability create biosensors. This can be achieved by conjugating cryptophanes to a targeting ligand, which is capable of binding to a specific biological target, such as receptors on tumors or sites of inflammation. For example, Dmoschowiski recently synthesized a cryptophane that was tethered to the carbonic anhydrase (CA)-specific ligand, benzenesulfonamide.<sup>17</sup> When the benzenesulfonamide cryptophane binds to CA isozymes I or II, it produces a distinctive chemical shift from the biosensor when it is free in solution.<sup>6</sup> Despite the synthesis of new water-soluble and ligand-functionalized cryptophanes, more sensitive techniques for detection of HP-  $^{129}\text{Xe}$  needs to be addressed.

## Hyper-CEST

Despite the high affinity of cryptophanes to bind  $^{129}\text{Xe}$ , long acquisition times are necessary to achieve well-resolved spectra of bound  $^{129}\text{Xe}$ . This issue is circumvented by incorporating a method called chemical exchange saturation transfer (CEST) to enhance detection of hyperpolarized  $^{129}\text{Xe}$ , when used in conjunction with hyperpolarized  $^{129}\text{Xe}$  this technique is called Hyper-CEST. Xenon is an ideal candidate for this method due to its long relaxation times and large chemical shift difference between bound and free  $^{129}\text{Xe}$ .<sup>14</sup>

Instead of directly detecting the  $^{129}\text{Xe}$  that is bound in a cryptophane, HyperCEST detects the depletion of free  $^{129}\text{Xe}$ . In order to do this, an off- and on-resonance spectra is acquired. The off-resonance spectrum is a reference spectra obtained by applying a continuous wave saturation (**Figure 5 A**). The on-resonance spectrum is obtained by applying a radio frequency pulse tuned to  $^{129}\text{Xe}$ @cryptophane signal (**Figure 5 B**).<sup>18</sup> The difference of the on and off resonance spectra results in signal only arising from the depletion of the free  $^{129}\text{Xe}$  peak.<sup>19</sup> The exchange of  $^{129}\text{Xe}$  from inside to outside the cryptophanes results in a reduction of the free  $^{129}\text{Xe}$  peak.

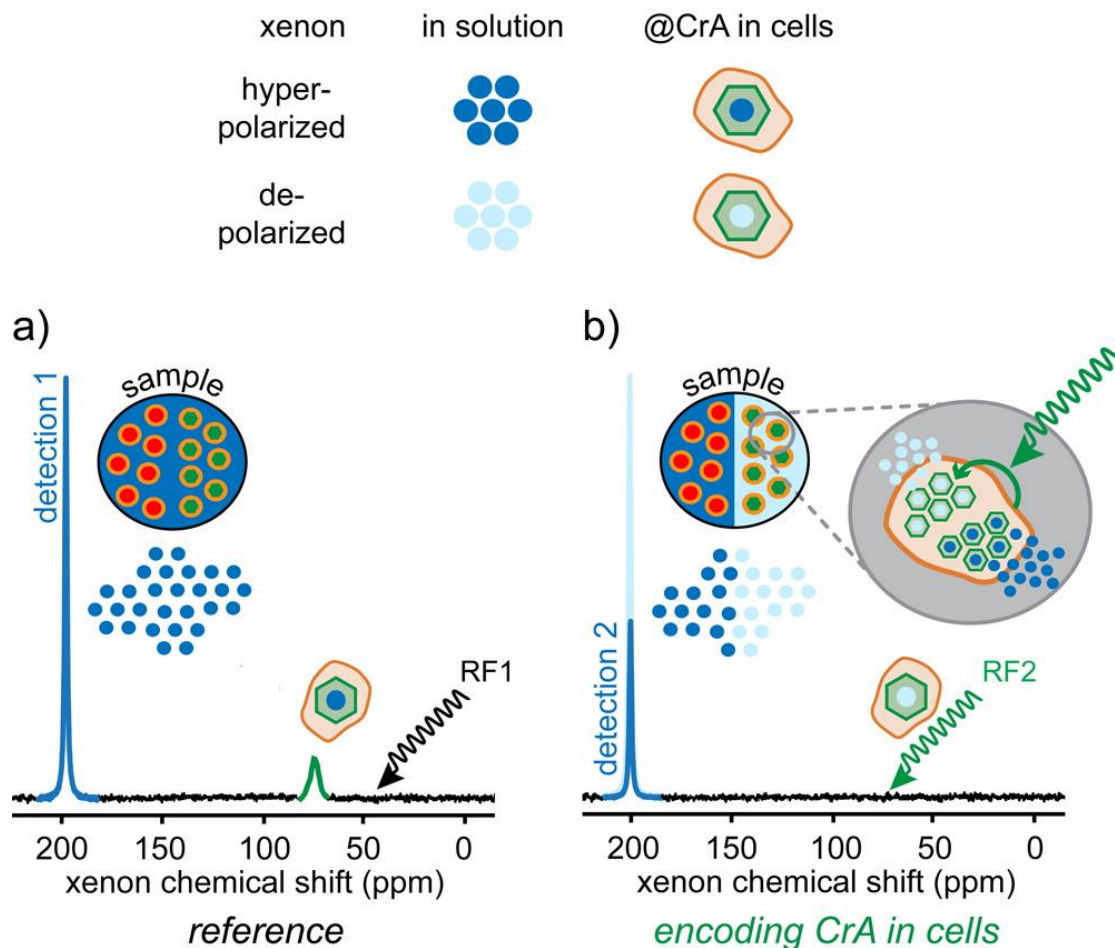


**Figure 5:** Depiction of Hyper-CEST: a) off -resonance spectra b) on-resonance spectra (modified from ref 18)<sup>18</sup>

When hyperpolarized  $^{129}\text{Xe}$  (GREEN) enters the cage a radio frequency pulse pre-saturates the bound xenon causing removal of polarization (RED) (**Figure 6**).<sup>17</sup> The depolarized  $^{129}\text{Xe}$  is then replaced by another polarized  $^{129}\text{Xe}$  atom through the natural in and out exchange. This cycle continues until there is an accumulation of depolarized  $^{129}\text{Xe}$ .



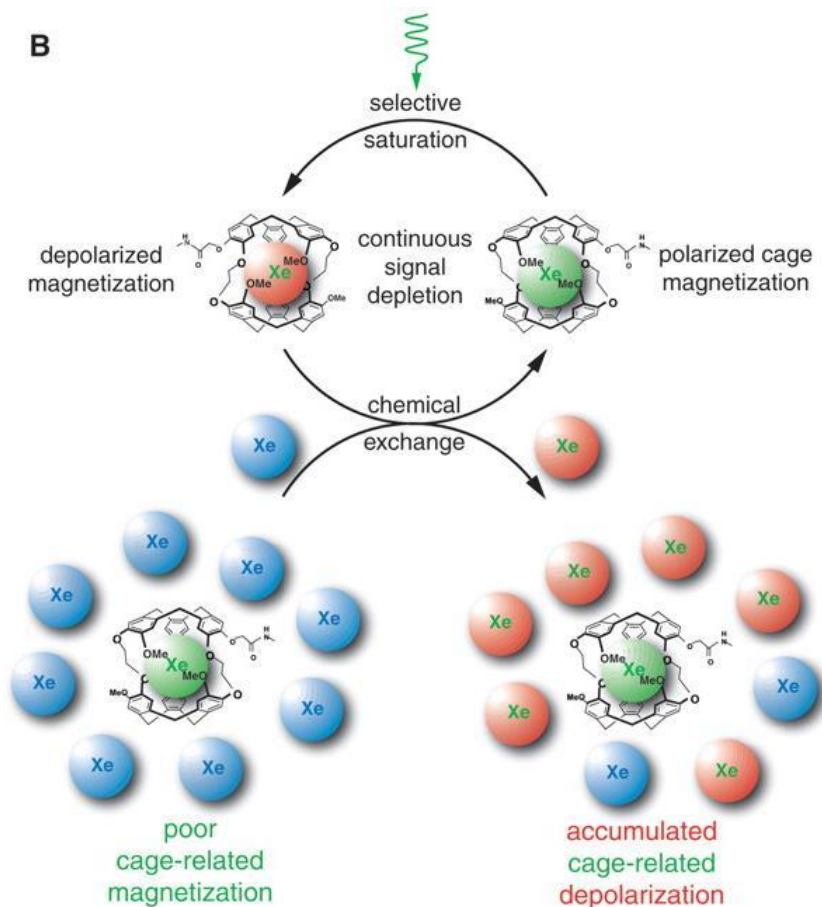


**Figure 6:** Hyper-CEST process <sup>17</sup>

Dmochowski applied this technique to detect a water soluble cryptophane (**Figure 3D**) at concentrations as low as 1.4 pM.<sup>20</sup> This indicates that HyperCEST should be an effective method for molecular imaging, as its detection limits are similar to those of PET and SPECT. HyperCEST has recently been applied to multi-channel detection of cryptophane-A and perfluorooctyl bromide nanodroplets as they both act as hosts for <sup>129</sup>Xe.<sup>18</sup>

## References

1. Gambhir, T. F. M. a. S. S., Molecular imaging in living subjects: seeing fundamental biological processes in a new light. *Genes and Development* **2003**, *17*, 545-580.
2. Lusic, H.; Grinstaff, M. W., X-ray-Computed Tomography Contrast Agents. *Chemical Reviews* **2012**, *113* (3), 1641-1666.
3. Louie, A. Y.; Huber, M. M.; Ahrens, E. T.; Rothbacher, U.; Moats, R.; Jacobs, R. E.; Fraser, S. E.; Meade, T. J., In vivo visualization of gene expression using magnetic resonance imaging. *Nat Biotech* **2000**, *18* (3), 321-325.
4. Broome, D. R.; Girguis, M. S.; Baron, P. W.; Cottrell, A. C.; Kjellin, I.; Kirk, G. A., Gadodiamide-Associated Nephrogenic Systemic Fibrosis: Why Radiologists Should Be Concerned. *American Journal of Roentgenology* **2007**, *188* (2), 586-592.
5. Jasanoff, A., Functional MRI using molecular imaging agents. *Trends in Neurosciences* **2005**, *28* (3), 120-126.
6. Taratula, O.; Dmochowski, I. J., Functionalized <sup>129</sup>Xe contrast agents for magnetic resonance imaging. *Current Opinion in Chemical Biology* **2010**, *14* (1), 97-104.
7. Albert, M. S.; Cates, G. D.; Driehuys, B.; Happer, W.; Saam, B.; Springer, C. S.; Wishnia, A., Biological magnetic resonance imaging using laser-polarized <sup>129</sup>Xe. *Nature* **1994**, *370* (6486), 199-201.

8. Lowery, T. J.; Garcia, S.; Chavez, L.; Ruiz, E. J.; Wu, T.; Brotin, T.; Dutasta, J.-P.; King, D. S.; Schultz, P. G.; Pines, A.; Wemmer, D. E., Optimization of Xenon Biosensors for Detection of Protein Interactions. *ChemBioChem* **2006**, *7* (1), 65-73.
9. Schröder, L., Xenon for NMR biosensing – Inert but alert. *Physica Medica: European Journal of Medical Physics* *29* (1), 3-16.
10. Mugler, J. P.; Altes, T. A., Hyperpolarized <sup>129</sup>Xe MRI of the human lung. *Journal of Magnetic Resonance Imaging* **2013**, *37* (2), 313-331.
11. Simon, B. A.; Kaczka, D. W.; Bankier, A. A.; Parraga, G., *What can computed tomography and magnetic resonance imaging tell us about ventilation?* 2012; Vol. 113, p 647-657.
12. Brotin, T.; Dutasta, J.-P., Cryptophanes and Their Complexes—Present and Future. *Chemical Reviews* **2008**, *109* (1), 88-130.
13. Fogarty, H. A.; Berthault, P.; Brotin, T.; Huber, G.; Desvaux, H.; Dutasta, J.-P., A Cryptophane Core Optimized for Xenon Encapsulation. *Journal of the American Chemical Society* **2007**, *129* (34), 10332-10333.
14. Hill, P. A.; Wei, Q.; Troxler, T.; Dmochowski, I. J., Substituent Effects on Xenon Binding Affinity and Solution Behavior of Water-Soluble Cryptophanes. *Journal of the American Chemical Society* **2009**, *131* (8), 3069-3077.
15. Berthault, P.; Huber, G.; Desvaux, H., Biosensing using laser-polarized xenon NMR/MRI. *Progress in Nuclear Magnetic Resonance Spectroscopy* **2009**, *55* (1), 35-60.

16. Huber, G.; Brotin, T.; Dubois, L.; Desvaux, H.; Dutasta, J.-P.; Berthault, P., Water Soluble Cryptophanes Showing Unprecedented Affinity for Xenon: Candidates as NMR-Based Biosensors. *Journal of the American Chemical Society* **2006**, *128* (18), 6239-6246.
17. Chambers, J. M.; Hill, P. A.; Aaron, J. A.; Han, Z.; Christianson, D. W.; Kuzma, N. N.; Dmochowski, I. J., Cryptophane Xenon-129 Nuclear Magnetic Resonance Biosensors Targeting Human Carbonic Anhydrase. *Journal of the American Chemical Society* **2008**, *131* (2), 563-569.
18. Klippel, S.; Freund, C.; Schröder, L., Multichannel MRI Labeling of Mammalian Cells by Switchable Nanocarriers for Hyperpolarized Xenon. *Nano Letters* **2014**, *14* (10), 5721-5726.
19. Schröder, L.; Lowery, T. J.; Hilty, C.; Wemmer, D. E.; Pines, A., Molecular Imaging Using a Targeted Magnetic Resonance Hyperpolarized Biosensor. *Science* **2006**, *314* (5798), 446-449.
20. Bai, Y.; Hill, P. A.; Dmochowski, I. J., Utilizing a Water-Soluble Cryptophane with Fast Xenon Exchange Rates for Picomolar Sensitivity NMR Measurements. *Analytical Chemistry* **2012**, *84* (22), 9935-9941.

**MANUSCRIPT 1**

Will be submitted to Bioorganic and Medicinal Chemistry Letters

December, 2014

Efforts Towards Cryptophanes functionalized with AuNPs

Marissa Simone and Brenton DeBoef\*

Corresponding author:

Prof. Brenton DeBoef

Department of Chemistry,

University of Rhode Island,

Kingston, Rhode Island 02881

bdeboef@chm.uri.edu

# MANUSCRIPT 1

## Efforts Towards Cryptophanes Functionalized with AuNPs

### **Abstract**

While advances in imaging have made it possible for the diagnosis of certain diseases, there are still many drawbacks. This paper aims to discuss the use of hyperpolarized xenon in conjunction with gold nanoparticles that are decorated with as a novel probe for magnetic resonance imaging (MRI). The synthesis of cryptophanes, optimization of click reactions, and addition of gold nanoparticles will be discussed.

### **General Introduction**

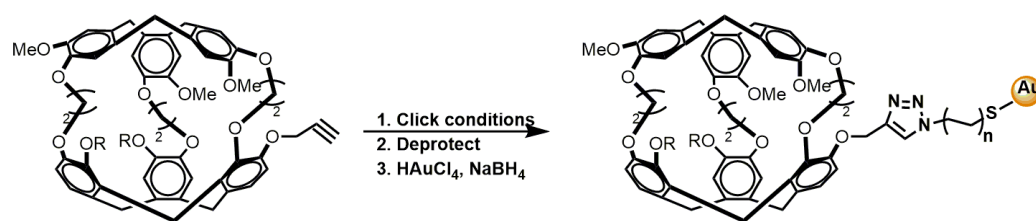
While conventional magnetic resonance imaging (MRI) allows for anatomical imaging, it is inherently insensitive due to the minimal amount of protons capable of aligning with the instrument's magnetic field. Minimization of the signal to noise issues that are inherent in  $^1\text{H}$  MRI, can be achieved by using  $^{129}\text{Xe}$  as a molecular probe, as it is not present in the body and has the ability to be hyperpolarized, thereby giving a 10,000-times stronger signal.<sup>1</sup> When  $^{129}\text{Xe}$  is encapsulated by a porous cage-shaped molecule, such as a cryptophane, a new signal, which is well resolved from the chemical shift of free  $^{129}\text{Xe}$ , is produced in the  $^{129}\text{Xe}$  NMR spectrum. In principle, magnetic resonance imaging techniques can translate this unique signal into a high-resolution 3D image. If these cryptophanes are attached to target-specific ligands, the cryptophane could serve as a biosensor, where its unique signal would be localized at a specific site within the body. This cryptophane-ligand biosensor will allow for the specific detection of molecular processes or receptors.

Using hyperpolarized chemical exchange saturation transfer (HyperCEST) provides another source of signal amplification allowing for detection of sub-micromolar concentrations of physiological targets. By selectively irradiating the  $^{129}\text{Xe}$ -cryptophane signal, the loss of magnetization of the larger bulk Xe peak is easily detected. This indirect detection method allows for very low detection limits, indicating that HyperCEST imaging could be used for true molecular imaging.<sup>1</sup> Cryptophanes can be synthesized into biosensors by functionalizing cryptophanes with antibodies or peptide ligands that are capable of binding to specific targets in the body, such as enzymes. By doing this they are capable of being delivered to human cells and achieving concentrations that would allow for in vivo hyperpolarized  $^{129}\text{Xe}$  MRI studies.<sup>2</sup> Recent HyperCEST NMR experiments of water soluble triacetic acid cryptophane A have shown depolarization of  $^{129}\text{Xe}$  at a rate of  $1.2 \times 10^4$  HP  $^{129}\text{Xe}$  atoms per second.<sup>3</sup> This sensitive detection was performed at picomolar concentrations—a huge improvement over previous work at micromolar concentrations.

Selective biosensors can be synthesized by functionalizing cryptophanes with antibodies or peptide ligands that are capable of binding to specific targets in the body, such as genes, receptors or enzymes. When the ligands on the biosensor bind to a specific target, a unique signal is produced allowing for detection of molecular events making it ideal for in vivo hyperpolarized  $^{129}\text{Xe}$  MRI studies.<sup>2,4</sup>

Gold nanoparticles (AuNPs) are capable of being functionalized with a myriad of organic or biological ligands that bind selectively to small molecules or biological targets. This is achieved by varying the type of capping ligand used and fast or slow addition of  $\text{NaBH}_4$ .<sup>5</sup> The use of gold nanoparticles in imaging has grown over the years

due to their unique optical properties. Along with the use of gold nanoparticles for various modes of imaging, they can be also used for drug delivery.<sup>7</sup> For instance, Kim et al., developed multifunctional gold nanoparticles capable of anticancer therapy and computed tomography (CT) imaging of cancer cells.<sup>8</sup> Further benefits of using gold nanoparticles is that they are nontoxic and non-immunogenic making them ideal drug delivery scaffolds.<sup>9</sup> Therefore, tethering both cryptophanes and biological ligands to gold nanoparticles would allow for targeted imaging via HP-<sup>129</sup>Xe MRI.



**Scheme 1:** Click reaction of cryptophane A to AuNPs (where n = # carbons)

The use of gold nanoparticles to facilitate drug delivery and imaging when tethered to a cryptophane is unprecedented. The proposed study will focus on efforts towards synthesizing a biosensor consisting of a cryptophane tethered to gold nanoparticles via a thiol linker. The addition of protected thiol linkers to cryptophanes will be accomplished via the copper-catalyzed Huisgen cycloaddition, the so-called azide-alkyne click reaction (**Scheme 1**). After deprotection of the thiol group, gold nanoparticles capped with thiol ligands will be added to AuNPs that have been previously capped with labile thiol ligands. These thiols will undergo ligand exchange with the thiols on the cryptophanes to yield the desired nanoparticles decorated with



cryptophanes. The amount of cryptophane loaded onto the nanoparticle surface will be quantified by infrared spectroscopy.

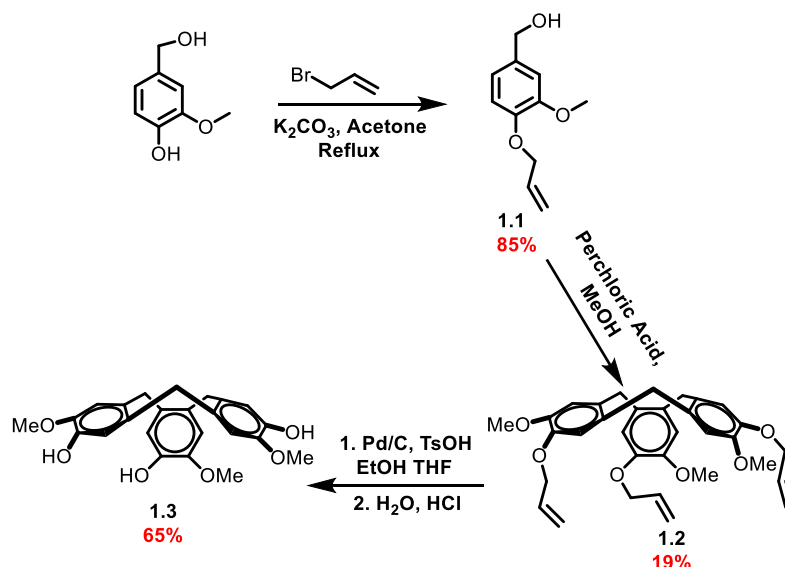
### **Cryptophanes and Gold Nanoparticles**

Over recent years, AuNPs have become increasingly popular in imaging due to their unique optical properties and ability to functionalize the surface with a myriad of organic compounds or biological ligands that selectively bind small molecules or biological targets.<sup>5</sup> Additionally, gold nanoparticles can be used as drug delivery vehicles, as gold nanoparticles have been shown to be non-toxic. Brown et al., achieved this by tethering the anti-cancer drug oxaliplatin to gold nanoparticles resulting in direct site drug delivery.<sup>6</sup>

Tethering gadolinium (Gd) chelates to AuNPs has the capability to enhance the contrast signal in <sup>1</sup>H MRI images. This enhancement is a result of the large number of Gd chelates on each AuNP, allowing for a more pronounced enhancement in contrast near the site of the AuNPs.<sup>7</sup> However, as previously discussed, the toxicity of Gd chelates renders them as less attractive modes of imaging. The capability to achieve signal enhancement utilizing gold nanoparticles initiated our investigation into developing AuNP-based <sup>129</sup>Xe biosensors using a cryptophane.

As originally reported by Dmochowski, the tripropargyl cryptophane-2,2,2 (2 refers to the number of carbons in the alkoxy bridge between cage top and cage bottom), derivative can be accomplished in ten steps.<sup>4</sup> The top of the cage, **1.3**, was synthesized in three steps (**Scheme 2**). Vanillyl alcohol is protected with an allyl group in order to avoid polymerization in the cyclization step (**Scheme 2**). Cyclization was achieved

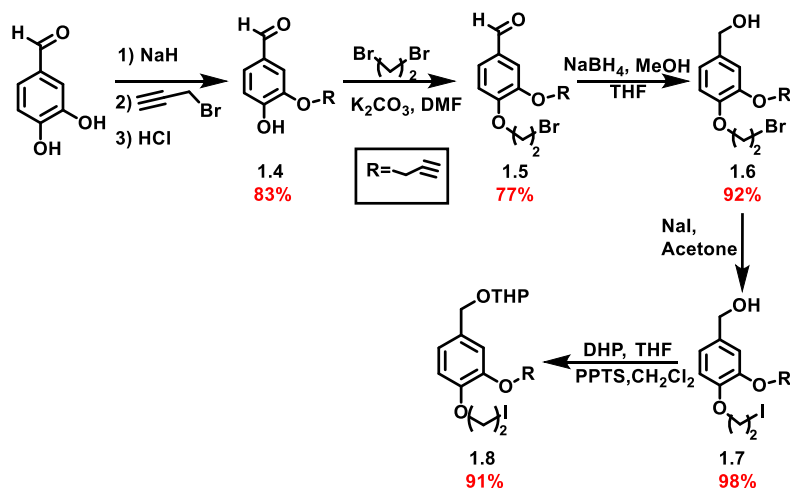
through a Friedel-Crafts cyclization using HClO<sub>4</sub> and MeOH. Deprotection of the allyl group required excess amounts of Pd/C and TsOH.



**Scheme 2:** Synthesis of cage top

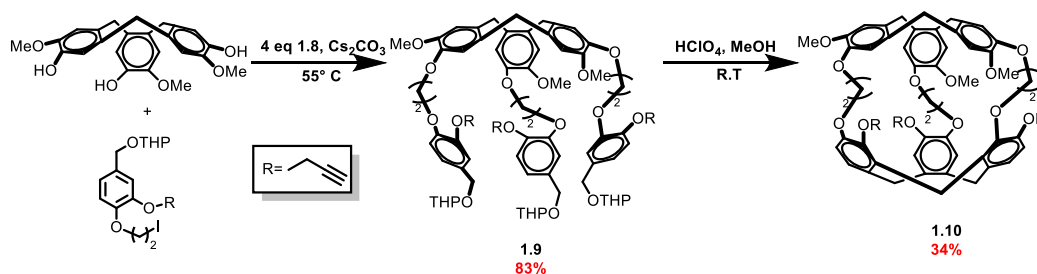
Though the number of carbons in the propargyl linker can be varied, incorporating ethylene bridges results in a cryptophane cavity size that allows for optimal binding and exchange of <sup>129</sup>Xe. Consequently, we set out to synthesize a cryptophane cage containing ethylene bridges between the two cyclotrivenatrylenes. The linker containing the propargyl group was synthesized in five steps (**Scheme 3**). The first step, selective addition of the propargyl linker to the 3-position the linker starting material, 3,4 dihydroxybenzaldehyde was achieved using NaH and propargyl bromide. Though both phenols are deprotonated, position 4 is stabilized through resonance, therefore not as reactive as the 3 position (**1.4**). Subsequent steps included the addition of an ethylene linker (**1.5**), reduction of the aldehyde (**1.6**), a Finkelstein reaction (**1.7**) and finally, protection of the benzyl alcohol as a tetrahydropyranyl (THP)

ether (**1.8**). This protection step was necessary to avoid any unwanted side products in the final steps, and was easily removed *in situ* during the last step. Until recently, the majority of the aforementioned reactions required purification using flash chromatography, but we have recently developed recrystallization conditions that allow for easier scale-up of these synthetic steps. Recrystallization using hexanes and minimal amounts of ethyl acetate was implemented for the purification of **1.4**, **1.5**, and **1.6**, resulting in analytically pure product. Since there is more of a possibility for side products during the first reaction, flash chromatography was kept as a purification procedure for the first step. When using recrystallization for the second step, a 77% yield was obtained, while using flash chromatography for the same step gave a 75% yield. Recrystallization for the reduction step resulted in comparable yields to when flash chromatography was used. Though similar yields were obtained, recrystallization is less time consuming and requires less solvent, so it became our preferred purification method.



**Scheme 3:** Synthesis of propargyl linker

Once the linker was synthesized, it was added in excess to the cage top and heated for two days under nitrogen at 55 °C in the presence of the base, cesium carbonate (**Scheme 4, 1.9**). The final step in the synthesis of the conjugatable cryptophane (**1.10**) was the cyclization of the cage bottom, through a second Friedel-Crafts reaction, mediated by perchloric acid (**Scheme 4**). The overall yield of this synthesis is rather low due unwanted polymerization.



**Scheme 4:** Synthesis of tripropargyl cryptophane A

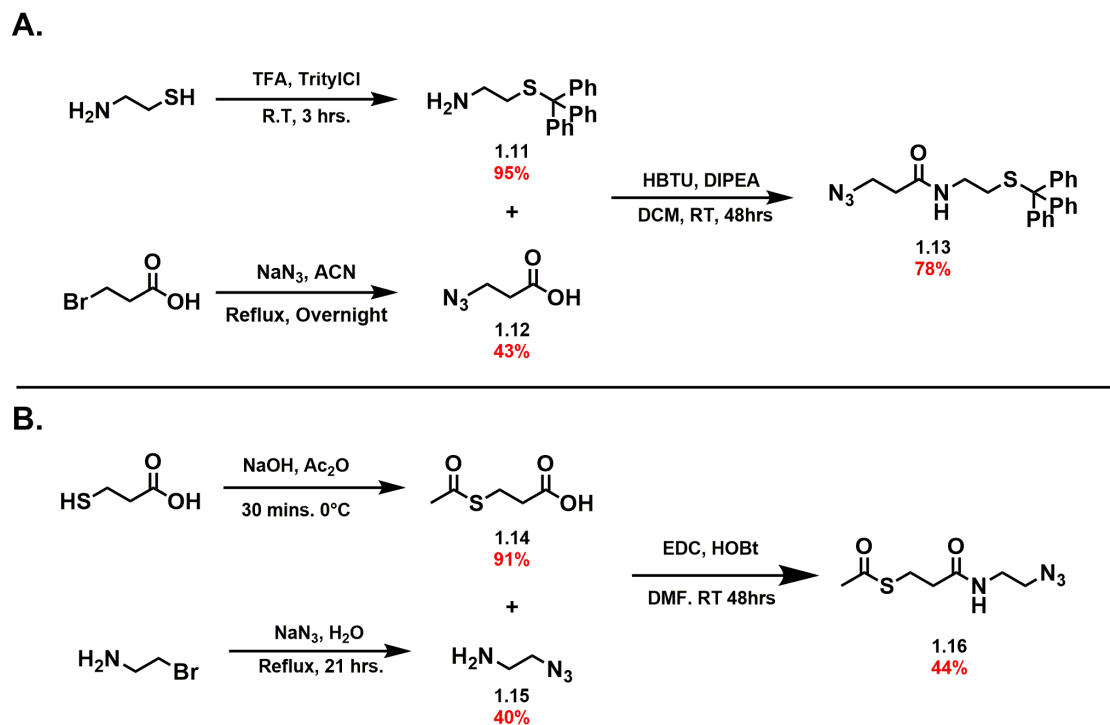
The conversion of tri-propargyl Cryptophane A to a biosensor can be achieved via copper(I)-catalyzed Huisgen cycloaddition “click” of a targeting moiety.<sup>2</sup> Our aim was to decorate gold nanoparticles (AuNPs) with cryptophane cages, which potentially could increase the cryptophanes’ water solubility improving their applicability for in-vivo imaging. Using gold nanoparticles also acts as a second scaffold to which biological ligands could be tethered.

There are multitudes of ways to synthesize gold nanoparticles. For our purposes, the Brust-Schiffron method was the most attractive, as the resulting thiol capped AuNPs are easily re-dispersed in organic solvents, which we envisioned to be an advantage for subsequent modification reactions. Additionally, the dodecanethiol capping ligand used in the AuNP synthesis is known to readily undergo ligand exchange of a variety of thiols.<sup>5, 8</sup> Copper(I) catalyzed azide-alkyne cycloaddition (CuAAC), click chemistry,

can be used to modify gold nanoparticles by employing an azide linker containing a thiol group.<sup>9</sup>

The modification of AuNPs using click chemistry can be achieved via indirect and direct pathways. The indirect method involves synthesizing AuNPs with a dodecanethiol capping ligand that readily undergoes ligand exchange with a thiol-azide linker. At this point click chemistry using the appropriate conditions can be carried out between a cryptophane bearing alkyne groups, such as **1.10**, and the azide-decorated AuNP.<sup>9a</sup> The direct method involves carrying out the click reaction with a protected-thiol-azide linker and a cryptophane like **1.10** in solution. Once completed, the thiol, which is now tethered to the cryptophane, can be deprotected and added as a capping ligand during the synthesis of AuNPs. Recent studies have found this method prevents aggregation of the consequent AuNPs.<sup>9a</sup> As a result, our initial attempts employed this method.

To carry out the click chemistry with the alkynes on cryptophanes, an azide-thiol linker needed to be synthesized. We attempted the synthesis of two azide-thiol linkers (**Scheme 5**). In order to avoid poisoning of the copper catalyst and unwanted side products during the click reaction, the thiol group needed to be protected. This was achieved using trityl chloride to protect 2-aminoethanethiol (**1.11**, **Scheme 5**) and acetate to protect mercaptopropionic acid (**1.14**). The synthesis of the azide portion of the two possible linkers was carried out by refluxing 3-bromopropionic acid or 2-bromoethylamine with sodium azide. Both reactions required extended reaction times and, unfortunately, were low yielding. The synthesis of both azide-thiol linkers was then achieved using peptide-coupling conditions.



**Scheme 5:** Synthesis of protected thiol azide linkers.

Previous click conditions utilized by Dmochowski, which required  $\text{Cu}_2\text{SO}_4$ ,  $\text{K}_2\text{CO}_3$ , 2,6-lutidine and sodium ascorbic acid, did not result in any product and also are not compatible with gold nanoparticles, as salts cause the aggregation of gold nanoparticles.<sup>4</sup> Therefore, new click conditions needed to be established and optimized. To achieve optimal yields when carrying out the click reaction with cryptophanes, the reaction was first optimized using the cryptophane linker, **1.5**, with the thiol-azide linkers.

Initially, copper sulfate pentahydrate and sodium ascorbic acid conditions were applied to click the trityl-thiol-azide linker (**1.13**) to **1.5** and eventually to tripropargyl cryptophane A, **1.10** (**Scheme 4**). Though yields were sufficient, the inability to deprotect the trityl group after the click reaction, resulting in the need to switch to the acetate protected thiol linker (**1.16**), in hopes that it would be easily deprotected.

Originally, the same conditions for the previous click reaction were applied to conjugate **1.16** to **1.5**, however, no product was formed. It is possible that the bulky trityl group on the thiol prevented the copper catalyst from coordinating with sulfur, whereas the thioacetate group may not hinder the poisoning of the catalyst. New click reactions involving copper(I) bromide [Cu(I)Br] and the hexabenzyltren (tren) ligand turned out to give better yields than the previously described conditions. Due to the air sensitivity of Cu(I)Br, these reactions were carried out in a Schlenk tube. The first conditions applied were using 1 equivalent of the alkyne, **1.5**, and 1.1 equivalents of the azide, **1.16**, with 30 mol% Cu(I)Br and the tren ligand, resulting in a 46% yield (**Table 1**). Decreasing the mole percentage of Cu(I)Br and tren actually led to an increase in yield, though the reaction took 72 hr to complete. Optimal reaction conditions were found to be 1 equivalent of **1.5**, 1.1 equivalent of **1.16**, 10 mol% Cu(I)Br and tren ligand at 65 °C for 48 hr, giving a 64% yield (**Table 1**).

**Table 1: Optimization click conditions**

Entry	<b>1.5</b> (equiv)	<b>1.16</b> (equiv)	Cu(I)Br	Tren Ligand	Solvent	Conditions	Yield
<b>1</b>	1	1.1	30%	30%	Toluene	60 °C 48 hr	46%
<b>2</b>	1	1	10%	10%	Toluene	60 °C 72 hr	54%
<b>3</b>	1	1.1	10%	10%	Toluene	65 °C 48 hr	64%

These optimal conditions were modified to achieve the click reaction at all three alkynes on the cryptophane. This was achieved by using 40 mol% Cu(I)Br and 40% tren





carry out the previously discussed direct method of functionalizing AuNPs, led us to explore the indirect method of AuNP functionalization.

As previously mentioned, the indirect method involved ligand exchange of the dodecanethiol capping ligand with an thiol-azide chain. Deprotection of the trityl-thiol-azide linker, **1.13**, was achieved using TFA and triethylsilane in DCM. This was then added to AuNPs in DCM and stirred for two days at room temperature. The solution was concentrated and washed with ethanol to remove any free ligands. Successful ligand exchange was verified by NMR (see supporting information). The click reaction between the azide-tethered AuNPs and cryptophane was performed using Cu(I)Br and the tren ligand. Unfortunately, the click reaction was not successful even with adding excess amounts of catalyst and extended reaction times.

Another pathway to functionalize nanoparticles was attempted by performing ligand exchange between dodecanethiol capping ligand and 11-bromoundecylthiol, which was converted into an azide via an  $S_N2$  reaction with sodium azide. The formation of the azide-decorated AuNPs was verified via NMR, allowing for click chemistry to be carried out with tri-propargyl cryptophane using Cu(I)Br and tren ligand. While the click reaction seemed to be successful, the AuNPs aggregated.

## **Conclusion**

Future work involves using different deprotection strategies and/or protecting groups. Additional routes for AuNP functionalization could be accomplished by synthesizing a different cryptophane starting material by substituting one of the propargyl linkers in the cryptophane for a linker that is functionalized with thiol group.

## References

1. Schröder, L.; Lowery, T. J.; Hilty, C.; Wemmer, D. E.; Pines, A., Molecular Imaging Using a Targeted Magnetic Resonance Hyperpolarized Biosensor. *Science* **2006**, *314* (5798), 446-449.
2. Chambers, J. M.; Hill, P. A.; Aaron, J. A.; Han, Z.; Christianson, D. W.; Kuzma, N. N.; Dmochowski, I. J., Cryptophane Xenon-129 Nuclear Magnetic Resonance Biosensors Targeting Human Carbonic Anhydrase. *Journal of the American Chemical Society* **2008**, *131* (2), 563-569.
3. Bai, Y.; Hill, P. A.; Dmochowski, I. J., Utilizing a Water-Soluble Cryptophane with Fast Xenon Exchange Rates for Picomolar Sensitivity NMR Measurements. *Analytical Chemistry* **2012**, *84* (22), 9935-9941.
4. Wei, Q.; Seward, G. K.; Hill, P. A.; Patton, B.; Dimitrov, I. E.; Kuzma, N. N.; Dmochowski, I. J., Designing <sup>129</sup>Xe NMR Biosensors for Matrix Metalloproteinase Detection. *Journal of the American Chemical Society* **2006**, *128* (40), 13274-13283.
5. Saha, K.; Agasti, S. S.; Kim, C.; Li, X.; Rotello, V. M., Gold Nanoparticles in Chemical and Biological Sensing. *Chemical Reviews* **2012**, *112* (5), 2739-2779.
6. Brown, S. D.; Nativo, P.; Smith, J.-A.; Stirling, D.; Edwards, P. R.; Venugopal, B.; Flint, D. J.; Plumb, J. A.; Graham, D.; Wheate, N. J., Gold Nanoparticles for the Improved Anticancer Drug Delivery of the Active Component of Oxaliplatin. *Journal of the American Chemical Society* **2010**, *132* (13), 4678-4684.

7. Debouttière, P. J.; Roux, S.; Vocanson, F.; Billotey, C.; Beuf, O.; Favre-Réguillon, A.; Lin, Y.; Pellet-Rostaing, S.; Lamartine, R.; Perriat, P.; Tillement, O., Design of Gold Nanoparticles for Magnetic Resonance Imaging. *Advanced Functional Materials* **2006**, *16* (18), 2330-2339.
8. Brust, M.; Walker, M.; Bethell, D.; Schiffrin, D. J.; Whyman, R., Synthesis of thiol-derivatised gold nanoparticles in a two-phase Liquid-Liquid system. *Journal of the Chemical Society, Chemical Communications* **1994**, (7), 801-802.
9. (a) Li, N.; Zhao, P.; Salmon, L.; Ruiz, J.; Zabawa, M.; Hosmane, N. S.; Astruc, D., "Click" Star-Shaped and Dendritic PEGylated Gold Nanoparticle-Carborane Assemblies. *Inorganic Chemistry* **2013**, *52* (19), 11146-11155; (b) Lim, J.; Yang, H.; Paek, K.; Cho, C.-H.; Kim, S.; Bang, J.; Kim, B. J., "Click" synthesis of thermally stable Au nanoparticles with highly grafted polymer shell and control of their behavior in polymer matrix. *Journal of Polymer Science Part A: Polymer Chemistry* **2011**, *49* (16), 3464-3474; (c) Sommer, W. J.; Weck, M., Facile Functionalization of Gold Nanoparticles via Microwave-Assisted 1,3 Dipolar Cycloaddition. *Langmuir* **2007**, *23* (24), 11991-11995; (d) Fleming, D. A.; Thode, C. J.; Williams, M. E., Triazole Cycloaddition as a General Route for Functionalization of Au Nanoparticles. *Chemistry of Materials* **2006**, *18* (9), 2327-2334.

## **Supporting Information**

Efforts Towards Functionalization of Cryptophanes for MRI

Marissa Simone, and Brenton DeBoef

University of Rhode Island, Department of Chemistry, 51 Lower College Road,

Kingston, RI 02881

## Experimental Section

### Reagents

All substrates and solvents were purchased from Sigma-Aldrich and Fisher Scientific.

Flash chromatography was performed using hand columns or a Teledyne ISCO

CombiFlashR<sub>f</sub> apparatus using RediSep R<sub>f</sub> Silica gel (60 Å, 40-60 μm).

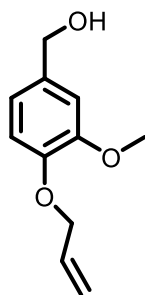
### Instrumentation

GC/MS analysis was carried out on an Agilent Technologies 6890 GC system fixed

with a 5973 mass selective detector. NMR spectra were acquired with a Bruker

Avance III 300 MHz spectrometer.

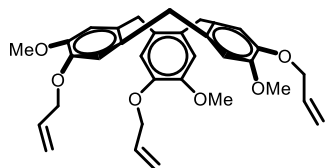
### Compound 1.1: 3-methoxy-4-(2-propenyloxy) benzenemethanol:



Acetone, vanillyl alcohol (15.48 g, 97.29 mmol), and allyl bromide (12.94 g, 107.01 mmol) were added to round bottom flask and stirred until homogeneous. K<sub>2</sub>CO<sub>3</sub> (13.44 g, 97.29 mmol) was added slowly and the mixture was refluxed overnight. The next day, the reaction was cooled to room temperature while stirring. Acetone was then removed under vacuum. The resulting white residue was dissolved in 50 mL of DCM and 40 mL of H<sub>2</sub>O. The biphasic solution was transferred to a separatory funnel, and the aqueous layer was removed, and the organic layer was washed with 1 M NaOH (3 x 50 mL) and brine (1 x 50 mL). The organic layer was collected, dried over MgSO<sub>4</sub>, filtered and the solvent was removed under vacuum to yield a yellow powder. 50 mL

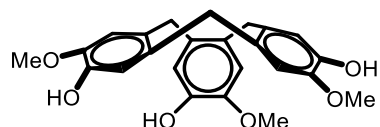
of EtOAc was added, and then removed under vacuum (to remove excess allyl bromide), resulting in **1.1** (15.54 g, 82%) as a fine white powder. All spectral information matched literature values.<sup>1</sup>

**Compound 1.2: 2,7,12-Trimethoxy-3,8,13-tris(2-propenyloxy)-10,15-dihydro-5H-tribenzo cyclononene**



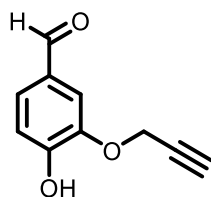
In a round bottom flask equipped with a stir bar, **1.1** (4.91 g, 25.29 mmol) was dissolved in methanol (36 mL) and cooled to 0 °C in an ice bath. Perchloric acid (15 mL) was added dropwise to the flask under N<sub>2</sub>. The solution turned magenta while it stirred overnight. The following day, DCM was added to the solution, and it was cooled again to 0 °C for 5 min. Then 32 mL of 5 M NaOH was added dropwise over 10 min followed by the dropwise addition of saturated NaHCO<sub>3</sub> (32 mL). The reaction was stirred at room temperature for 1-2 hours. The organic layer was then filtered, dried with MgSO<sub>4</sub> and concentrated. Diethyl ether was added and the resulting suspension was sonicated for 1 hr. The suspension was allowed to stir overnight at room temperature. The thickened product was isolated by filtration and the solid was dried under high vacuum to yield **1.2** (2.01 g, 15%) as an off-white solid. All spectral information matched literature values.<sup>1</sup>

**Compound 1.3**



In a round bottom **1.2** (3.36 g, 6.34 mmol) was dissolved in THF (100 mL) and EtOH (68 mL) in a vacuum-dried flask under N<sub>2</sub>. In a separate round bottom flask Pd/C (4.06 g, mmol) and TsOH (0.72 g, 4.22 mmol) was dissolved in 25 mL of H<sub>2</sub>O and then added to the other flask. The solution was heated to 75 °C for 2 days. Upon completion, the reaction was cooled to room temperature, and filtered over celite. The filtrate was concentrated and dissolved with THF and EtOAc. The organic solutions was washed 3x with 100 mL of saturated solution of NaHCO<sub>3</sub> and 2x with 100 mL of brine. The organic layers were isolated, dried over MgSO<sub>4</sub>, and concentrated to dryness. The solid was then digested by stirring in chloroform for 1 hr. The solid was filtered to obtain **1.3** (1.68 g, 35%) as a fine white powder. All spectral information matched literature values.<sup>1</sup>

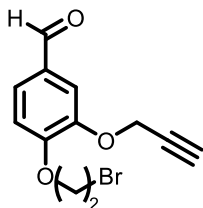
**Compound 1.4: 3 propargyloxy-4-hydroxybenzaldehyde:**



To a flame dried 3-neck flask, NaH (0.96 g, 40 mmol) was added, followed by the addition of 20mL of DMSO in one portion, and was stirred until dissolved. 3,4-dihydroxy benzaldehyde (2.76 g, 20 mmol) was then dissolved in DMSO (12 mL) and was added all once at 0C. Once all aldehyde was added, the flask was removed from the ice bath, and propargyl bromide (2.37g, 20mmole) was added drop wise by syringe. The reaction was stirred overnight at room temperature. Reaction was poured over ice and neutralized with 1M HCl and extracted with EtOAc (3 x 75 mL). Organic

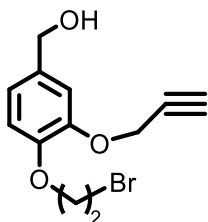
layers were washed with brine (3 x 50 mL), dried over MgSO<sub>4</sub>, filtered, and the solvent was removed under pressure. Flash chromatography to separated, using 20/80/1 of ethyl acetate/hexane/ glacial acetic acid. Pure product, **1.4** (2.60 g, 74%) was isolated. All spectral information matched literature values.<sup>1</sup>

**Compound 1.5 propargyloxy-4-(2-bromoethoxy)benzaldehyde:**



Added **1.4**, propargyloxy-4-hydroxybenzaldehyde (1.65 g, 9.4 mmol), K<sub>2</sub>CO<sub>3</sub> (6.00 g, 46.9 mmol), and DMF to a three neck flask. Reaction was stirred at room temperature for 30 minutes. Dibromoethane (94 mmol, 6 mL) was then added in one portion and heated overnight at 60 °C under N<sub>2</sub> atmosphere. Mixture was poured over 350 mL of water and was extracted using 3 x 10 mL (4 x 75mL) of ethyl acetate. Organic layers were washed with NaOH 1M (2 x 75 mL), H<sub>2</sub>O (75 mL), then brine (3 x 75 mL). Organic layer dried over MgSO<sub>4</sub>, filtered and solvent removed under vacuum. Using hexanes and minimal ethyl acetate product was recrystallized to give **1.5** (2.06 g, 77%) as a white solid. All spectral information matched literature values.<sup>1</sup>

**Compound 1.6 [3 propargyloxy-4-(2-bromoethoxy)phenyl]methanol**

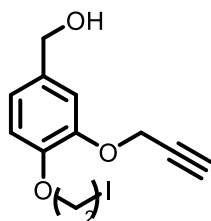


To a three neck flask with N<sub>2</sub> inlet, **1.5** (1.58 g, 5.60 mmol), was dissolved in methanol/THF solvent. Solution was cooled to -9°C in (MeOH/ice) followed by



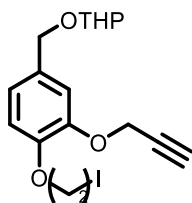
addition NaBH<sub>4</sub> (0.25g, 6.70mmole). Mixture was stirred at 0°C for 20 min then allowed to warm to rt for an additional 40 min. Mixture was concentrated under vacuum and then cooled to 0 °C and acidified with 150 mL of dilute HCl. Sample was extracted with ethyl acetate (3 x 50 mL), then washed with brine (3 x 50 mL) and dried over MgSO<sub>4</sub>. Sample was filtered, and concentrated in vacuum and purified using recrystallization with hexanes to yield **1.6** (1.48g, 92%) as a white solid. All spectral information matched literature values.<sup>1</sup>

**Compound 1.7 [3 propargyloxy-4-(2-iodoethoxy)phenyl]methanol:**



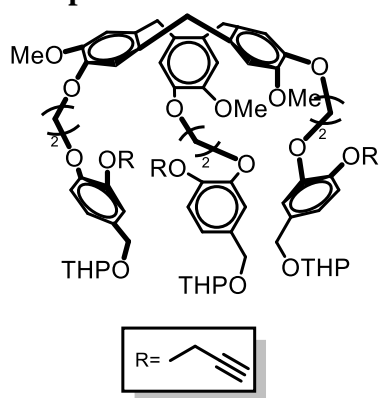
In a round bottom flask, sodium iodide (4.86 g, 32.46 mmol) and **1.6** (2.30 g, 8.11 mmol) were dissolved in acetone and refluxed overnight. Solvent was removed under vacuum and solid was dissolved in DCM and subsequently washed with sodium thiosulfate (2 x 50 mL), water (50 mL) and brine (2 x 50 mL). The organic layer was dried over MgSO<sub>4</sub>, filtered and solvent was removed under vacuum to yield pure **1.7** (2.44 g, 98%) as a white solid. All spectral information matched literature values.<sup>1</sup>

**Compound 1.8 [3-propargyloxy-4-(2-iodoethoxy)phenyl]methanol:**



In a three neck flask **1.7** (1.82 g, 5.48mmol) was dissolved in THF, to which DHP (0.55 g, 6.58 mmol) was then added. In a separate flask PPTS (0.13 g, 0.54 mmol) was dissolved in DCM and then added to main reaction flask. The reaction was stirred at room temperature overnight. Upon completion the reaction was concentrated under reduced pressure and subsequently diluted with EtOAc and washed with water and brine. It was then dried over MgSO<sub>4</sub>, filtered and concentrated by vacuum. The crude product was purified using flash chromatography with 20/80 EtOAc/Hexane. Product isolated to yield **1.8** (2.08 g, 91%) as yellow oil. All spectral information matched literature values.<sup>1</sup>

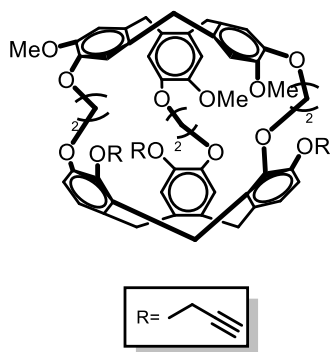
### Compound 1.9



Cesium carbonate (1.27 g, 3.89 mmol) and **1.3** (0.26 g, 0.65 mmol) were added to a dried three neck flask with a stir bar and purged with nitrogen. Dry DMF was then added with a syringe and mixture was allowed to stir for 30 minutes at room temperature. Then using minimal amounts of DMF, **1.8** was added (1.07 g, 2.59 mmol). The reaction was stirred under N<sub>2</sub> at 65°C for 48 hours. Upon completion the reaction was cooled to room temperature and was poured into 100 mL of water. The aqueous layer was then extracted with 3 x 75 mL of EtOAc. Combined organic layers were washed with 3 x 100 mL of brine. The organic layer was isolated, dried over

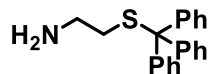
MgSO<sub>4</sub> and concentrated under vacuum. The crude product was purified by flash chromatography using 50/50, 60/40, and 75/25 EtOAc/Hex. Product was isolated and concentrated down to yield **1.9** (0.52 g, 63%). All spectral information matched literature values.<sup>1</sup>

### Compound 1.10 Tri-Propargyl Cryptophane A



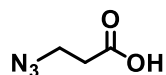
To a round bottom containing methanol (165 mL), **1.9** (0.21 g, 0.16 mmol) dissolved in DCM (5mL) was added. The reaction mixture was then cooled to 0°C and HClO<sub>4</sub> (165 mL) is added in a drop-wise fashion. Reaction was stirred at room temperature for 48 hrs. Upon completion the reaction was quenched with H<sub>2</sub>O (165 mL) and brine (165 mL) and stirred for 1 hour. Half of the mixture was extracted with 4 x 100mL of DCM, the organic layer is put aside and the second half of the reaction mixture was extracted with 4x100mL of DCM. Organic layers were combined and washed with H<sub>2</sub>O, saturated NaHCO<sub>3</sub>, and brine. Flash chromatography was performed using a gradient of DCM/Acetone 2%-10% to afford pure **1.10** (0.054g, 34%) as a white solid. All spectral information matched literature values.<sup>1</sup>

### Compound 1.11: 2-(tritylthio)ethanamine



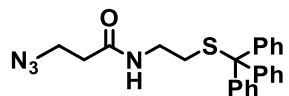
To a round bottom containing thiol ethylamine (1 g, 8.8 mmol), TFA(6.3 mL) was added followed by the addition of trityl chloride (2.45 g, 8.8 mmol) and stirred at room temperature for three hours. The reaction was then concentrated, diluted with EtOAc, washed with 3N NaOH (4 x 15 mL), H<sub>2</sub>O (15 mL), and saturated NaHCO<sub>3</sub> (15 mL), and brine (15 mL). The organic layer was dried over MgSO<sub>4</sub> and concentrated down. The reaction was recrystallized using DCM and hexanes yielding **1.11** (2.68 g, 95%) as white solid. All spectral information matched literature values.<sup>2</sup>

**Compound 1.12: 3-(azido)propionic acid**



Bromopropionic acid (1.52 g, 10mmol) was dissolved in acetonitrile (20 mL) and to it NaN<sub>3</sub> (1.3 g, 20 mmol) was added. Reaction was refluxed overnight. Acetonitrile was removed under vacuum and resulting solid was dissolved in EtOAc (100 mL), washed with 0.1M HCl (3 x 60 mL), water (3 x 60 mL), and brine (100 mL). Organic layer dried with MgSO<sub>4</sub> and concentrated down yielding 3-(azido)propionic acid, **1.12** (0.50g, 43%) as a yellow oil. All spectral information matched literature values.<sup>3</sup>

**Compound 1.13:**

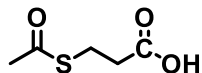


To a round bottom equipped with a stir bar, compounds **1.11** (1.16 g, 3.6 mmol), and **1.12** (0.38 g, 3.3 mmol) were added. Followed by the addition of HBTU (1.50 g, 3.96 mmol), round bottom was purged with N<sub>2</sub> and then dry DCM (20 mL) was added followed by DIPEA (1.2 mL, 6.6 mmol). Reaction was stirred at room temperature,

under N<sub>2</sub> for two days. Upon completion the reaction was washed with NaHCO<sub>3</sub> (50 mL) and brine (50 mL). Organic layer dried with MgSO<sub>4</sub>, filtered, and concentrated down onto silica. The crude product was purified using a 20/80 - 70/30 solvent gradient of EtOAc/Hex. The product was isolated and concentrated down to yield **1.13** (78%) as a white solid.

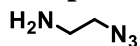
**<sup>1</sup>H NMR (300 MHz, CDCl<sub>3</sub>):** δ 7.46 – 7.35 (Ar CH, m, 6H), 7.33 – 7.27 (Ar CH, m, 6H), 7.25 – 7.19 (Ar CH, m, 3H), 3.57 (COCH<sub>2</sub>, t, *J* = 6.5 Hz, 2H), 3.10 (-NHCH<sub>2</sub>, q, *J* = 6.1 Hz, 2H), 2.44 (-N<sub>3</sub>CH<sub>2</sub>-, t, *J* = 6.3 Hz, 2H), 2.32 (SCH<sub>2</sub>-, t, *J* = 6.5 Hz, 2H).  
**<sup>13</sup>C NMR (75 MHz, CDCl<sub>3</sub>):** δ 169.72, 144.65, 129.57, 128.06, 126.90, 66.90, 47.31, 38.35, 35.67, 31.87.

#### Compound 1.14: Propionithioacetate



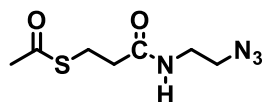
Mercaptopropionic acid (1.4 mL 20mmol) was added to NaOH (2 M) at 0°C. Acetic anhydride was then added and reaction was stirred for 30 minutes at 0°C. Reaction was acidified to a pH ≈ 2 with 6N HCl. Then the mixture was extracted with EtOAc (3 x 30 mL). Organic layers were combined, dried with MgSO<sub>4</sub>, and concentrated down reduced pressure to yield **1.14** (2.68 g, 91%) as white crystals. All spectral information matched literature values.<sup>4</sup>

#### Compound 1.15: 2-azidoethylamine



Bromoethylamine (2.5 g, 12.20 mmol) was dissolved in 10 mL of water, followed by the addition of NaN<sub>3</sub> (2.38 g, 36.36 mmol) and was refluxed for 21 hrs. Reaction was then cooled to 0°C and KOH (4g) was slowly added. The reaction mixture was then extracted using diethyl ether (3 x 10 mL) and organic layers were collected, dried over MgSO<sub>4</sub> and concentrated until 10 mL was left (0.41g, 40%). All spectral information matched literature values.<sup>5</sup>

### Compound 1.16



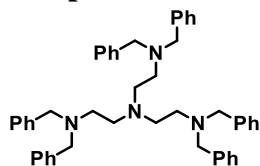
To round bottom containing **1.15** (0.67 g, 4.5mmol) and **1.14** (0.43 g, 5.00 mmol) were dissolved in DMF. EDC (2.96 g, 15.4 mmol) and HOBT (1.25 g, 8.19 mmol) were then added and the reaction was stirred at room temperature for two days.

Reaction was diluted with water and extracted with DCM (3 x 50 mL). Organic layers were then washed with brine, isolated, dried over MgSO<sub>4</sub>, filtered and concentrated down. Purification was performed using flash chromatography (gradient of EtOAc/Hexane) to give pure **1.16**, (0.42g 44%) as a yellow oil.

<sup>1</sup>H NMR (300 MHz, CDCl<sub>3</sub>): δ 5.92 (NH, s, 1H), 3.38 (d, *J* = 3.9 Hz, 4H), 3.08 (t, *J* = 7.0 Hz, 2H), 2.45 (t, *J* = 7.0 Hz, 2H), 2.27 (CH<sub>3</sub>-CO s, 3H).

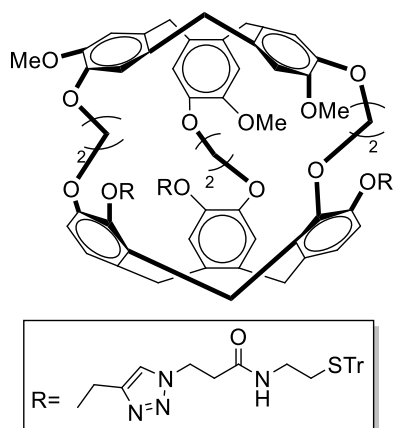
<sup>13</sup>C NMR (75 MHz, CDCl<sub>3</sub>): δ 196.21, 170.95, 50.85, 38.97, 36.20, 30.61, 24.85.

### Compound 1.17



Tris (2 aminoethyl) amine (0.18 g, 1.3 mmol), phenylbenzylbromide (1.05 mL, 8.8 mmol), and K<sub>2</sub>CO<sub>3</sub> (1.90 g, 13.8 mmol), were refluxed in CH<sub>3</sub>CN under N<sub>2</sub> for 48 hrs. Upon completion it was cooled on an ice bath and washed with acetonitrile, water, methanol and then dissolved in hot toluene. Toluene washed with brine and dried over MgSO<sub>4</sub> and solvent was removed. Product was precipitated in methanol giving **1.17** (0.69 g, 77%) as a yellow oil. All spectral information matched literature values.<sup>6</sup>

### Compound 1.18

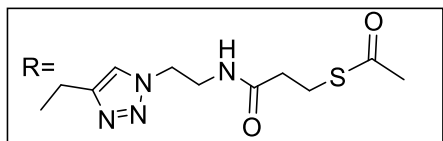
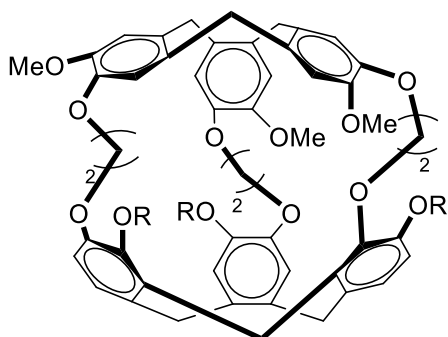


To a vial equipped with a stir bar, **1.10** (0.11 g, 0.11mmol) and **1.13** (0.14 g, 0.33 mmol) were dissolved in THF (5 mL). An aqueous solution of  $\text{CuSO}_4 \cdot 5\text{H}_2\text{O}$  was added, followed by the slow addition of a freshly prepared aqueous solution of sodium ascorbic acid. Reaction was monitored by TLC (98%DCM/2% Acetone), upon disappearance of **1.10**, THF was removed under vacuum.

DCM and 3mL of concentrated  $\text{NH}_3\text{OH}$  were added and stirred for 30 minutes. The organic layer was then washed with water and brine, dried over  $\text{MgSO}_4$  and filtered. Crude product was dried onto silica and purified using a 25 gram column (gradient of 2/98-20/80 acetone/DCM) on the combi-fash. Product was isolated to yield **1.18** (52%) as a white solid.

**$^1\text{H}$  NMR (300 MHz,  $\text{CDCl}_3$ ):**  $\delta$  7.72 (tetrazole CH, s, 3H), 7.42 – 7.36 (m, 20H), 7.30 – 7.19 (m, 32H), 6.81 (s, 3H), 6.77 (d,  $J = 1.4$  Hz, 6H), 6.66 (s, 3H), 5.52 (-NH, t,  $J = 5.7$  Hz, 3H), 5.15 – 4.98 (- $\text{OCH}_2\text{C}$ , m, 6H), 4.67 (- $\text{COCH}_2$ , t,  $J = 6.4$  Hz, 6H), 4.53 (- $\text{OCH}_2\text{CH}_2\text{O}$ -, dd,  $J = 13.6, 6.3$  Hz, 6H), 4.17 (-Ar $\text{CH}_2$ , s, 12H), 3.56 (- $\text{OCH}_3$ , s, 9H), 3.37 (- $\text{OCH}_2\text{CH}_2\text{O}$ -, dd,  $J = 14.2, 3.9$  Hz, 6H), 3.03 (-NH $\text{CH}_2$ -, dt,  $J = 7.3, 3.6$  Hz, 6H), 2.75 (-N $\text{CH}_2$ -, t,  $J = 6.4$  Hz, 6H), 2.40 (- $\text{CH}_2\text{S}$ -, t,  $J = 6.3$  Hz, 6H).  
 **$^{13}\text{C}$  NMR (75 MHz,  $\text{CDCl}_3$ ):**  $\delta$  168.85, 149.63, 148.37, 147.71, 146.52, 144.52, 134.06, 133.23, 131.63, 129.47, 128.01, 126.87, 123.98, 121.65, 120.72, 117.99, 114.46, 69.26, 66.93, 63.81, 56.03, 45.90, 38.33, 36.13, 31.64.

## Compound 1.19



To a Shlenk tube equipped with a stir bar, **1.10** (61 mg, 0.064 mmol), **1.16** (41 mg, 0.19 mmol), and **1.17** (35 mg, 0.051 mmol) were added under N<sub>2</sub> and dissolved in 2 mL of THF. In the glove box Cu(I)Br (7.3 mg, 0.051 mmol) was added to the Shlenk tube. The reaction was heated at 65°C for two days and monitored by TLC (2/98 acetone/DCM), upon disappearance of **1.10**, the reaction was worked up by removing THF under reduced pressure. Then DCM was added and the organic layer was washed with water and brine, dried over MgSO<sub>4</sub>, filtered and then dried onto silica for purification. Purified using 25 gram column and a gradient (2/98-20/80) of acetone/DCM on combi-fash. The product was isolated to yield **1.19** (59%) as a white solid.

**<sup>1</sup>H NMR (300 MHz, CDCl<sub>3</sub>):**  $\delta$  7.60 (s, 3H), 6.80 (s, 3H), 6.69 (d,  $J = 13.4$  Hz, 6H), 6.59 (s, 3H), 6.12 (s, 2H), 5.15 – 5.00 (m, 6H), 4.49 (q,  $J = 6.7, 6.3$  Hz, 12H), 4.12 (s, 12H), 3.75 (d,  $J = 5.6$  Hz, 6H), 3.56 (-OCH<sub>3</sub>, s, 9H), 3.32 (d,  $J = 13.7$  Hz, 6H), 3.06 (t,  $J = 7.0$  Hz, 7H), 2.42 (t,  $J = 6.9$  Hz, 6H), 2.25 (-COCH<sub>3</sub>, s, 9H).

**<sup>13</sup>C NMR (75 MHz, CDCl<sub>3</sub>):**  $\delta$  196.01, 171.30, 149.56, 148.29, 147.77, 146.45, 134.10, 133.37, 131.68, 129.57, 123.70, 121.40, 120.58, 114.41, 69.20, 63.93, 56.07, 49.71, 39.46, 36.11, 30.63, 24.76.



**Compound 1.20: AuNPs**

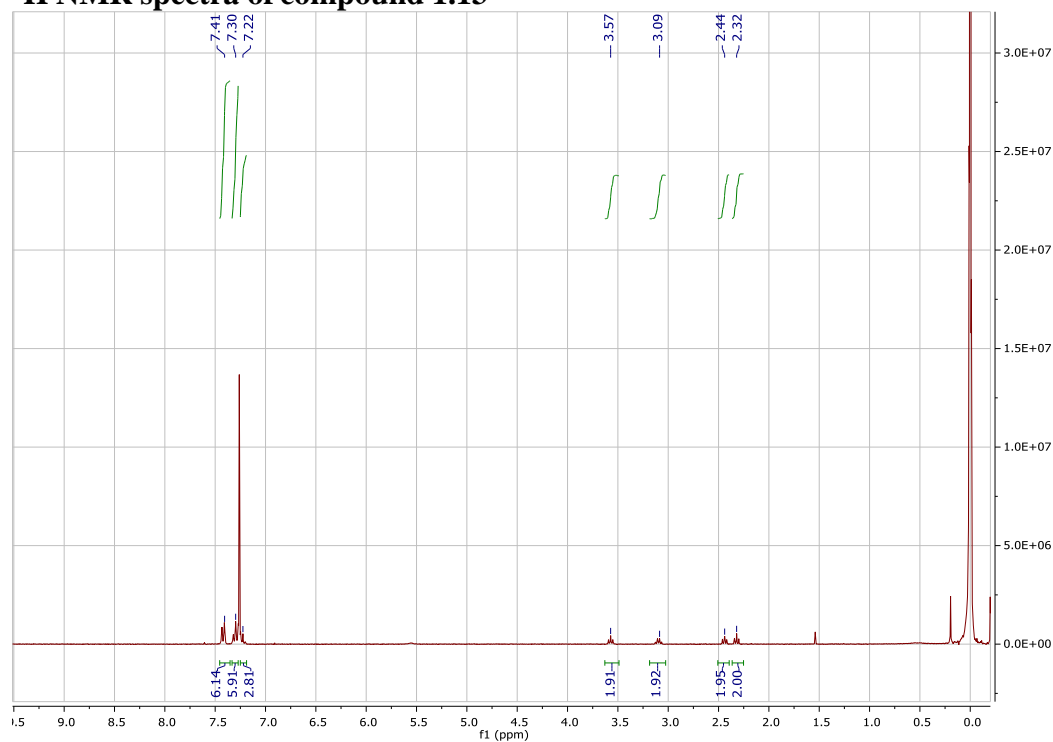
Gold nanoparticles were synthesized with dodecanethiol capping ligands using the Brust-Schiffrin “two-phase” method.<sup>7</sup> An aqueous solution of  $\text{HAuCl}_4 \cdot \text{H}_2\text{O}$  (0.10 g, 0.30 mmol) was mixed with tetraoctylammonium bromide (0.71 g, 1.31 mmol) in toluene. The solution was stirred vigorously until all of the gold was transferred into the organic layer. Dodecanethiol (0.055g, 0.27 mmol) was then added and stirred for 20 mins, at which point the solution turned clear. An aqueous solution of  $\text{NaBH}_4$  (0.12 g, 3.24 mmol) was slowly added and the resulting solution turned brown. The reaction was then stirred for 3 hrs at room temperature. The organic phase was then isolated and concentrated down to ~5 mL, which was then mixed with 200 mL of EtOH and kept at  $-18^\circ \text{C}$  for 4 hours. The dark brown precipitate was then filtered off and re-dissolved in 5 mL of toluene, which was then precipitated again using 100 mL EtOH. The suspension was then filtered and washed with copious amounts of EtOH to remove any free dodecane thiol, product was dried under vacuum overnight. Transmission electron microscopy validated the presence of AuNPs.

**Compound 1.21: Azide-AuNPs**

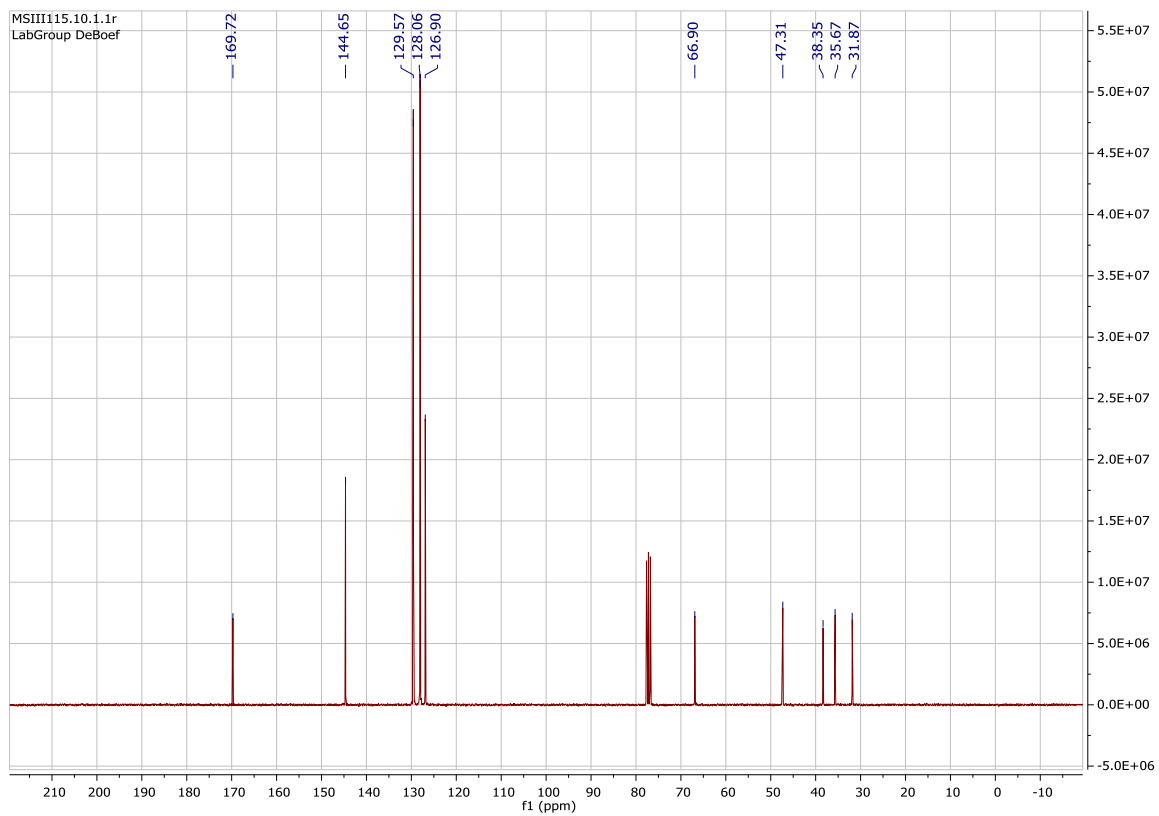
The 11-bomoundecylthioacetate (0.10 g, 0.32 mmol) was dissolved in 1 mL of ethanol. NaOH was added (0.1 mL) and reaction mixture was refluxed for 2 hrs. The reaction was then neutralized with 6 mL of 2 M HCl. The mixture was transferred to separatory funnel and then 10 mL of diethyl ether was added followed by the addition of with 5 mL of  $\text{H}_2\text{O}$ . The organic layer was washed with 5 mL of  $\text{H}_2\text{O}$ , isolated, dried of  $\text{MgSO}_4$  and then filter. The solvent was removed and product was left to dry under

vacuum overnight. The deprotected 11-bromoundecylthiol was then dissolved in DCM and added to AuNPs. AuNPs functionalized with 11-bromoundecylthiol (28 mg) were dissolved in DCM (6 mL) and added to a solution of sodium azide (70 mg) in DMSO (6 mL). The solution was stirred for 2 days at room temperature. An IR was taken to verify the presence of an azide and once complete water was added and the organic layer was isolated. The AuNPs were washed with ethanol and then dried under vacuum to yield AuNPs-N<sub>3</sub> (0.021 g). FTIR: 2094.06 cm<sup>-1</sup>

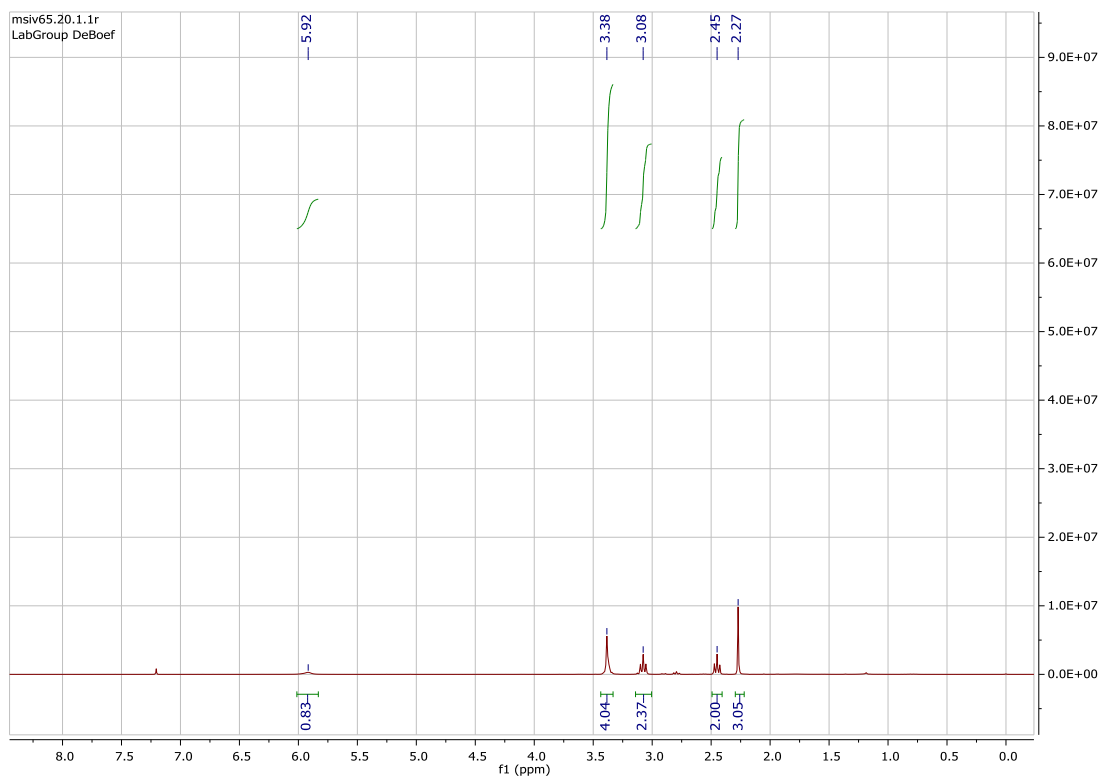
### <sup>1</sup>H NMR spectra of compound 1.13



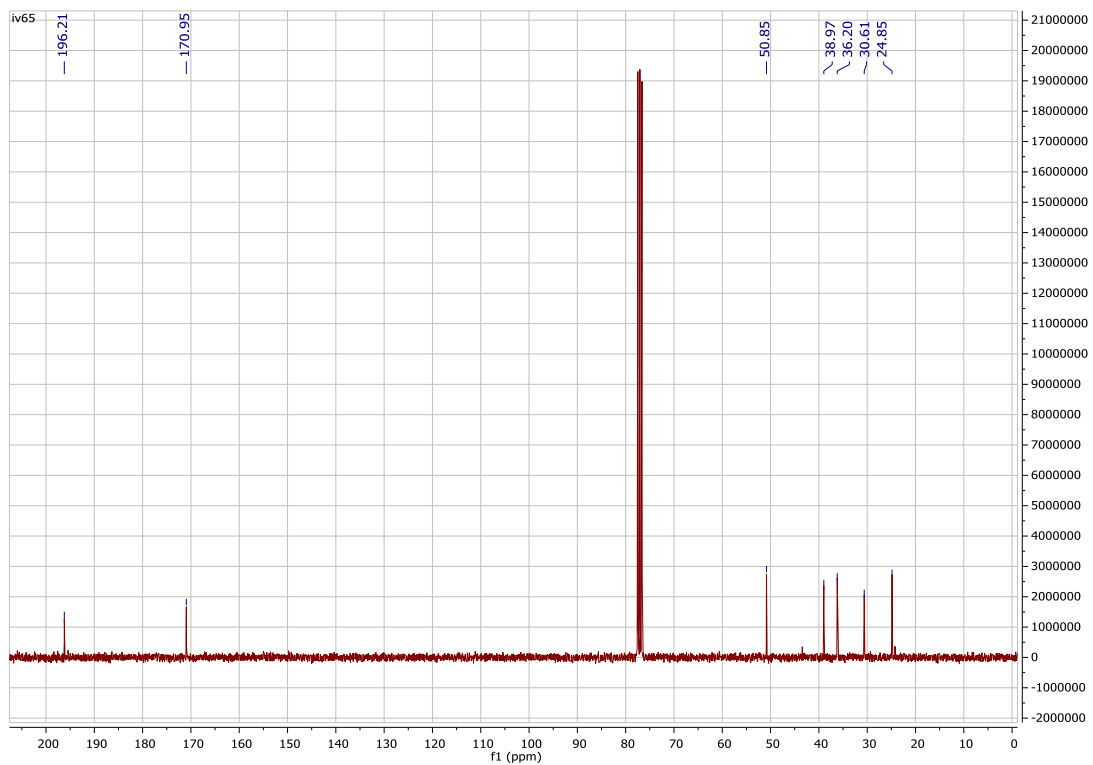
### <sup>13</sup>C NMR spectra of compound 1.13



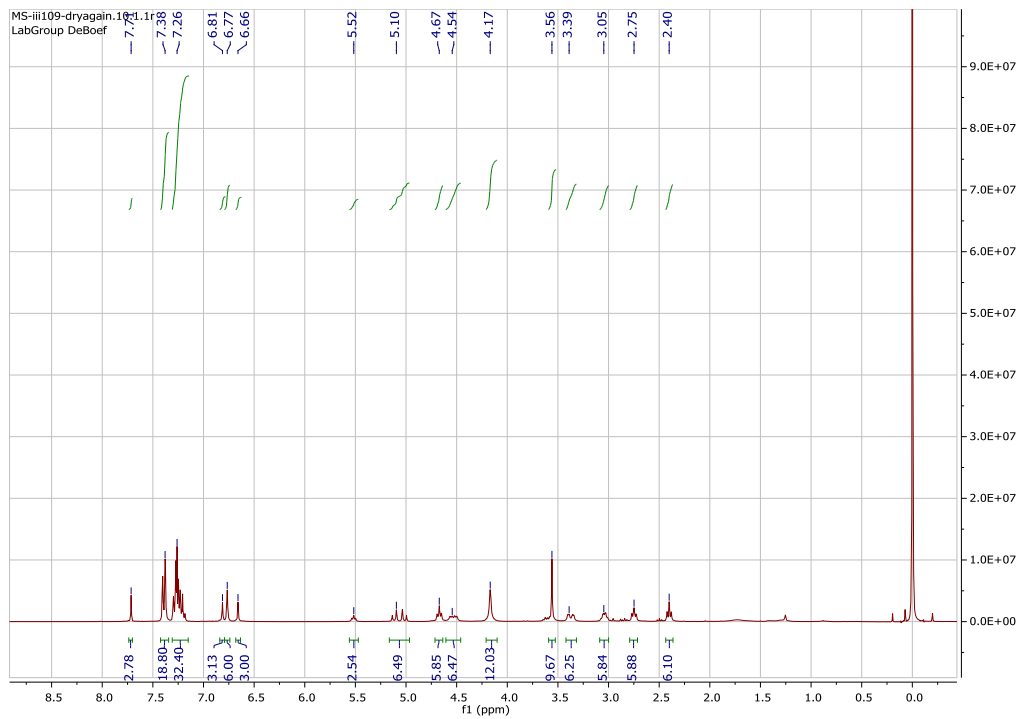
**$^{13}\text{C}$  NMR spectra of compound 1.16**



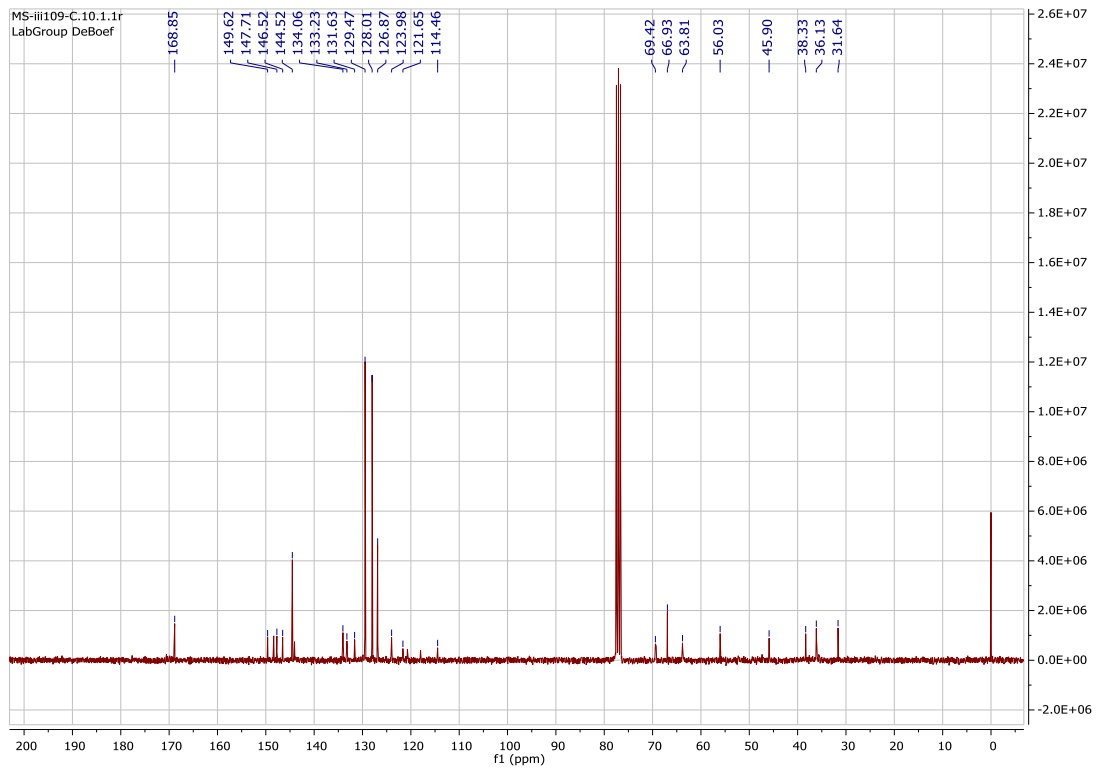
**$^{13}\text{C}$  NMR spectra of compound 1.16**



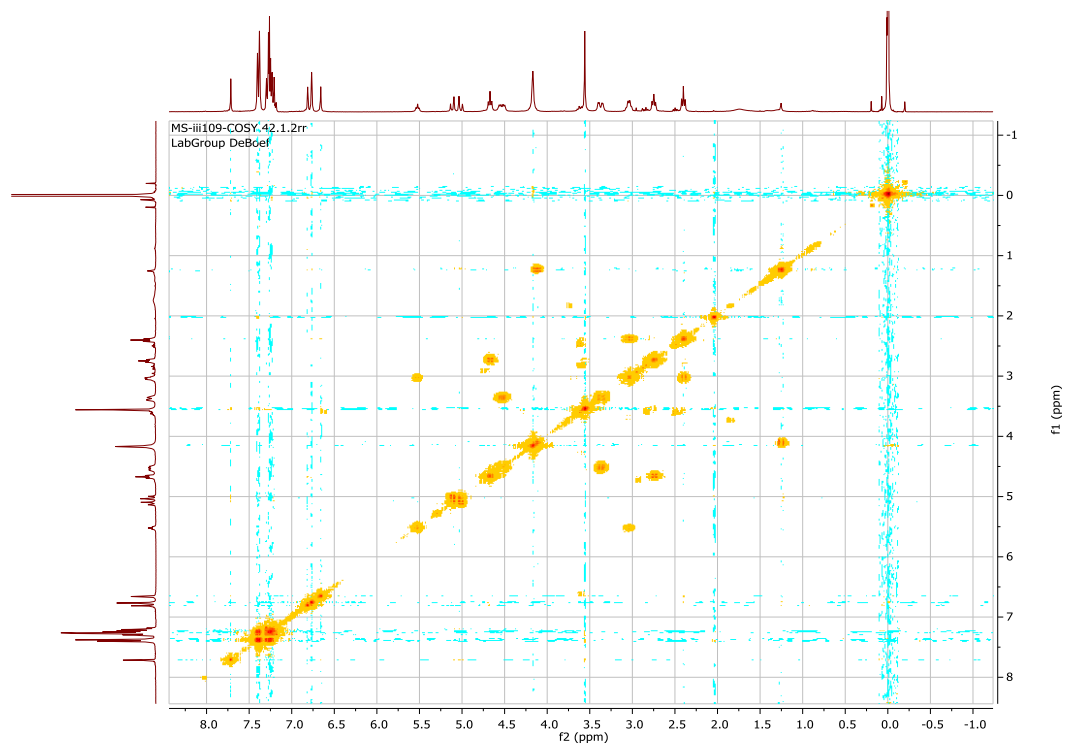
$^1\text{H}$  NMR spectra of compound 1.18



**<sup>13</sup>C NMR spectra of compound 1.18**

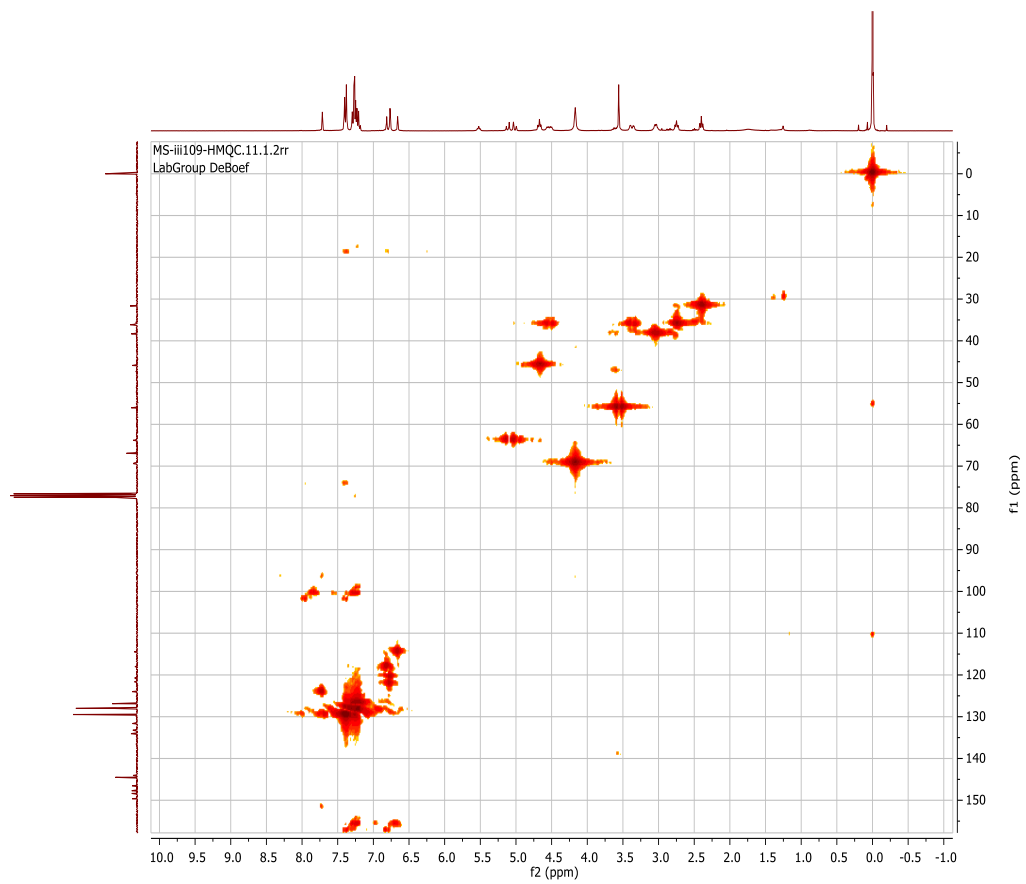


**COSY of 1.18**

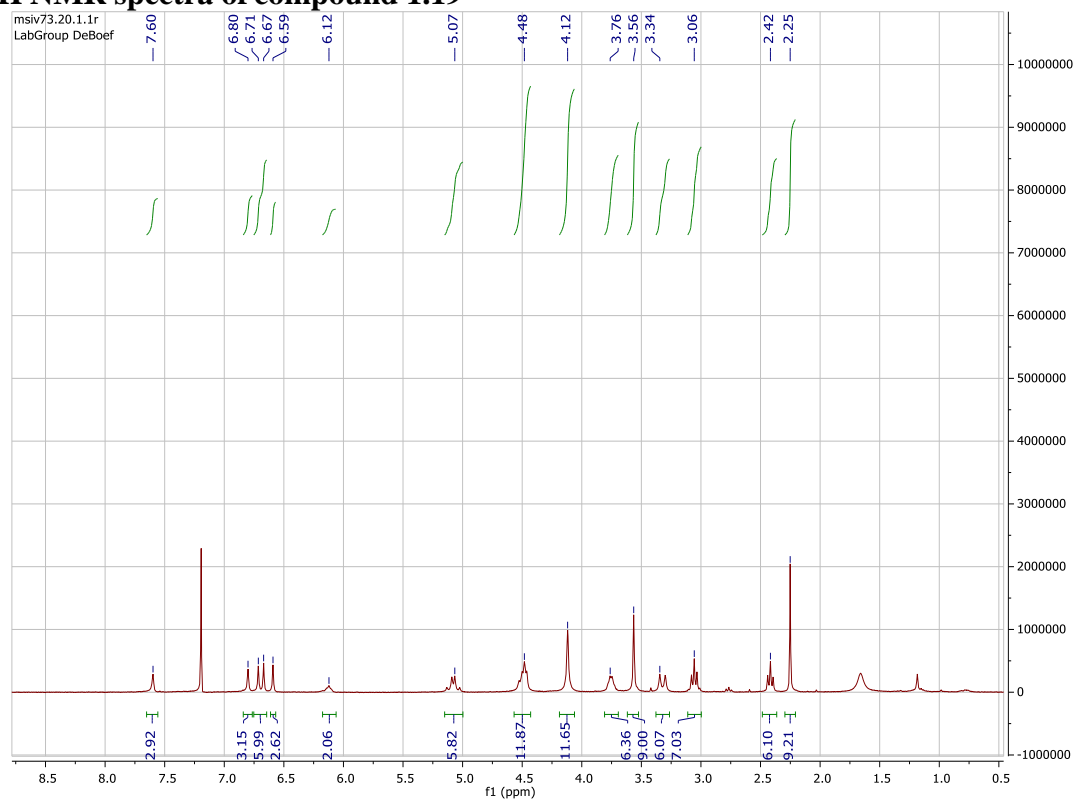


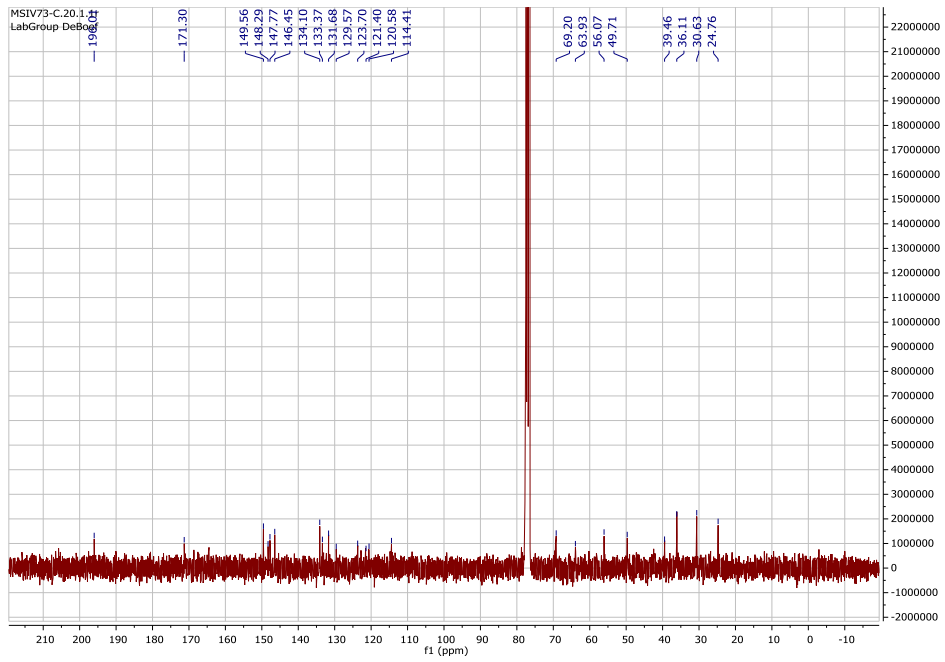
**HMQC of Compound 1.18**



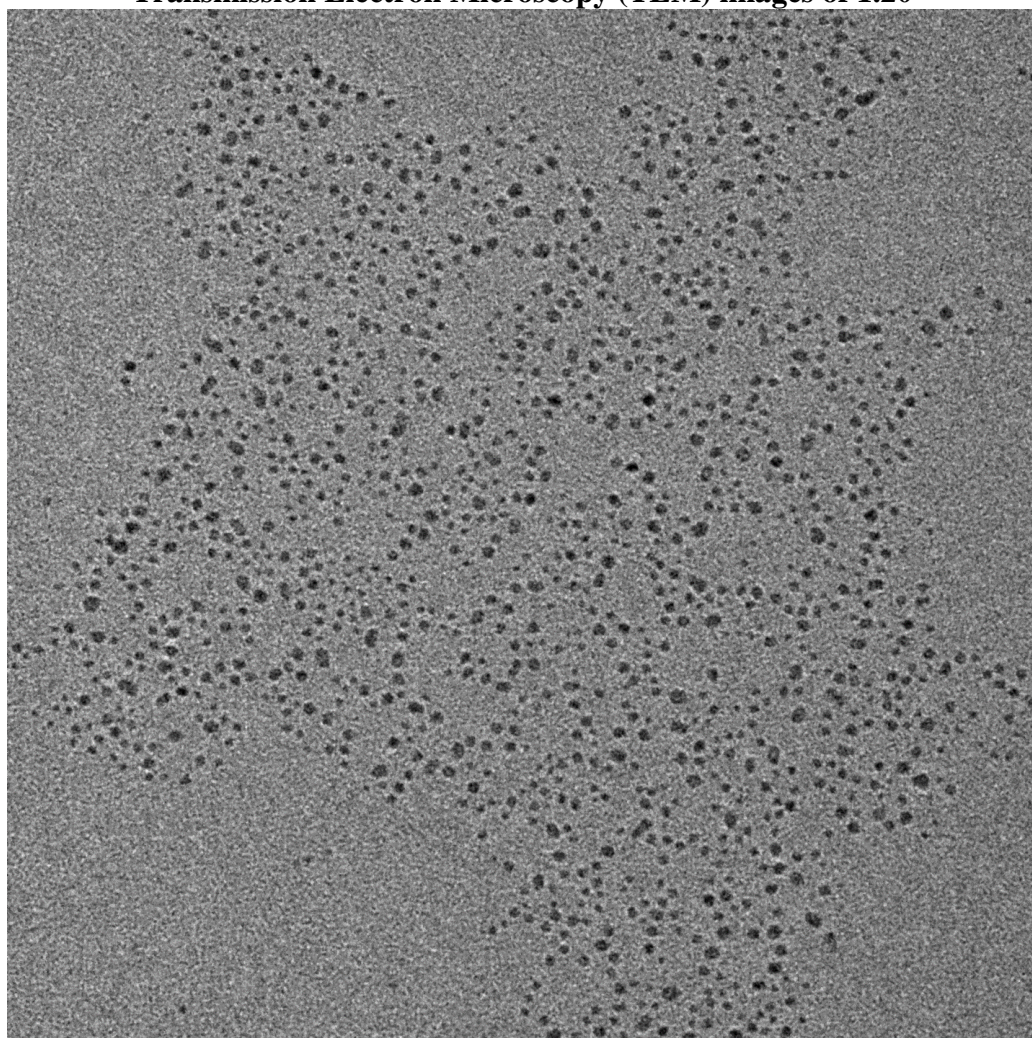


# <sup>1</sup>H NMR spectra of compound 1.19





**Transmission Electron Microscopy (TEM) images of 1.20**



aunp-14-02-06\_005

Print Mag: 737000x @ 7.0 in

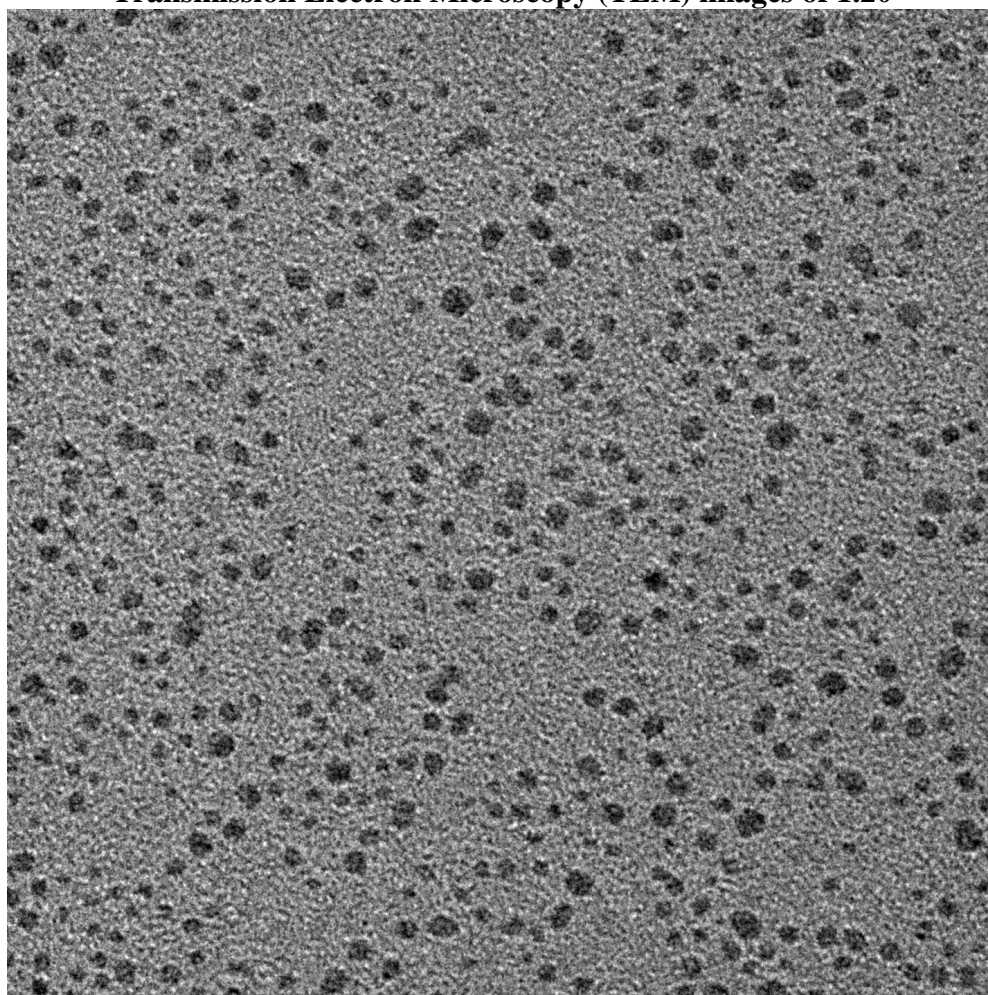
10:01:09 2/6/2014

20 nm

Direct Mag: 100000x

URI TEM

## Transmission Electron Microscopy (TEM) images of 1.20



aunp-14-02-06\_006

Print Mag: 1470000x @ 7.0 in

10:01:58 2/6/2014

20 nm

Direct Mag: 200000x

URI TEM

### References

1. Hill, P. A.; Wei, Q.; Eckenhoff, R. G.; Dmochowski, I. J., Thermodynamics of Xenon Binding to Cryptophane in Water and Human Plasma. *Journal of the American Chemical Society* **2007**, *129* (30), 9262-9263.

2. Ruggles, E. L.; Deker, P. B.; Hondal, R. J., Synthesis, redox properties, and conformational analysis of vicinal disulfide ring mimics. *Tetrahedron* **2009**, *65* (7), 1257-1267.
3. Shi, Z.; Cui, Y.-Z.; Huang, S.; Li, Z. a.; Luo, J.; Jen, A. K. Y., Dipolar Chromophore Facilitated Huisgen Cross-Linking Reactions for Highly Efficient and Thermally Stable Electrooptic Polymers. *ACS Macro Letters* **2012**, *1* (7), 793-796.
4. Lee, S.; Rosazza, J. P. N., First Total Synthesis of Mycothiol and Mycothiol Disulfide. *Organic Letters* **2004**, *6* (3), 365-368.
5. Mayer, T.; Maier, M. E., Design and Synthesis of a Tag-Free Chemical Probe for Photoaffinity Labeling. *European Journal of Organic Chemistry* **2007**, *2007* (28), 4711-4720.
6. Liang, L.; Ruiz, J.; Astruc, D., The Efficient Copper(I) (Hexabenzyl)tren Catalyst and Dendritic Analogues for Green “Click” Reactions between Azides and Alkynes in Organic Solvent and in Water: Positive Dendritic Effects and Monometallic Mechanism. *Advanced Synthesis & Catalysis* **2011**, *353* (18), 3434-3450.
7. Brust, M.; Walker, M.; Bethell, D.; Schiffrin, D. J.; Whyman, R., Synthesis of thiol-derivatised gold nanoparticles in a two-phase Liquid-Liquid system. *Journal of the Chemical Society, Chemical Communications* **1994**, (7), 801-802.

**MANUSCRIPT 2**

Will be submitted to *Tetrahedron Lett.* November, 2014

Vanadium Catalyzed Oxidative Coupling of  $sp^3$  C-H Bonds to Heteroarenes

Marissa Simone, Ashley L. Porter, Brenton DeBoef\*

Corresponding author:

Prof. Brenton DeBoef

Department of Chemistry,

University of Rhode Island,

Kingston, Rhode Island 02881

bdeboef@chm.uri.edu

## MANUSCRIPT 2

### Vanadium Catalyzed Oxidative Coupling of $sp^3$ C-H Bonds to Heteroarenes

#### Abstract

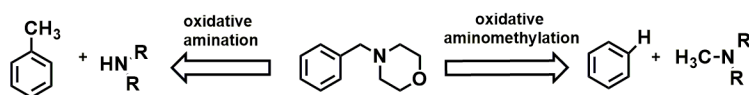
The vanadium-catalyzed oxidative coupling of substituted 2-phenyl-imidazo[1,2-a]pyridines to N-methylmorpholine which acts as the sacrificial oxidant has been achieved. This reaction was applied to various 2-phenyl-imidazo[1,2-a]pyridines substrates resulting in yields as high as 90%.

#### Introduction

Incorporating new carbon-carbon and carbon-nitrogen bonds into organic molecules is an apparent need in today's chemical industry. There have been many recent advances in this field, most using metal catalysis, however most require pre-functionalization steps and have poor atom economy.<sup>1</sup> The ability to oxidatively couple two carbon hydrogen bonds (or carbon-hydrogen and nitrogen-hydrogen) to form a carbon-carbon bond (or carbon-nitrogen bond) with no pre-functionalization would be ideal.<sup>2</sup> Incorporating C-N bonds via cross dehydrogenative coupling can be accomplished through direct oxidative amination or oxidative aminomethylation. The direct formation of C-N bonds under oxidative conditions has been achieved through various methods.<sup>3</sup> Aminomethylation is an alternative and convenient way to incorporate C-N bonds (**Scheme 1**). The less common oxidative aminomethylation is shown by Uang et al., who achieved oxidative aminomethylation of naphthalenes.<sup>5</sup> Another example of aminomethylation is shown by Mitchel et al., who developed a method for installing N-methylmorpholine on imidazopyridines structures, a precursor to an active



pharmaceutical ingredient that could serve as a treatment of several myeloproliferative disorders.<sup>10</sup>



**Scheme 1- Amination vs Aminomethylation**

There are numerous methods to oxidatively couple two  $sp^2$  hybridized carbons in high yields.<sup>2</sup> The coupling of an  $sp^3$  to an  $sp^2$  hybridized carbon is much less common due to the less reactive nature of  $sp^3$  hybridized C–H bonds compared to that of  $sp^2$  C–H bonds.<sup>4</sup> In order to achieve  $sp^3$  C–H bond activation, reactive directing groups are often needed.<sup>3</sup> Another difficulty is the potential for  $\beta$ -hydride elimination after C–H activation of  $sp^3$  bonds.<sup>4</sup> The oxidative coupling of a  $sp^3$  C–H bond to a  $sp^2$  C–H bond has received little attention,<sup>4,5,6,7</sup> so there is still a great need to invent new ways of oxidatively coupling  $sp^3$ - $sp^2$  carbon bonds in an efficient and green way.

Pharmaceuticals such as necopidem, saripidem, and zolpidem contain a substituted imidazo[1,2-a]pyridines back bone (**Figure 1**).<sup>8</sup> Providing a way to oxidatively couple the 3 position of 2-phenyl-imidazo[1,2-a]pyridine with alkyl derivatives would be a useful tool to have when synthesizing pharmaceuticals. This paper proposes a vanadium catalyzed oxidative coupling of imidazopyridines with N-methylmorpholine oxide which serves as both  $sp^3$  hybridized coupling partner and the sacrificial oxidant. Using these conditions we were able to perform oxidative aminomethylation of imidazopyridines.

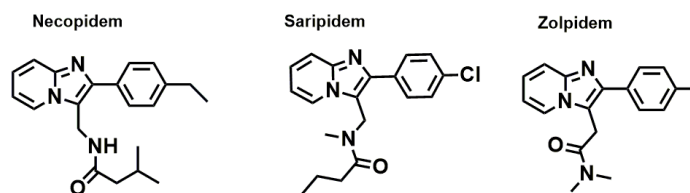
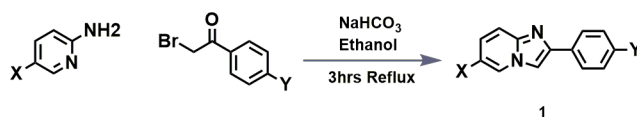


**Figure 1: Pharmaceuticals with imidazo[1,2-a]pyridines backbones**

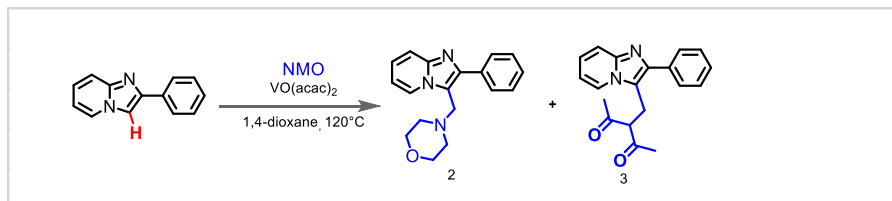
The synthesis of the starting material is accomplished in one step via an imminium formation followed by a nucleophilic cyclization (**Scheme 2**).<sup>9</sup> The nature of the substituents on pyridine or bromoacetophenone did not greatly affect the starting material yields **1**.



**Scheme 2: Synthesis of Starting Material**

## Results and Discussion

In order to achieve optimum conditions we screened solvent, catalyst, catalyst loading, time, and equivalents of NMO. Ethanol, toluene, and tetrahydrofuran were initially tested as alternative solvents (**Table 1** entries **4**, **5**, and **6**). Nevertheless, none had comparable yields to methylene chloride. The mole percent of vanadium (III) acetylacetonate, VO(acac)<sub>2</sub> was varied from 25% to 10%, showing that lower catalyst loading provided minimal impurities. To ensure that VO(acac)<sub>2</sub> was the ideal catalyst to use we tested V<sub>2</sub>O<sub>5</sub> (entries **9,10,16** and **17**). While it eliminated the formation of the impurity, **3**, it required longer reaction times and low amounts of NMO (entry 16), which still did not result in comparable yields to when VO(acac)<sub>2</sub> was used under the same conditions (entry 14). The best yield was achieved using 10% of



entry	VO(acac) <sub>2</sub>	NMO	Solvent	Time (hrs)	Product Yield <sup>a</sup>	3
	Mol%					
1	25	10	DCM	18	59	3.7
2	10	10	DCM	18	68	0.3
3	20	10	DCM	18	62	2.7
4	20	10	Ethanol	18	33	1.5
5	20	10	Toluene	18	30	28.5
6	20	10	THF	18	57	1.3
7	20	10	DCM	18	68	2.2
8	20	5	DCM	18	68	10.7
9	20 <sup>b</sup>	5	DCM	5	58	15
10	20 <sup>b</sup>	5	DCM	4	31	14.9
11	10	5	DCM	18	72	4.6
12	10	5	DCM	6	88	5.8
13	20	5	Dioxane	12	80 <sup>c</sup>	0
14	20	3	DCM	18	69	18.7
15	20	3	DCM	4	incomplete conversion	--
16	20 <sup>b</sup>	3	DCM	18	57	0
17	20 <sup>b</sup>	1.2	DCM	18	36	5
18	20	1	DCM	18	52	34.2

(a) Product yield determined by NMR (b) V<sub>2</sub>O<sub>5</sub> used as catalyst (c) Actual yield

**Table 1- Optimization of the Reaction Conditions**

(VO(acac)<sub>2</sub>), 5 equivalents of NMO for 6 hours in methylene chloride (entry **12**). However by changing the solvent from methylene chloride to 1,4 - dioxane and increasing the catalyst loading VO(acac)<sub>2</sub>, we were able to avoid any of **3** from forming and achieve an 80% yield. Performing a GC time study gave further insight into when the reaction would produce the least impurity (see **Chart 1**). The starting material was always present in small amounts as was **3**. We stopped the reaction at 12 hours despite

the presence of starting material to avoid product decomposition. As such we decided to perform our substrate scope using entry **13** as our optimized conditions.

Performing this reaction using substrates with electron withdrawing groups on the para position of the phenyl substituent resulted in less favorable yields or did not react. While electron donating groups in the para position lead to higher yields. Looking at the substrate scope (**table 2**) entry **10** has a nitro substituent in the para position resulted in no product while entry **8** with an ether substituent in the same position gave us an 84% yield. The addition of a second electron donating substituent led to lower yields than only one electron donating group (**4**). Changing the position of the methyl group at C6 (entry **6**) as to C8 (entry **7**) gave a slightly higher yield. Yields varied with different halogens substituted at the phenyl para position. For instance, a chlorine substituted phenyl ring had a much higher yield than when a bromine or fluorine was substituted in the same position. The addition of a methyl group at C7 on the Br para substituted ring gave a lower yield than fluorine. Methyl groups at the C6 position for both fluorine and chlorine substituted rings had high yields.

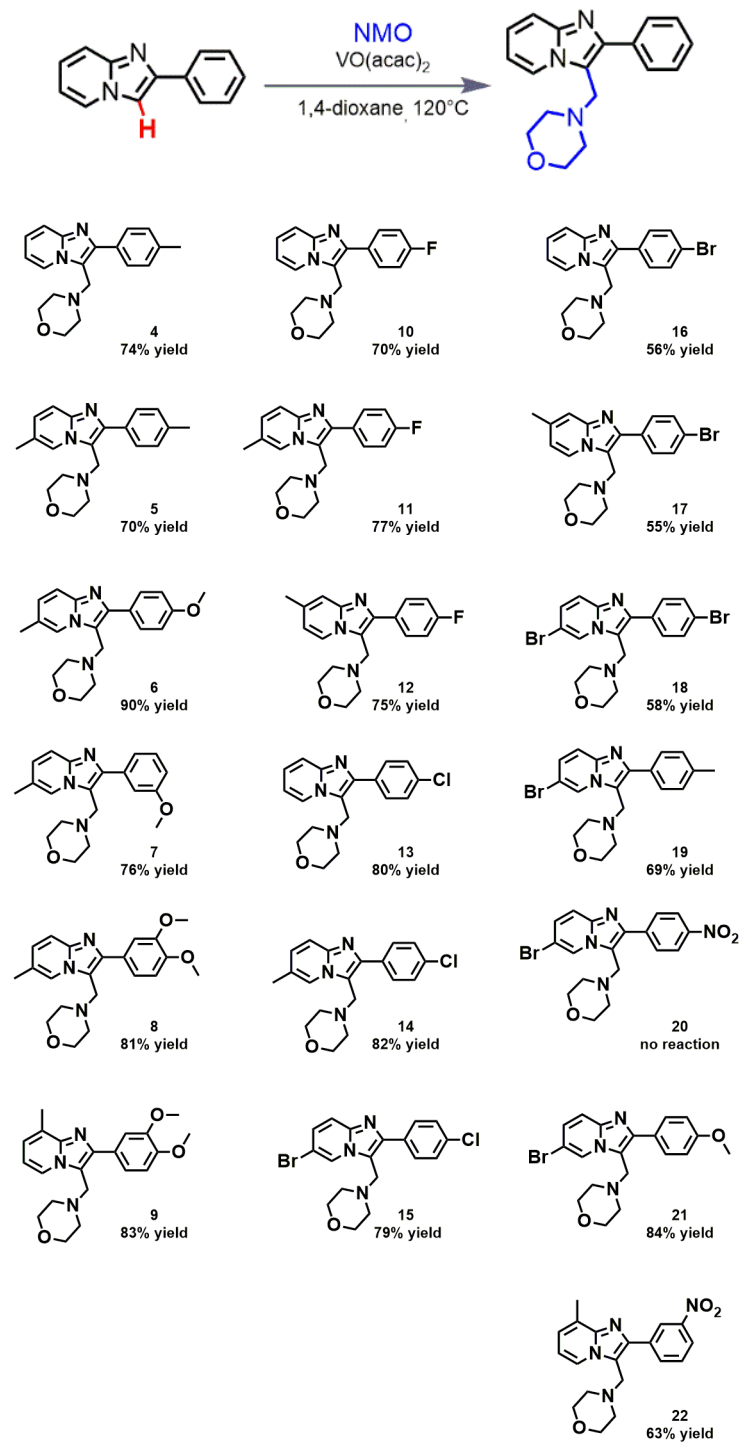
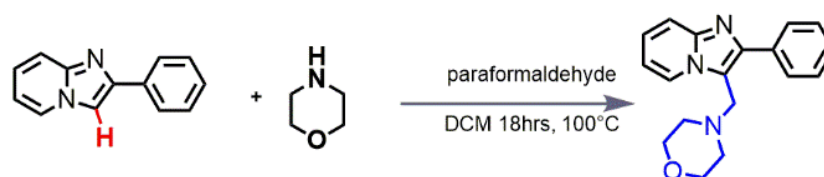


**Table 2: Substrate Scope**

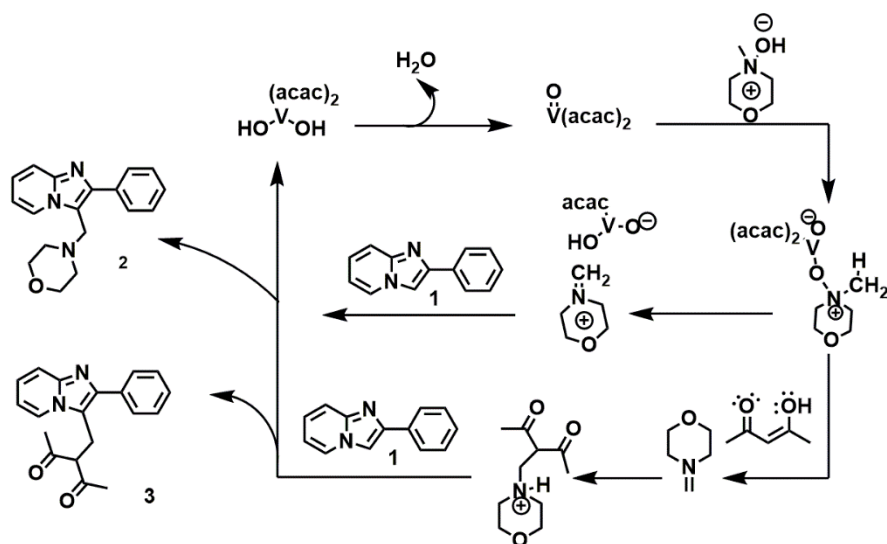
Previous studies of vanadium oxidative coupling of structures similar to **1** propose a radical mechanism,<sup>10</sup> while others theorize product is formed by way of a

Mannich-type reaction.<sup>5</sup> We propose a Mannich type mechanism is responsible for the formation of our product (**Scheme 4**). This was determined by running a Mannich reaction using **1**, formaldehyde, and morpholine to make the iminium in situ resulting in yields up to 98% (**scheme 3**). Running our normal reaction conditions in the presence of TEMPO, a radical inhibitor, did not prevent product from forming further proving this reaction a Mannich-type mechanism is responsible.



**Scheme 3-Pure Mannich Conditions**

As such we believe the product is formed by the following mechanism (**scheme 4**). The N- methyl morpholine oxidizes the VO(acac)<sub>2</sub> catalyst resulting in the formation of the iminium ion. The vanadium species extracts a proton from **1** which then attacks the iminium ion forming our product **2**. The elimination of water from vanadium regenerates the catalyst. We believe the main impurity is formed when the iminium ion reacts with one of the ligands from the vanadium catalyst.



Scheme 4- Proposed mechanism of product and impurity

## Conclusions

The vanadium catalyzed oxidative coupling of substituted imidazole pyridines to N-methylmorpholine was achieved in yields up to 90%. Despite the ability to produce this product using true Mannich conditions we believe this to be a useful method to demonstrate oxidative coupling.

## References

1. For reviews of C–H activation, see: (a) Lyons, T.W.; Sanford, M.S. *Chem.Rev.* **2010**, 110, 1147 (b) Shilov, A.E., Shul'pin, G.B. *Chem.Rev.* **1997**, 97, 2879 (c) Ritleng, V., Sirlin, C., Pfeffer, M. *Chem. Rev.* **2002**, 102, 1731. (d) Kantak, A., DeBoef, B., *Science of Synthesis*; Thieme: New York, **2013**, Vol 3, p 585
2. For examples of oxidative cross-dehydrogenative coupling see: (a) Yeung, C.S.; Dong, V.M. *Chem. Rev.* **2011**, 111, 1215. (b) Qin, X.; Feng, B.; Dong, J.; Li, X.; Xue, Y.; Lan, J.; You, J. *J. Org. Chem.* **2012**, 77, 7677. (c) Zhang, C., Zong, X., Zhang, L., Jiao, Ning. *Org. Lett.* **2012**, 14, 3280
3. For examples of oxidative aminanition: *Org. Lett.*, **2011**, 13 (3), pp 522–525
4. Stowers, K. J.; Fortner, K. C.; Sanford, M. S. *J. Am. Chem. Soc.* **2011**, 133, 6541.
5. Wasa, M.; Engle, K. M.; Yu, J. Q. *J. Am. Chem. Soc.* **2010**, 132, 3680
6. Hwang, D. R.; Uang, B. J. *Org. Lett.* **2002**, 4, 463.
7. Guo, X.; Li, C. *Org. Lett.* **2011**, 13, 4977.
8. Yang, H.; Liping Y.; Luan L.; Fan Z.; Huajie L.; Bing, Y. *Catal. Commun.* **2012**, 26, 11.
9. Zhu, D. J.; Chen, J. X.; Liu, M. C.; Ding, J. C.; We, H. Y. *J.Braz.Chm. Soc.* **2009** 3, 482
10. Mitchell, D.; Cole, K.P.; Pollock, P.M.; Coppert, D.M.; Burkholder, T.P.; Clayton, J.R.; *Org. Process Res. Dev.* **2012**, 16, 70.



## **Supporting Information**

Vanadium Catalyzed Oxidative Coupling of  $sp^3$  C-H Bonds to Heteroarenes

Ashley Porter, Marissa Simone, and Brenton DeBoef

University of Rhode Island, Department of Chemistry, 51 Lower College Road,

Kingston, RI 02881

## Experimental Section

### Reagents

All substrates were purchased from Sigma Aldrich and Fisher Scientific. Flash chromatography was performed using Teledyne ISCO CombiFlashRf Apparatus using RediSep Rf Silica gel (60 Angstroms, 40-60 microns).

### Instrumentation

GC/MS analysis was carried out on an Agilent Technologies 6890 GC system fixed with a 5973 mass selective detector]. NMR spectra were acquired with a Bruker Avance III 300 MHz spectrometer.

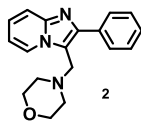
**General Synthesis of 2-phenyl- Imidazo[ 1,2-a] pyridines:**

2-amino pyridine (1.3 g 13.8 mmol), 1-bromoacetophenone (2.19 g, 11.1 mmol), sodium bicarbonate (1.45 g, 17.25 mmol) and ethanol (9 ml) were added to a flask. A stir bar was added and the reaction was stirred at 60°C for 4hrs. The reaction was monitored by TLC at a 50:50 ethyl acetate: hexanes solvent system. After reaction was completed, the ethanol was rotavapped off, and 50mL of water was added in portions to dissolve the solid. The water was then extracted with two 50mL portions of ethyl acetate and dried with sodium sulfate. The filtrate was rotavapped off. A column was ran (80 g column on a gradient) to yield 1.66 g (78%) of product. All spectral information matched literature values.<sup>1</sup>

**Representative Procedure for Synthesis of substituted imidazole pyridines with N- methylmorpholene**

Imidazo[1,2-a]pyridine (1 mmol), NMO (5 mmol), VO(acac)<sub>2</sub> (20 mol%), were dissolved in 1,4-dioxane (4 mL), and refluxed for 12 hrs. Upon completion the reaction was evaporated and diluted with water (10mL) and extracted with EtOAc (2x10mL). Organic layers were dried of Na<sub>2</sub>SO<sub>4</sub> and concentrated. Purified by column chromatography using 4/1 EtOAc:Hex.

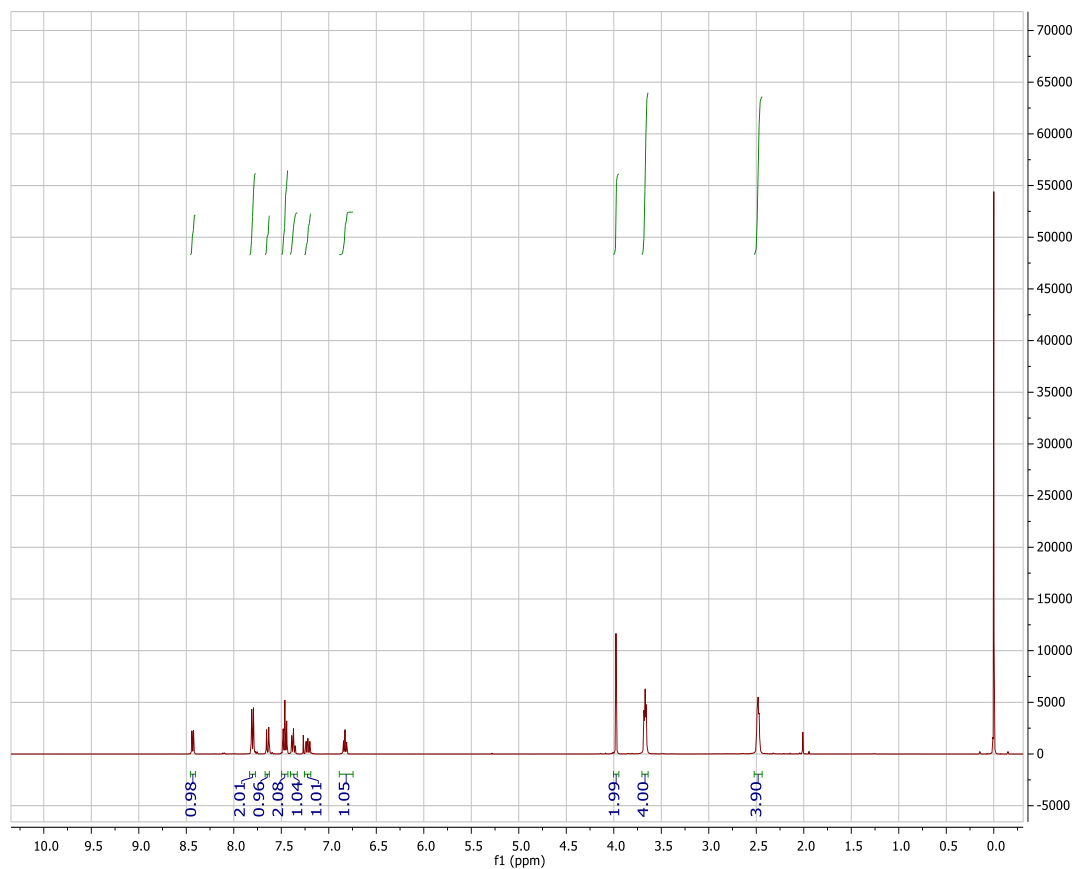
**Characterization of Compounds:**  
**Characterization of Compound 2**

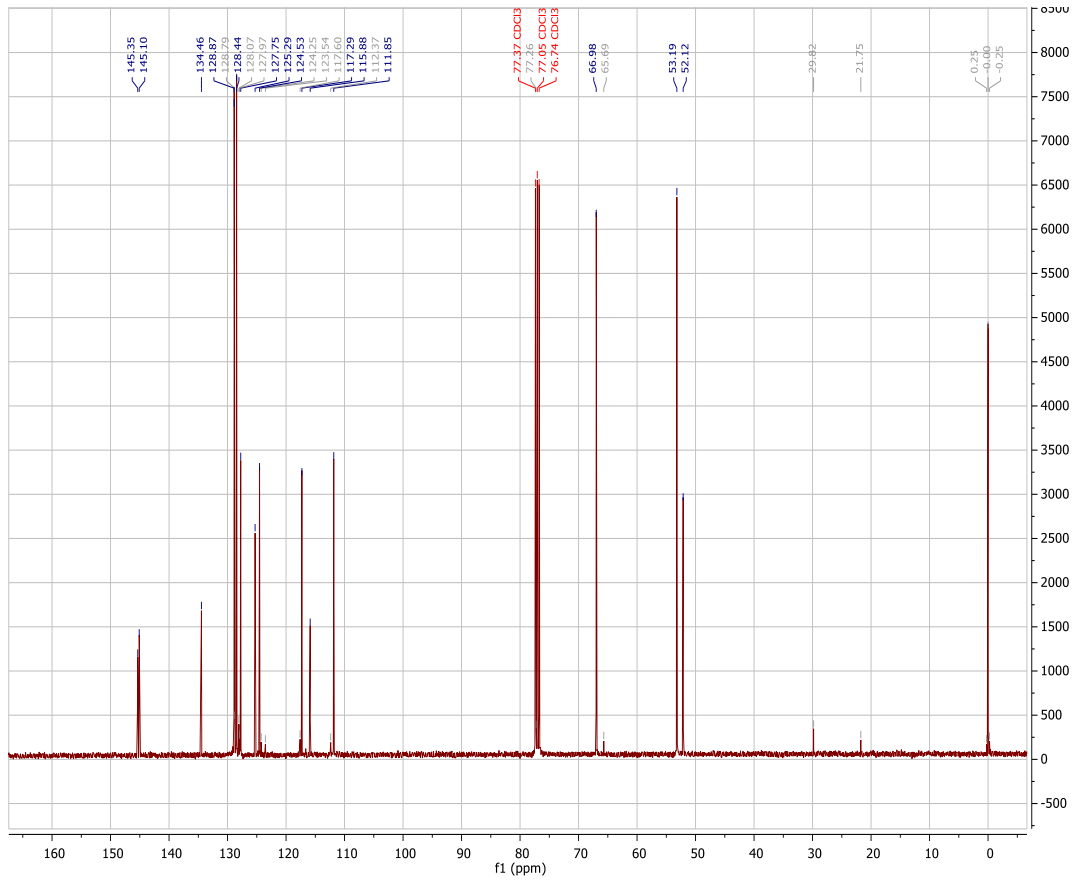


**<sup>1</sup>H NMR (300 MHz, CDCl<sub>3</sub>):** δ 8.43 (dd), 7.80 (m), 7.64(dt), 7.46(m), 7.38 (m), 7.22 (ddd), 3.98 (s), 3.67(t), 2.48 (t)

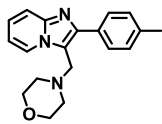
**<sup>13</sup>C NMR (101 MHz, CDCl<sub>3</sub>):** δ 145.35, 145.10, 134.46, 128.87, 128.44, 127.74, 125.29, 124.53, 117.29, 115.88, 111.85, 66.98, 53.19, 52.12.

**LRMS EI (m/z):** [M<sup>+</sup>] calc'd for C<sub>18</sub>H<sub>19</sub>N<sub>3</sub>O 293.15, observed 293.10





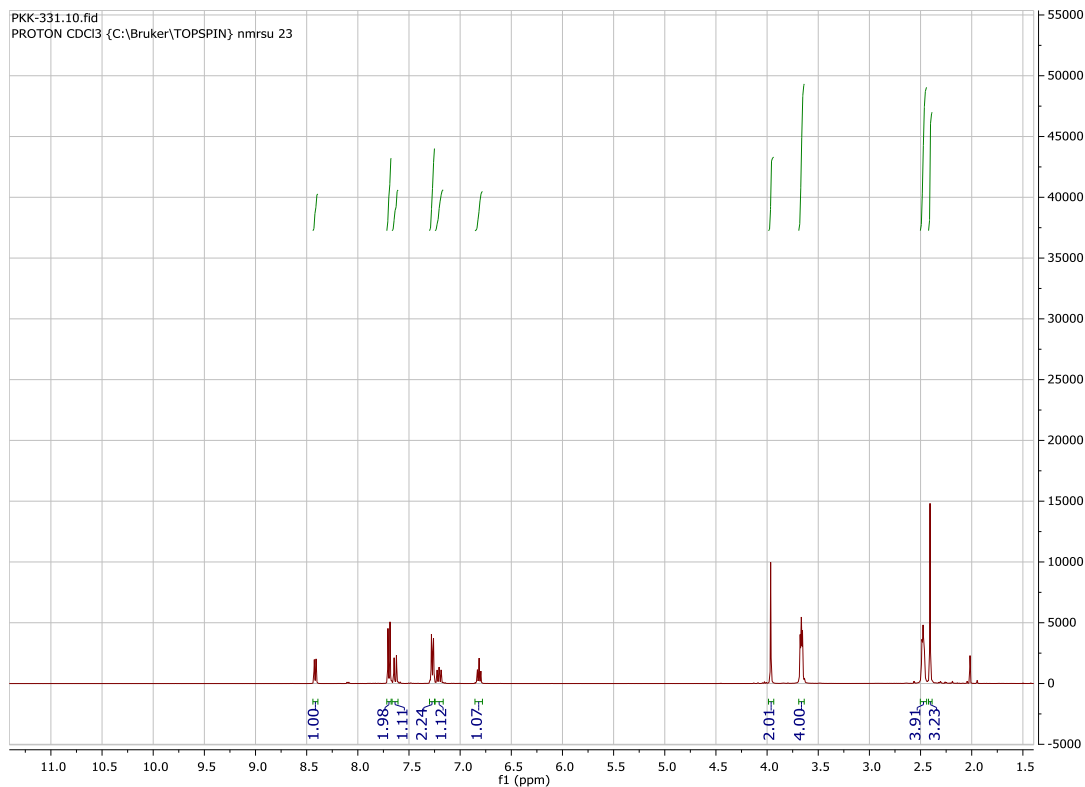
**Spectroscopic Data for Novel Compounds in Table 3:  
Characterization of Compound 3.4**

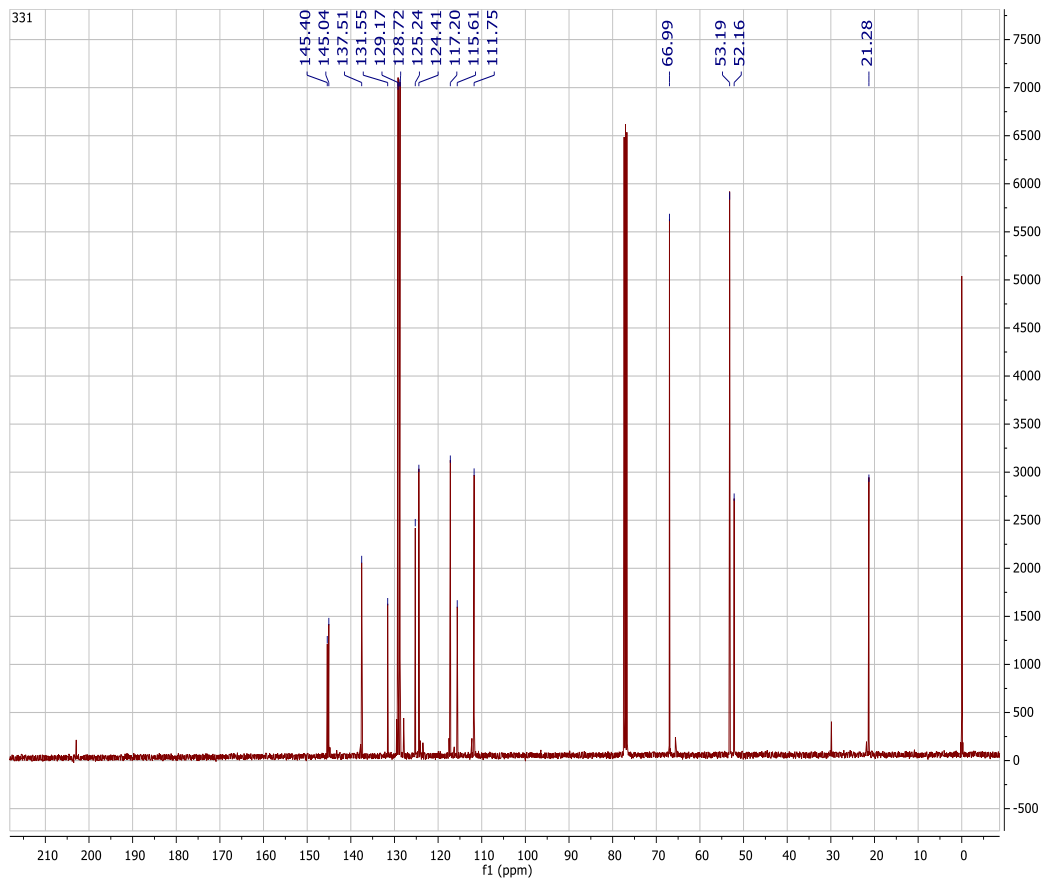


**<sup>1</sup>H NMR (400 MHz, CDCl<sub>3</sub>):** δ 8.42 (d, J = 6.9 Hz, 1H) 7.70 (d, J = 8.39 Hz, 2H), 7.63 (d, J = 9.2 Hz, 1H), 7.27 (d, J = 7.9 Hz, 2H), 7.24 – 7.17 (m, 1H), 6.82 (t, J = 6.4 Hz, 1H), 3.96 (s, 2H), 3.67 (t, J = 4.6 Hz, 4H), 2.48 (t, J = 4.6 Hz, 4H), 2.41 (s, 3H)

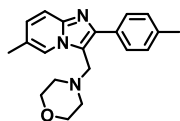
**<sup>13</sup>C NMR (101 MHz, CDCl<sub>3</sub>):** δ 145.40, 145.04, 137.51, 131.55, 129.17, 128.17, 125.24, 124.41, 117.20, 115.61, 111.75, 66.99, 53.19, 52.16, 21.28.

**LRMS EI (m/z):** [M<sup>+</sup>] calc'd for C<sub>19</sub>H<sub>21</sub>N<sub>3</sub>O 307.17, observed 307.20





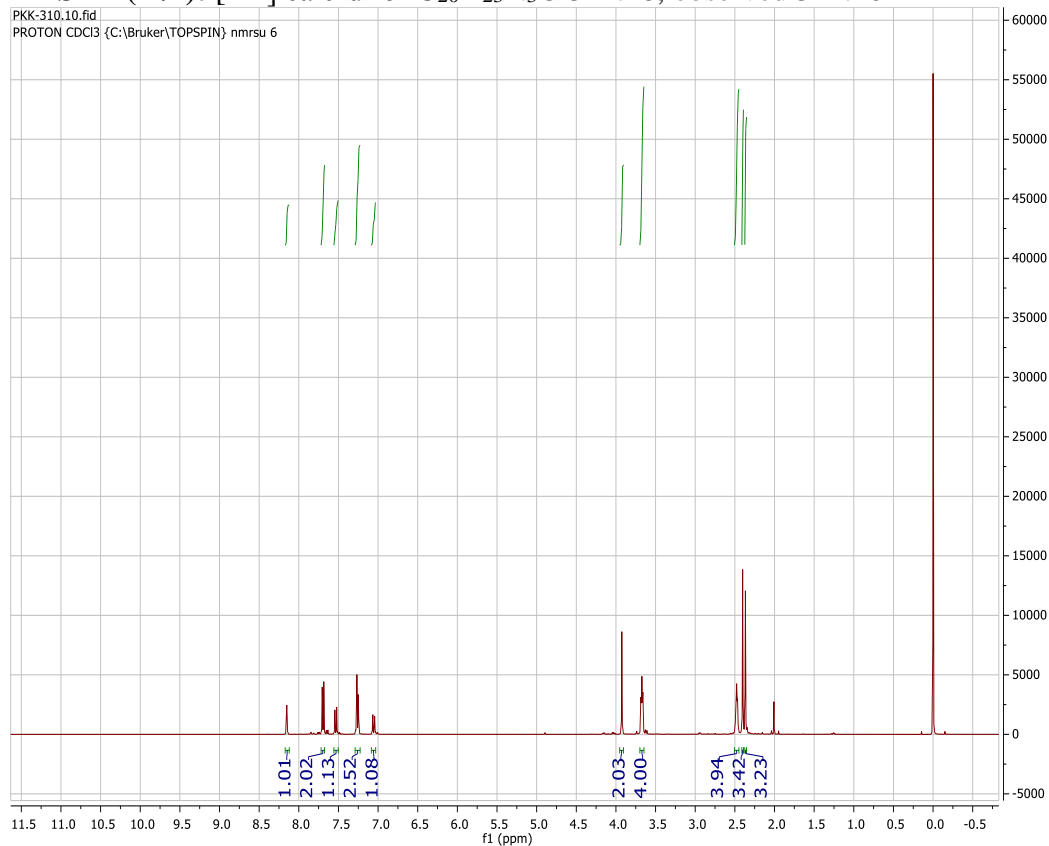
### Characterization of Compound 3.5



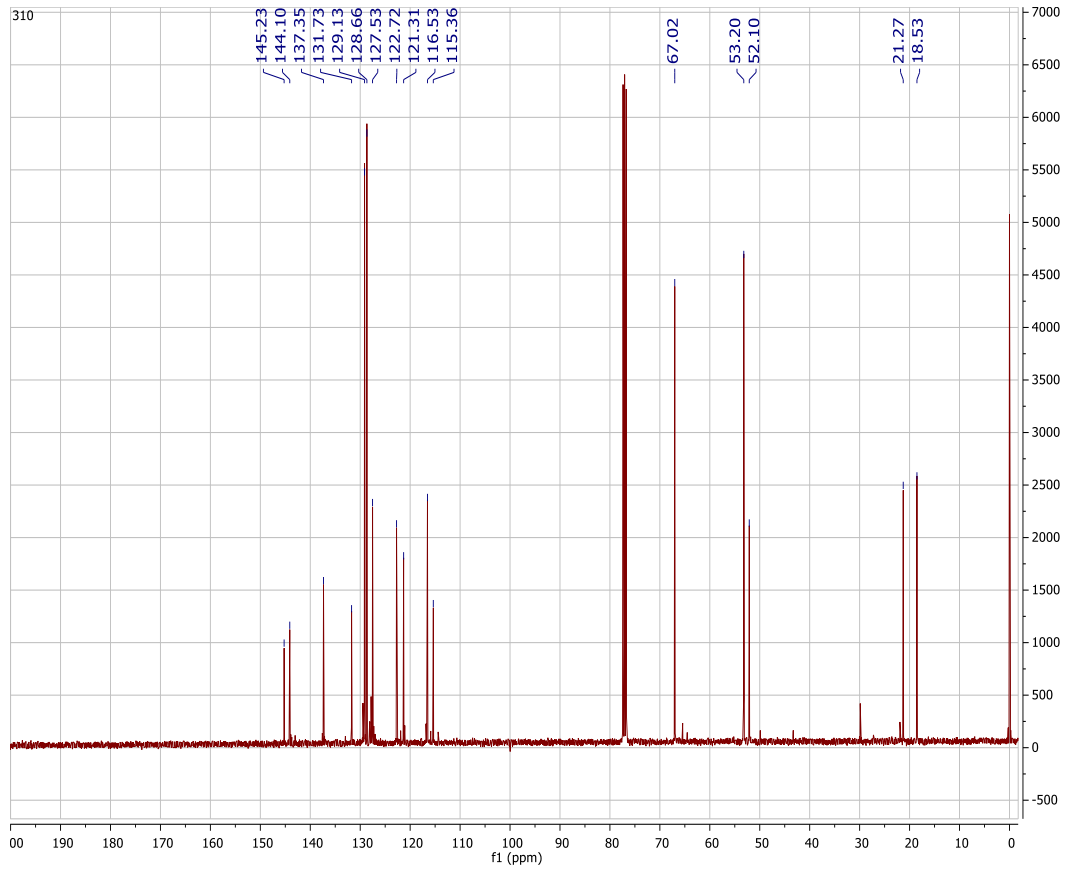
**<sup>1</sup>H NMR (400 MHz, CDCl<sub>3</sub>):** δ 8.51 (s, 1H), 7.69 (d, J = 8.0, 2H), 7.53 (d, J = 9.0, 1H), 7.26 (d, J = 7.4, 2H), 7.06 (d, J = 9.3, 1H), 3.93 (s, 2H), 3.67 (t, J = 4.4, 4H), 2.48 (t, J = 4.4, 4H), 2.40 (s, 3H), 2.37 (s, 3H)

**<sup>13</sup>C NMR (101 MHz, CDCl<sub>3</sub>):** 145.23, 144.10, 137.35, 131.73, 129.13, 128.66, 127.53, 122.72, 121.31, 116.53, 115.36, 67.02, 53.20, 52.10, 21.27, 18.53.

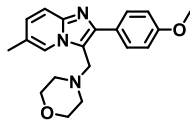
**LRMS EI (m/z):** [M<sup>+</sup>] calc'd for C<sub>20</sub>H<sub>23</sub>N<sub>3</sub>O 321.18, observed 321.20







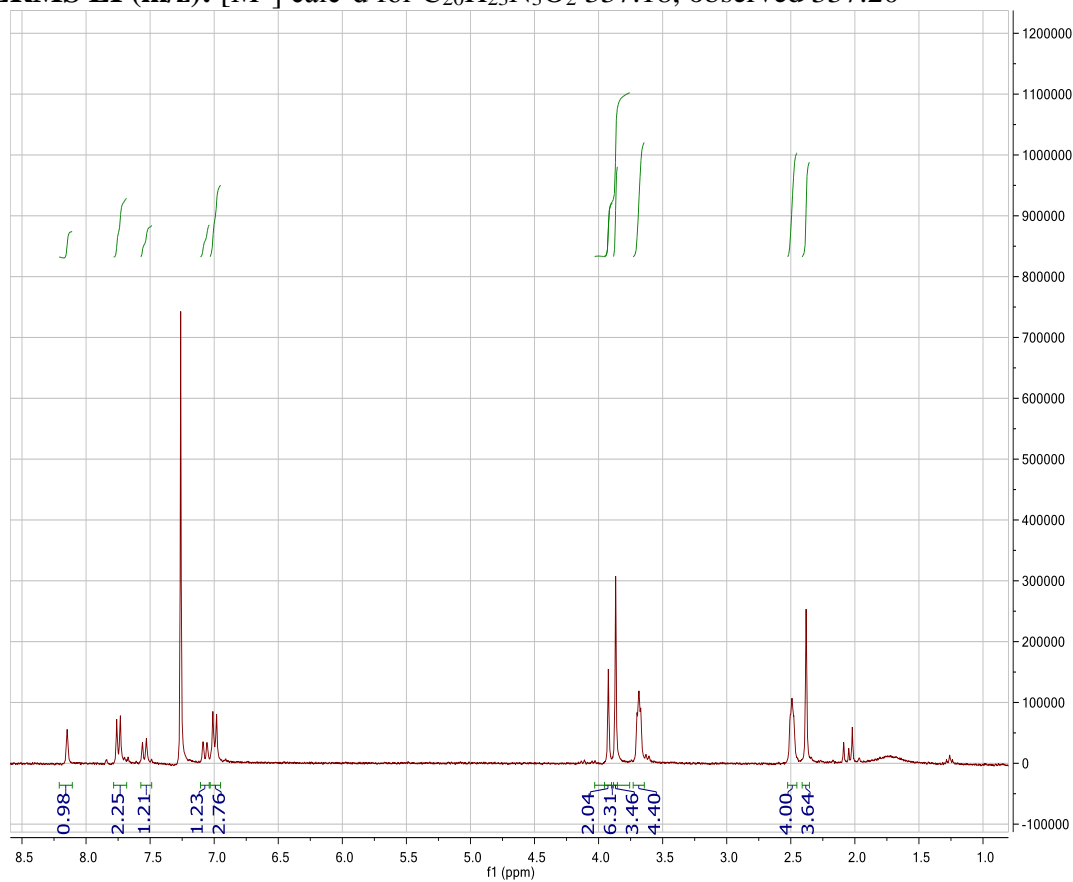
### Characterization of Compound 3.6

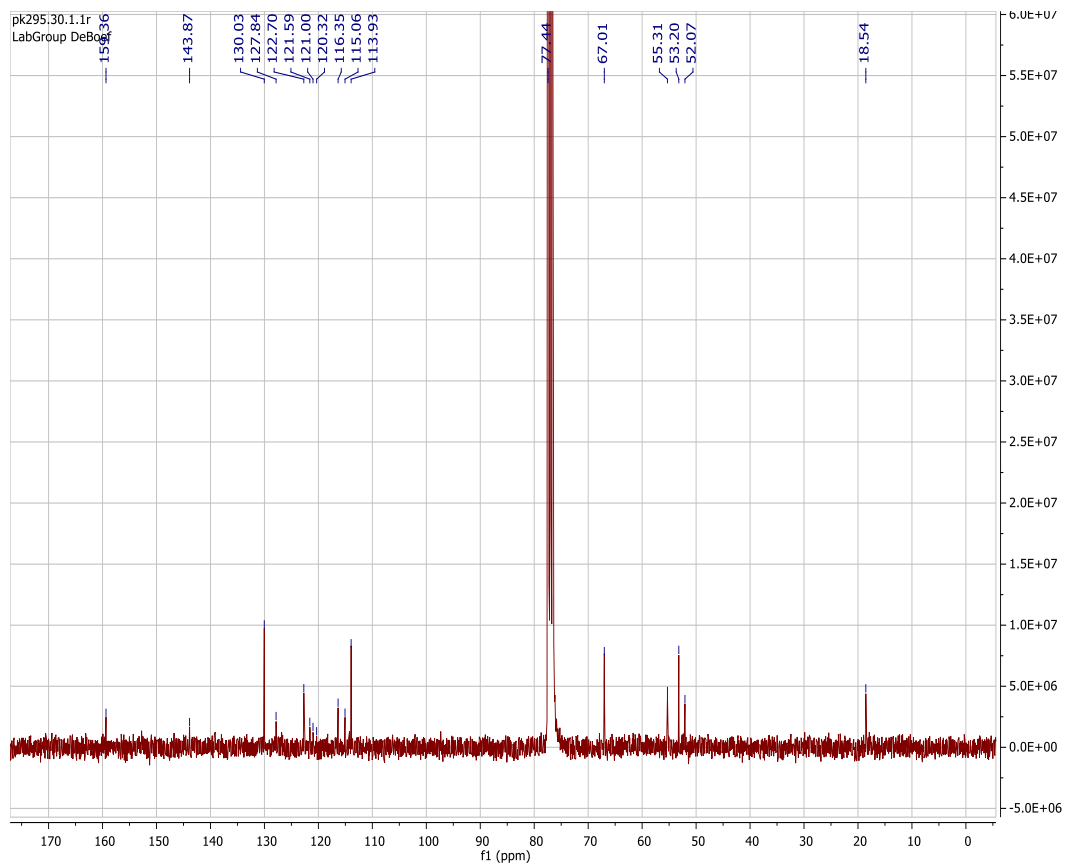


**<sup>1</sup>H NMR (300 MHz, CDCl<sub>3</sub>):** δ 8.15, (s, 1H), 7.75 (d, J=8.72 Hz, 2H), 7.53 (d, J=9.55 Hz 1H), 7.08 (d, J=9.45 Hz, 1H), 7.00 (d, J=8.86 Hz, 2H), 3.92 (s, 2H), 3.87 (s, 3H), 3.69 (t, J= 4.47 Hz, 4H), 2.49 (t, J =4.49 Hz ,4H), 2.38 (s, 3H)

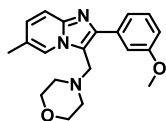
**<sup>13</sup>C NMR (75 MHz, CDCl<sub>3</sub>):** δ 159.36, 143.87, 130.03, 127.84, 122.70, 121.59, 121.00, 120.32, 116.35, 115.06, 113.93, 77.44, 67.01, 55.31, 53.20, 52.07, 18.54.

**LRMS EI (m/z):** [M<sup>+</sup>] calc'd for C<sub>20</sub>H<sub>23</sub>N<sub>3</sub>O<sub>2</sub> 337.18, observed 337.20





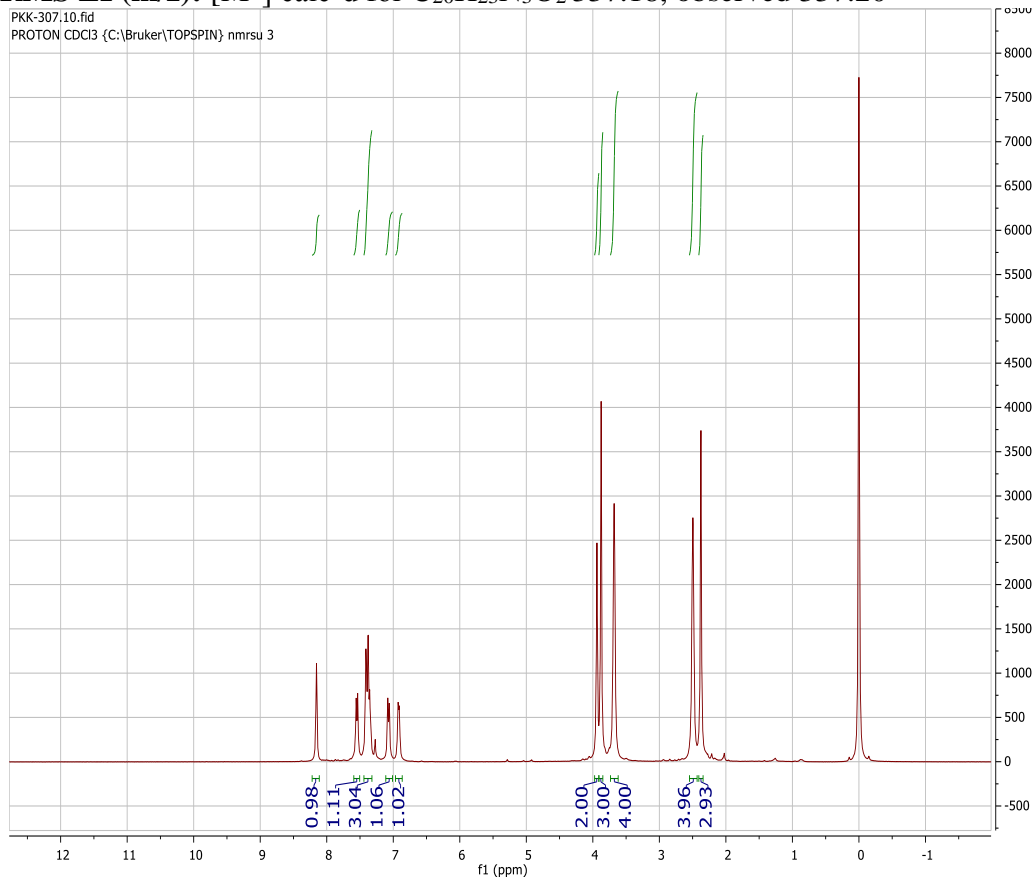
### Characterization of Compound 3.7

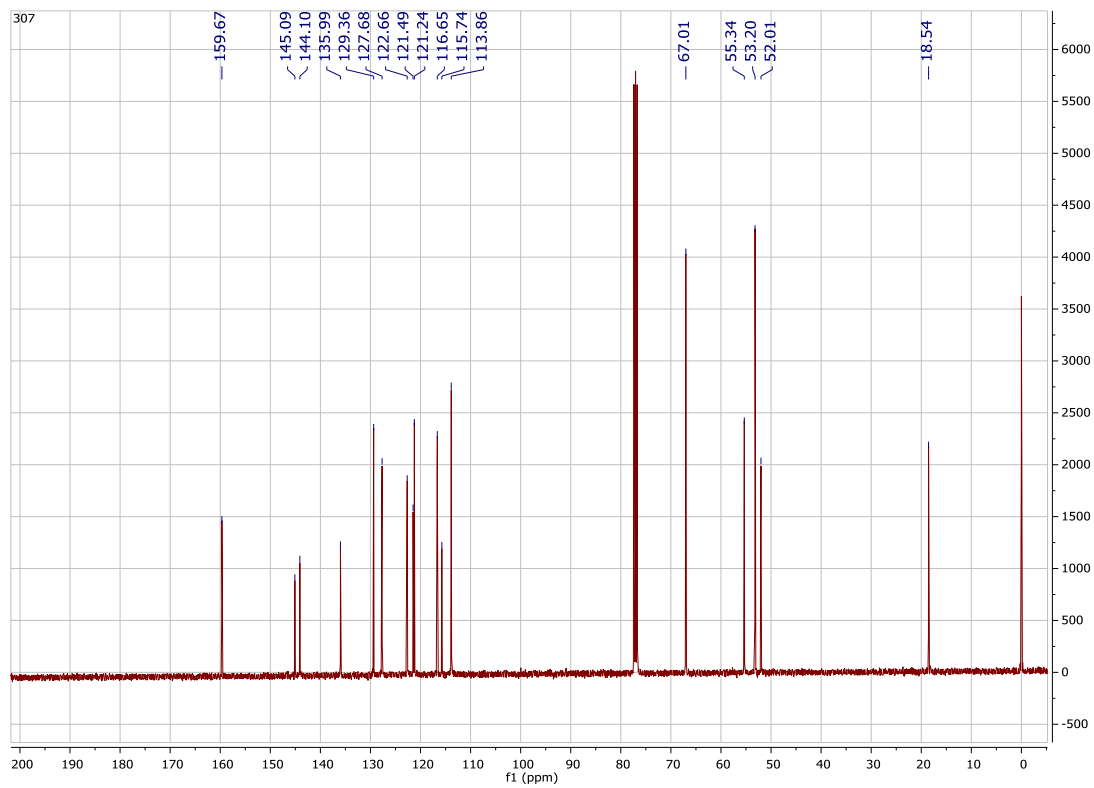


**<sup>1</sup>H NMR (400 MHz, CDCl<sub>3</sub>):** δ 8.15 (s, 1H), 7.55 (d, J=9.2 Hz 1H), 7.33 – 7.41 (m, 3H), 7.07 (d, J =9.2 Hz 1H), 6.92 (d, J = 7.5 Hz 1H), 3.94 (s, 2H), 3.88 (s, 3H), 3.68 (t, J = 4.4 Hz, 4H), 2.50 (t, 4H), 2.38 (s, 3H)

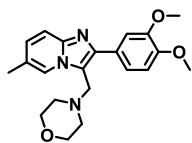
**<sup>13</sup>C NMR (101 MHz, CDCl<sub>3</sub>):** δ 159.67, 145.09, 144.10, 135.99, 129.36, 127.68, 122.66, 121.49, 121.24, 116.65, 115.74, 113.86, 67.01, 55.34, 53.20, 52.01, 18.54.

**LRMS EI (m/z):** [M<sup>+</sup>] calc'd for C<sub>20</sub>H<sub>23</sub>N<sub>3</sub>O<sub>2</sub> 337.18, observed 337.20





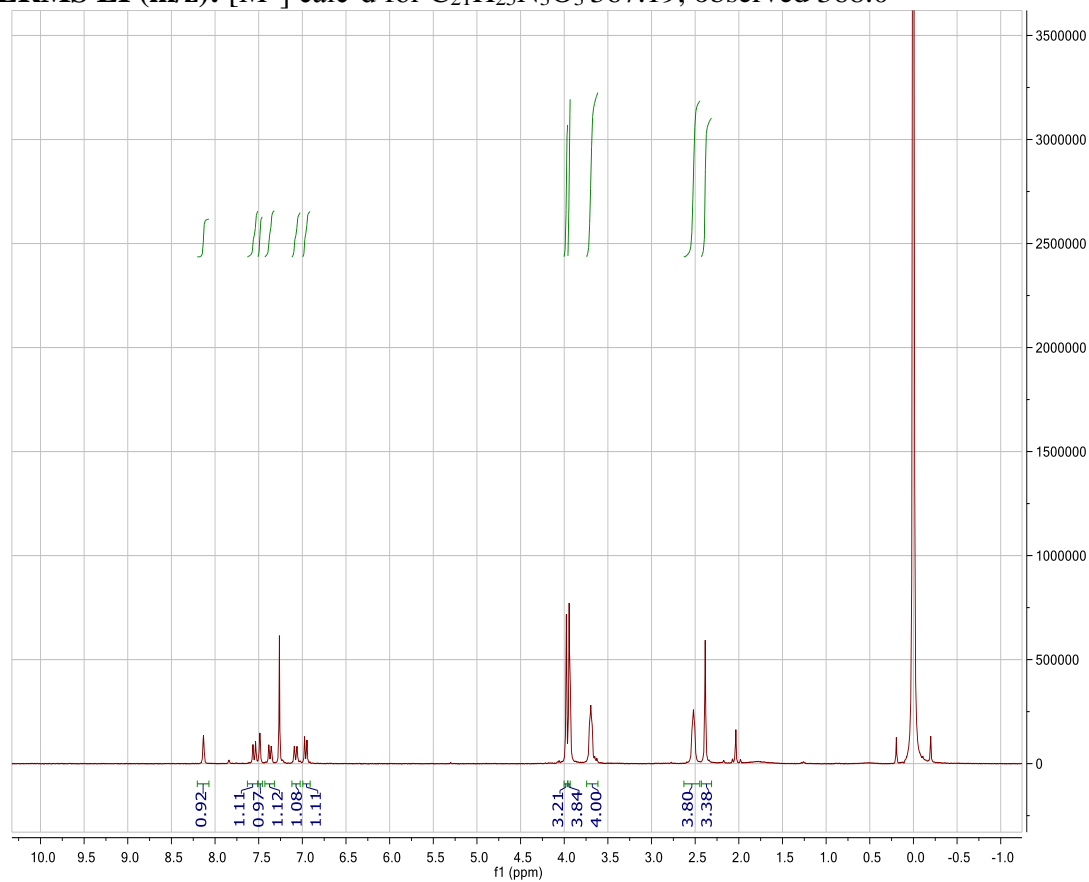
## Characterization of Compound 3.8

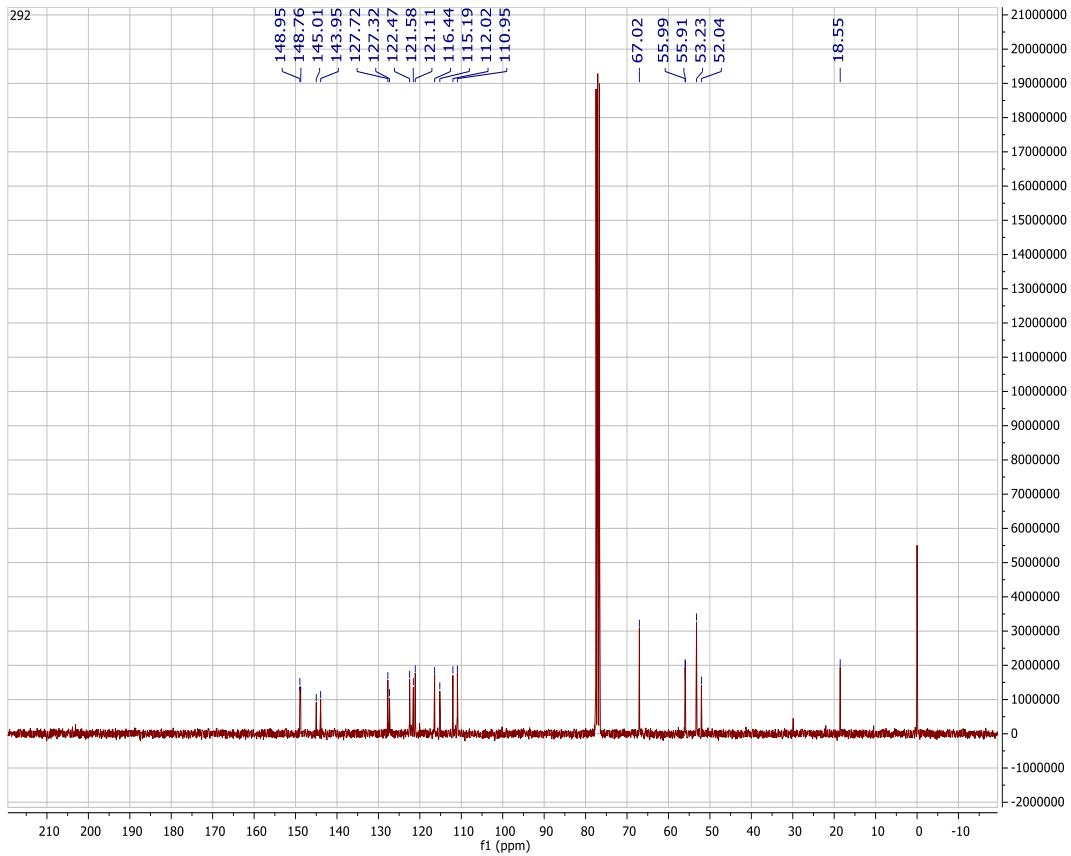


**<sup>1</sup>H NMR (300 MHz, CDCl<sub>3</sub>):**  $\delta$  8.13 (s, 1H), 7.55 (d,  $J = 9.2$  Hz, 1H), 7.49 (s, 1H), 7.37 (d,  $J = 8.3$ , 1H), 7.08 (d,  $J = 9.6$  Hz, 1H), 6.96 (d,  $J = 8.2$  Hz, 1H), 3.98 (s, 3H), 3.94 (s, 3H), 3.70 (t,  $J = 4.4$  Hz, 4H), 2.52 (t,  $J = 4.5$  Hz, 4H), 2.39 (s, 3H).

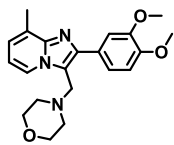
**<sup>13</sup>C NMR (75 MHz, CDCl<sub>3</sub>):**  $\delta$  148.95, 148.76, 145.01, 143.95, 127.72, 127.32, 122.47, 121.58, 121.11, 116.44, 115.19, 112.02, 110.95, 67.02, 55.99, 55.91, 53.23, 52.04, 18.55.

**LRMS EI (m/z):** [M<sup>+</sup>] calc'd for C<sub>21</sub>H<sub>25</sub>N<sub>3</sub>O<sub>3</sub> 367.19, observed 368.0





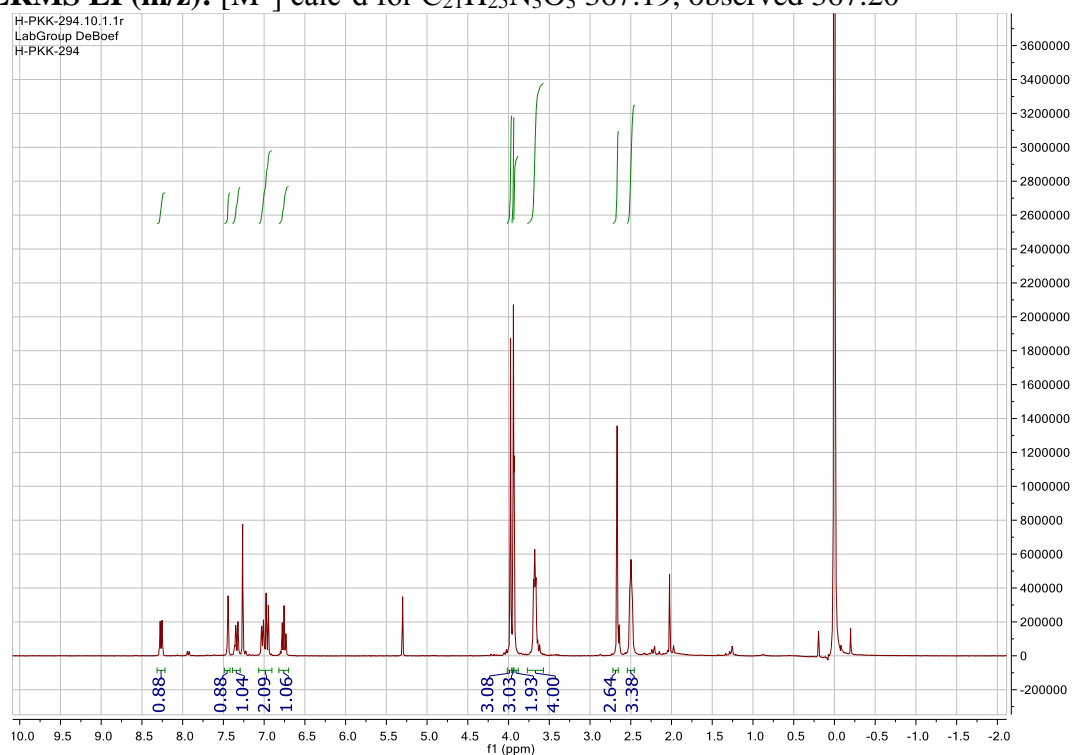
### Characterization of Compound 3.9



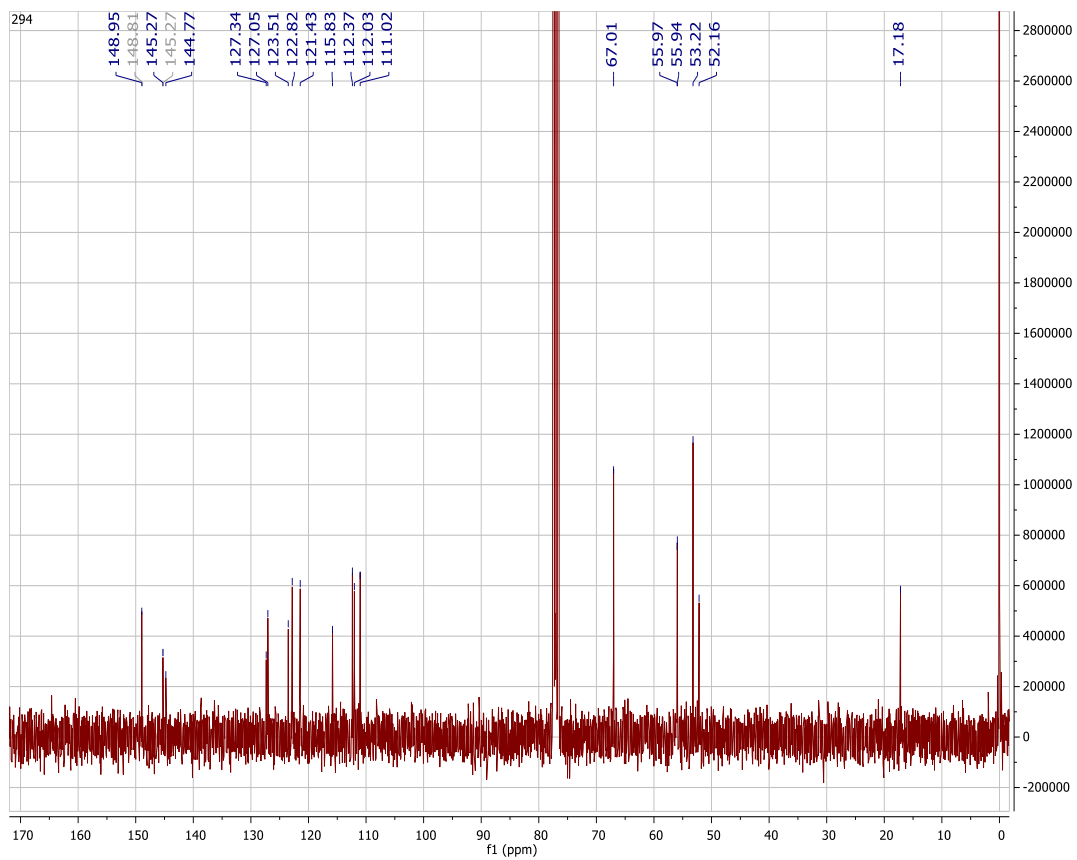
**<sup>1</sup>H NMR (300 MHz, CDCl<sub>3</sub>):** δ 8.27 (d, *J* = 6.8 Hz, 1H), 7.44 (d, *J* = 1.9 Hz, 1H), 7.39 – 7.29 (m, 1H), 7.02 (d, *J* = 7.0 Hz, 1H), 6.96 (d, *J* = 8.3 Hz, 7.6 Hz, 1H), 6.76 (t, *J* = 6.8 Hz, 1H), 3.98 (s, 3H), 3.94 (s, 3H), 3.93 (s, 2H), 3.68 (t, *J* = 4.5 Hz, 4H), 2.67 (s, 3H), 2.50 (t, *J* = 4.5 Hz, 3H).

**<sup>13</sup>C NMR (75 MHz, CDCl<sub>3</sub>)** δ 148.95, 148.81, 145.27, 144.77, 127.34, 127.05, 123.51, 122.82, 121.43, 115.83, 112.37, 112.03, 111.02, 67.01, 55.97, 55.94, 53.22, 52.16, 17.18.

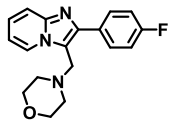
**LRMS EI (m/z):** [M<sup>+</sup>] calc'd for C<sub>21</sub>H<sub>25</sub>N<sub>3</sub>O<sub>3</sub> 367.19, observed 367.20







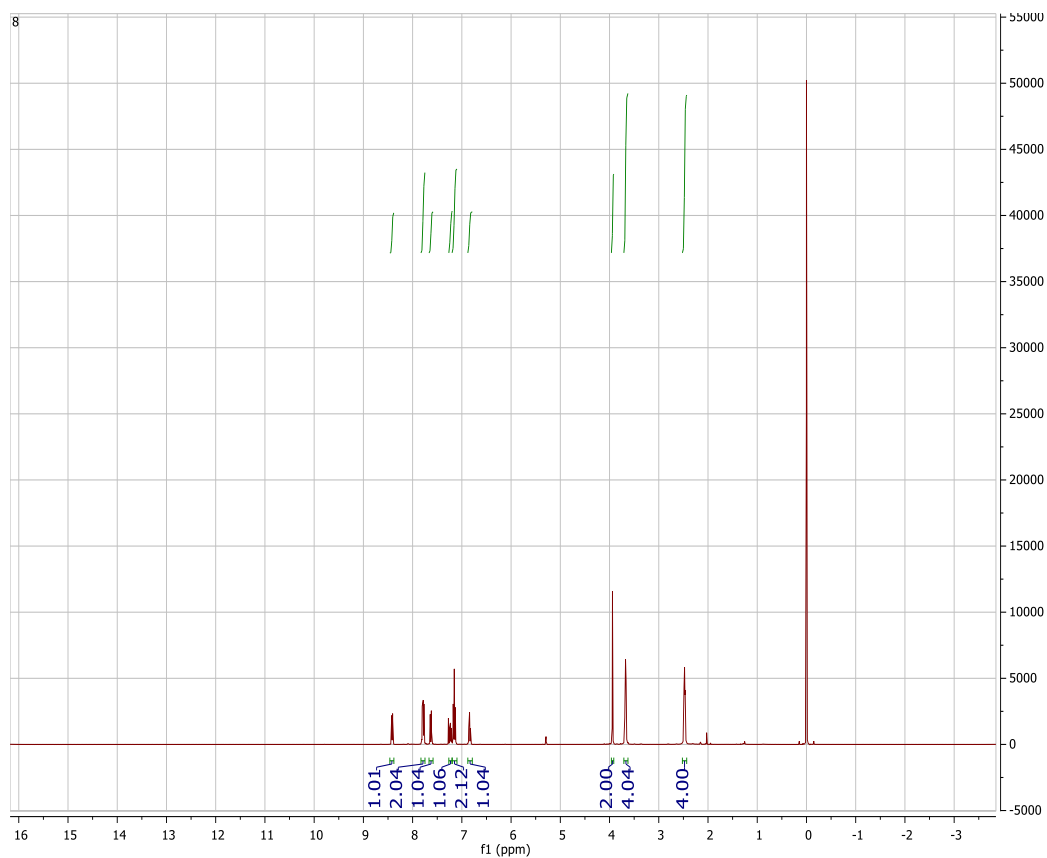
### Characterization of Compound 3.10



**<sup>1</sup>H NMR (400 MHz, CDCl<sub>3</sub>):** δ 8.40 (d, *J* = 7.1 Hz, 1H), 7.81 – 7.74 (m, 2H), 7.64 (d, *J* = 9.06 Hz, 1H), 7.22 (t, *J* = 6.7 Hz, 1H), 7.11 (m, 2H), 6.83 (t, *J* = 6.7 Hz, 1H), 3.93 (s, 2H), 3.67 (t, *J* = 4.4 Hz, 4H), 2.47 (t, *J* = 4.4 Hz, 4H).

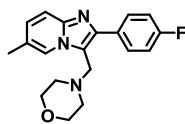
**<sup>13</sup>C NMR (101 MHz, CDCl<sub>3</sub>):** δ 162.57 (*J*<sub>CF</sub> = 253 Hz), 145.07, 144.48, 130.63, 130.53 (*J*<sub>CF</sub> = 9 Hz), 125.18, 124.67, 117.28, 115.42 (*J*<sub>CF</sub> = 21 Hz), 115.32, 111.98, 66.96, 53.20, 52.05.

**LRMS EI (m/z):** [M<sup>+</sup>] calc'd for C<sub>18</sub>H<sub>18</sub>FN<sub>3</sub>O 311.14, observed 311.10





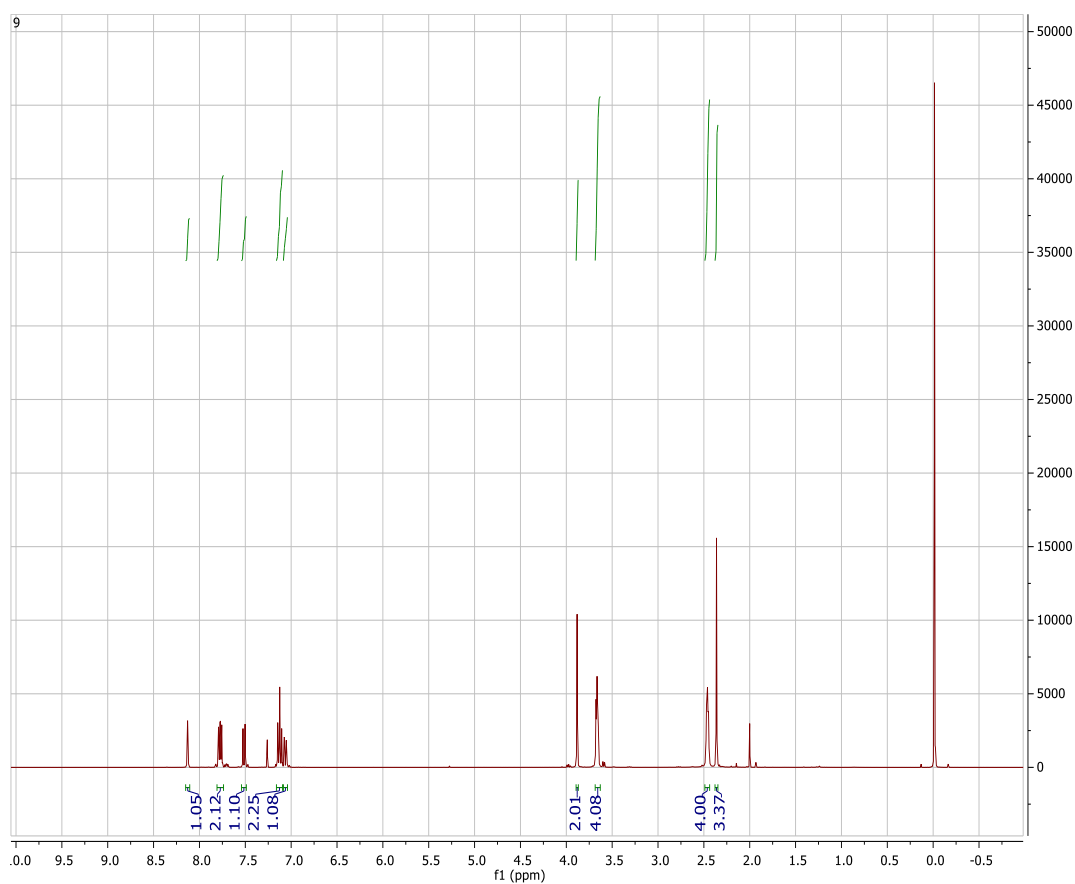
### Characterization of Compound 3.11

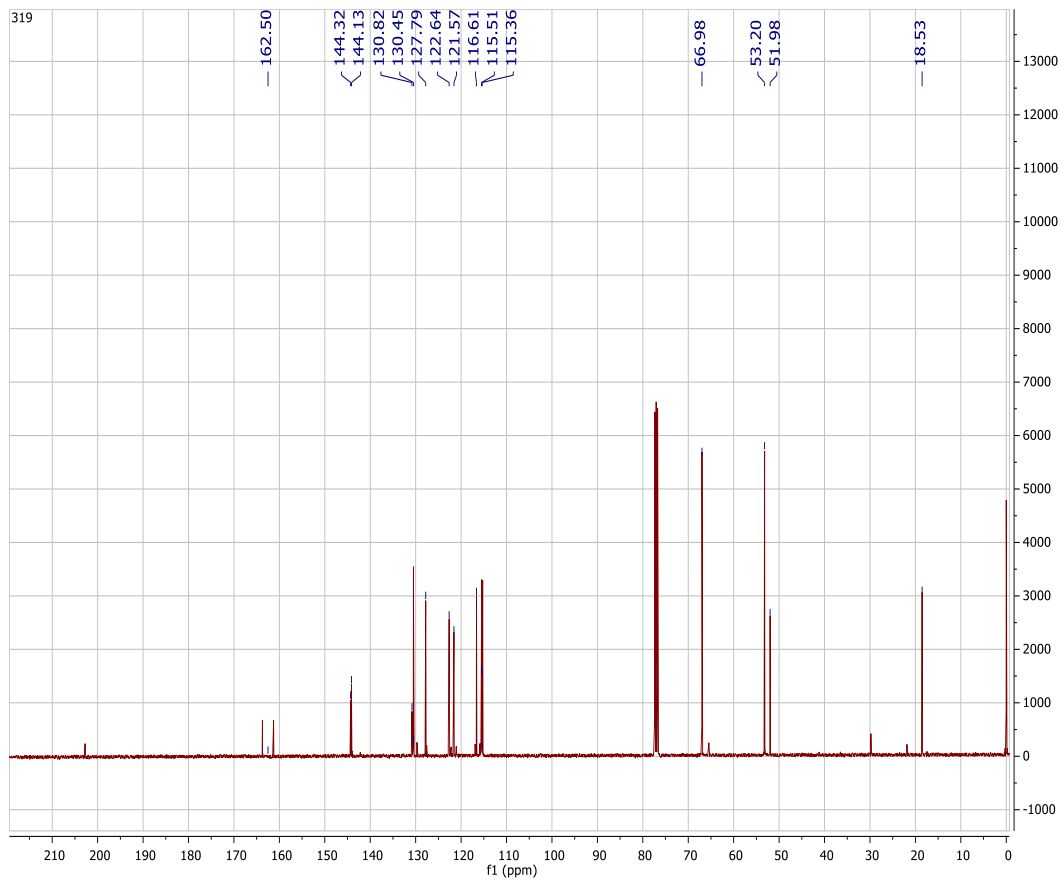


**<sup>1</sup>H NMR (400 MHz, CDCl<sub>3</sub>):** δ 8.13 (s, 1H), 7.81 – 7.74 (m, 2H), 7.51 (d, *J* = 9.2 Hz, 1H), 7.16 – 7.09 (m, 2H), 7.06 (dd, *J* = 9.2, 1.7 Hz, 1H), 3.88 (s, 2H), 3.66 (t, *J* = 4.6 Hz, 4H), 2.46 (t, *J* = 4.6 Hz, 4H), 2.36 (s, 3H).

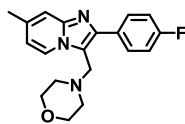
**<sup>13</sup>C NMR (101 MHz, CDCl<sub>3</sub>):** δ 162.50 (*J*<sub>CF</sub> = 245 Hz), 161.28, 144.32, 144.13, 130.45 (*J*<sub>CF</sub> = 8 Hz), 127.79, 122.64, 121.57, 116.61, 115.51, 115.37 (*J*<sub>CF</sub> = 21 Hz), 66.98, 53.20, 51.98, 18.53.

**LRMS EI (m/z):** [M<sup>+</sup>] calc'd for C<sub>19</sub>H<sub>20</sub>FN<sub>3</sub>O 325.16, observed 325.20





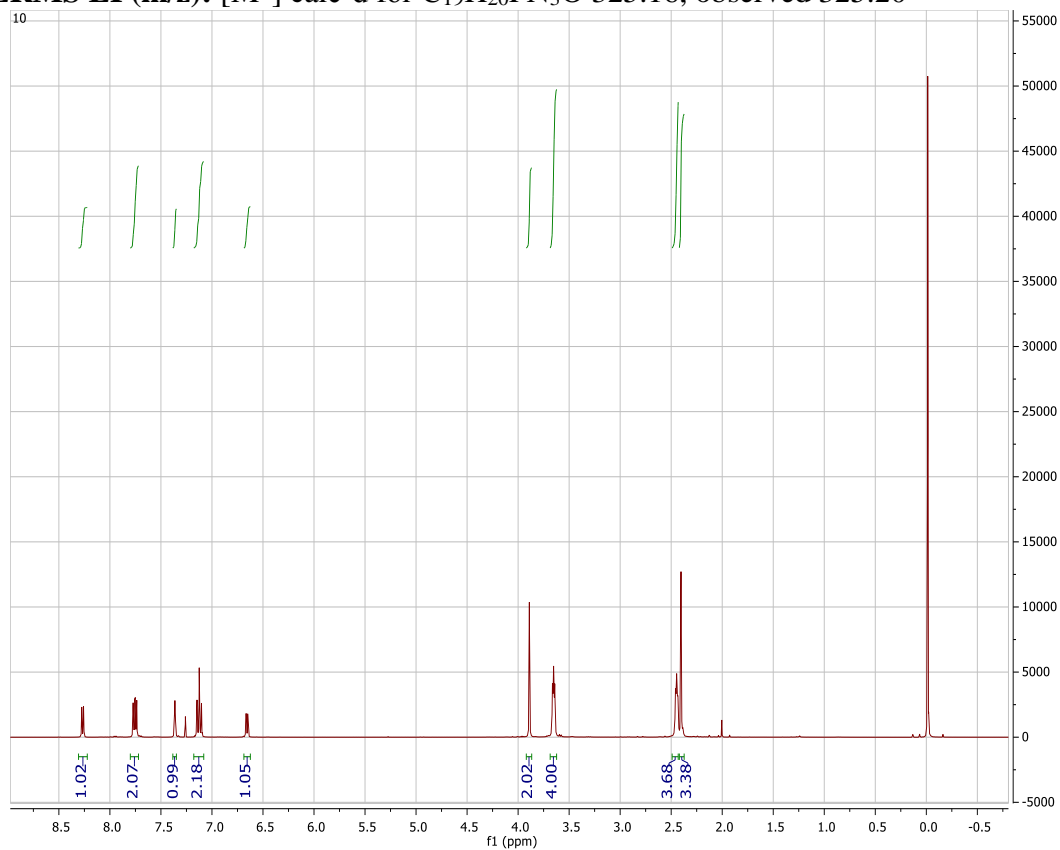
### Characterization of Compound 3.12

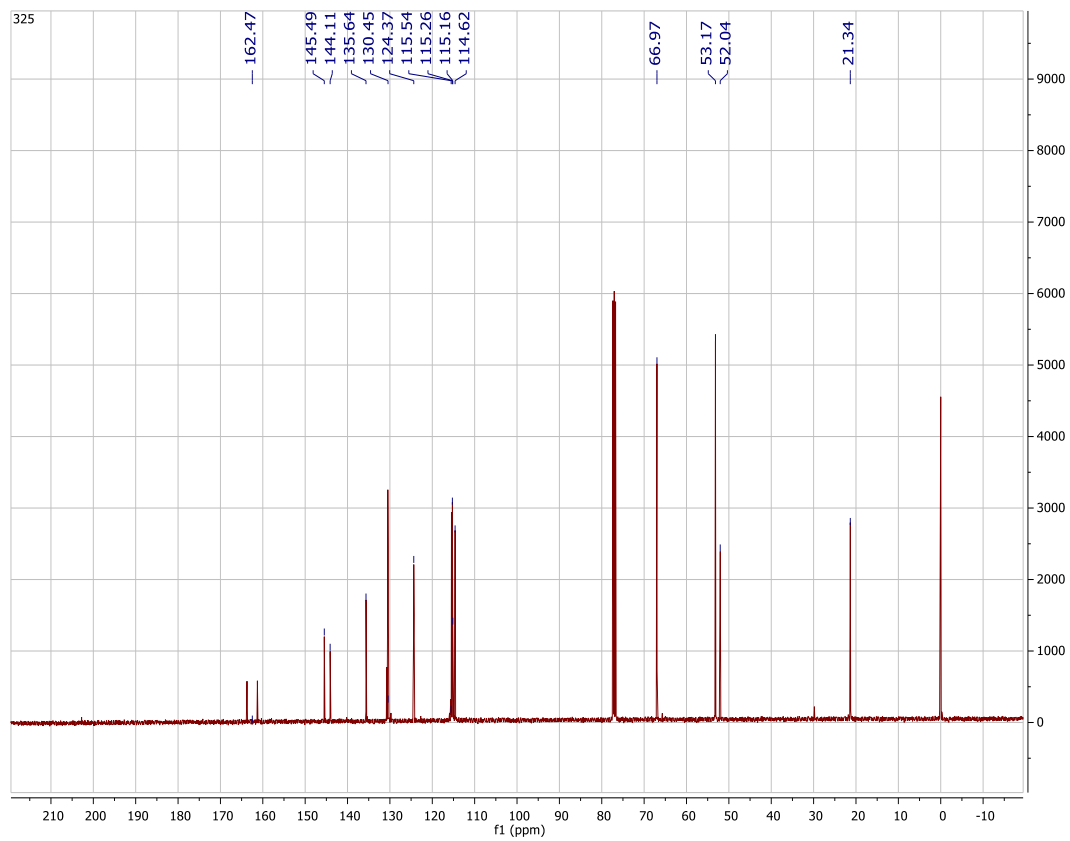


**<sup>1</sup>H NMR (400 MHz, CDCl<sub>3</sub>):**  $\delta$  8.27 (d,  $J$  = 6.9 Hz, 1H), 7.80 – 7.72 (m, 2H), 7.36 (s, 1H), 7.18 – 7.08 (m, 2H), 6.66 (dd,  $J$  = 7.1, 1.7 Hz, 1H), 3.89 (s, 2H), 3.65 (t,  $J$  = 4.6 Hz, 4H), 2.45 (t,  $J$  = 4.4, 4H), 2.40 (s, 3H).

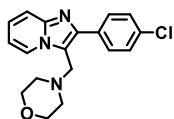
**<sup>13</sup>C NMR (101 MHz, CDCl<sub>3</sub>):**  $\delta$  162.4 ( $J_{CF}$  = 250 Hz), 161.28, 145.49, 144.11, 135.64, 130.45 ( $J_{CF}$  = 9 Hz), 124.37, 115.55 ( $J_{CF}$  = 20 Hz), 115.16, 115.26, 114.62, 66.97, 53.17, 52.04, 21.34.

**LRMS EI (m/z):** [M<sup>+</sup>] calc'd for C<sub>19</sub>H<sub>20</sub>FN<sub>3</sub>O 325.16, observed 325.20





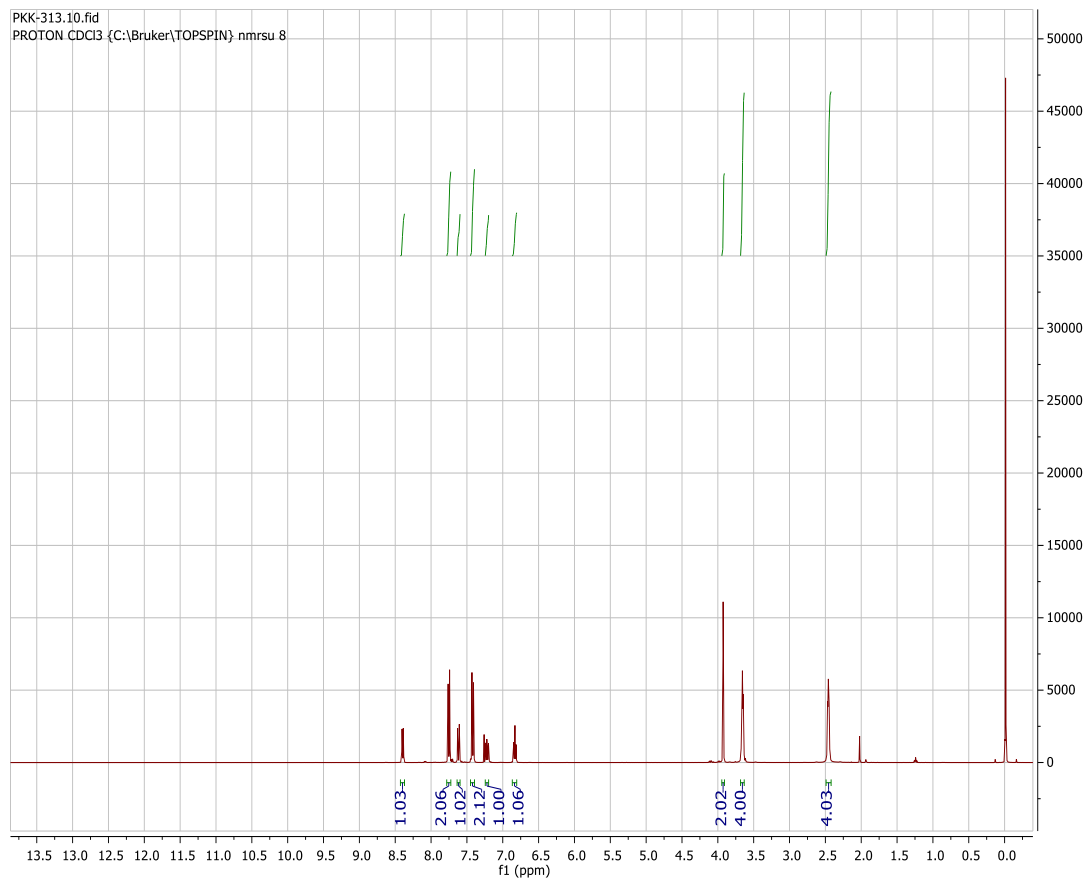
### Characterization of Compound 3.13



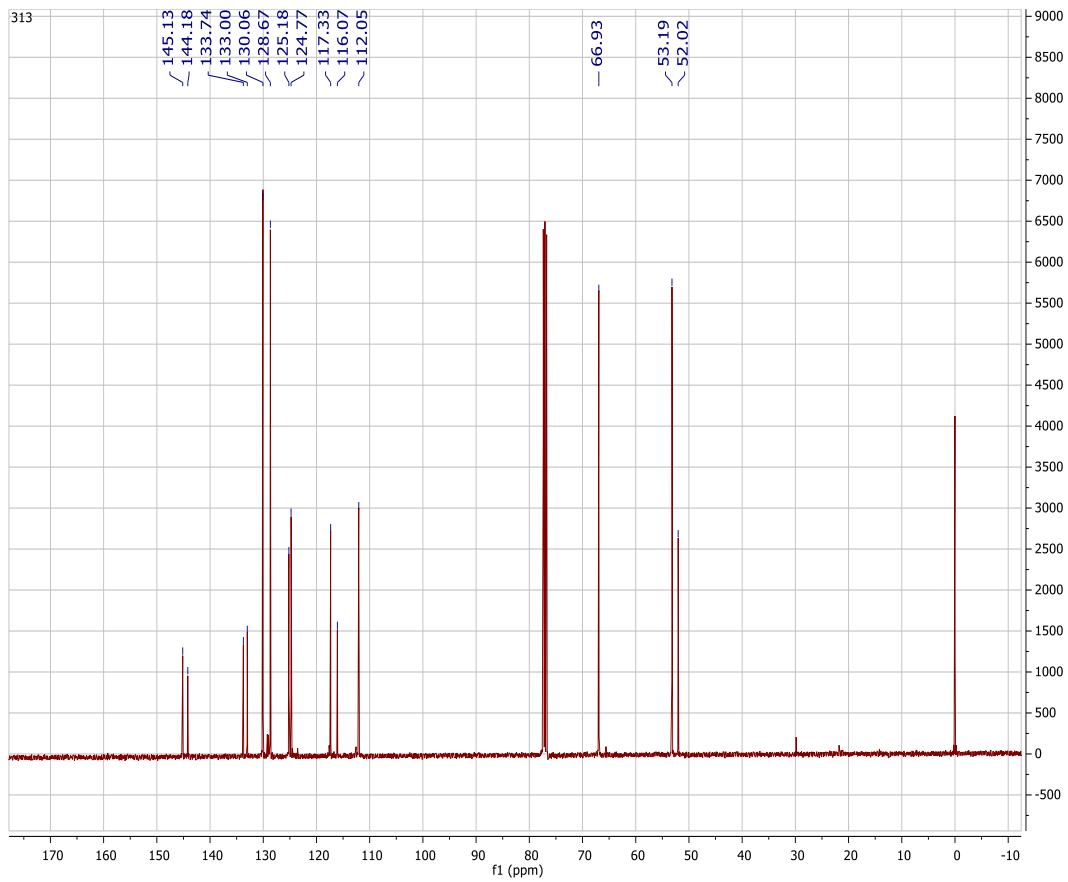
**<sup>1</sup>H NMR (400 MHz, CDCl<sub>3</sub>):**  $\delta$  8.40 (d,  $J = 7.0, 1.2$  Hz, 1H), 7.78 – 7.72 (m, 2H), 7.62 (d,  $J = 9.0$  Hz, 1H), 7.45 – 7.39 (m, 2H), 7.22 (ddd,  $J = 9.2, 6.7, 1.3$  Hz, 1H), 6.83 (t,  $J = 6.9$  Hz, 1H), 3.93 (s, 2H), 3.66 (t,  $J = 4.6$  Hz, 4H), 2.46 (t,  $J = 4.6$  Hz, 4H).

**<sup>13</sup>C NMR (101 MHz, CDCl<sub>3</sub>)**  $\delta$  145.13, 144.18, 133.74, 133.00, 130.06, 128.67, 125.18, 124.77, 117.33, 116.07, 112.05, 66.93, 53.19, 52.02.

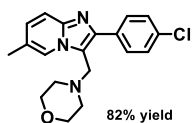
**LRMS EI (m/z):** [M<sup>+</sup>] calc'd for C<sub>18</sub>H<sub>18</sub>ClN<sub>3</sub>O 327.11, observed 327.10







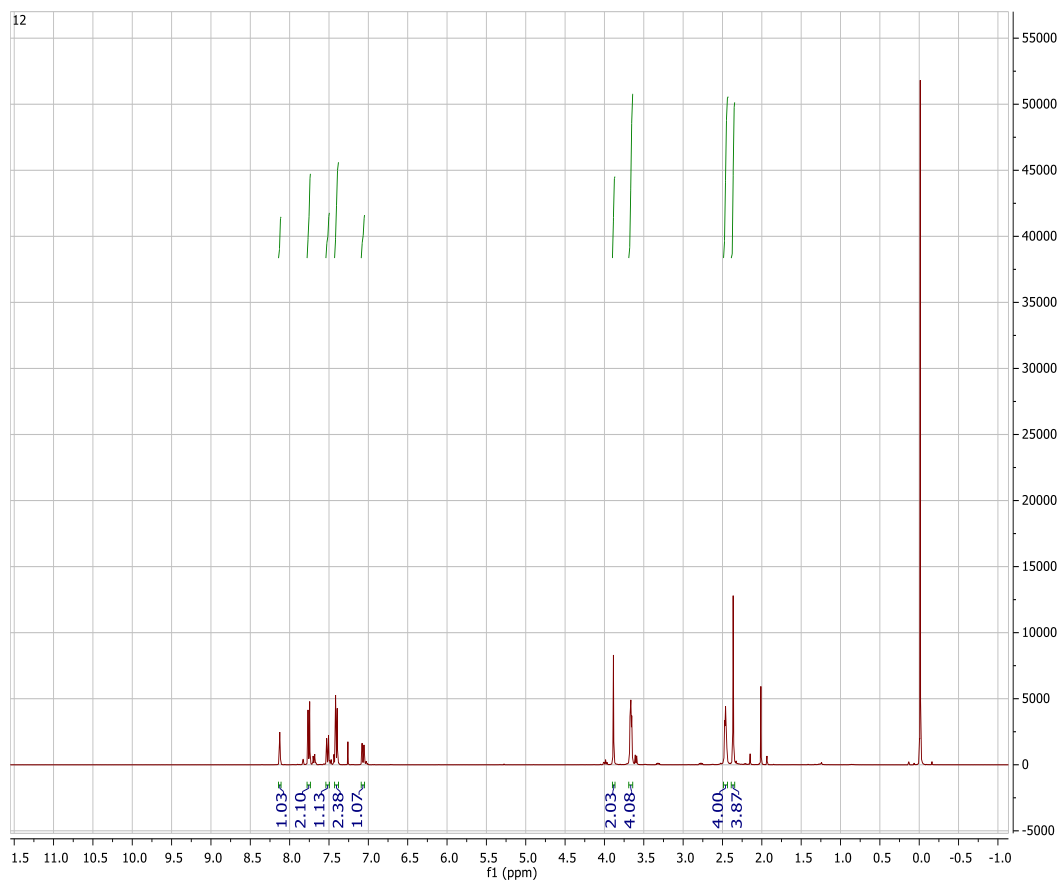
## Characterization of Compound 3.14

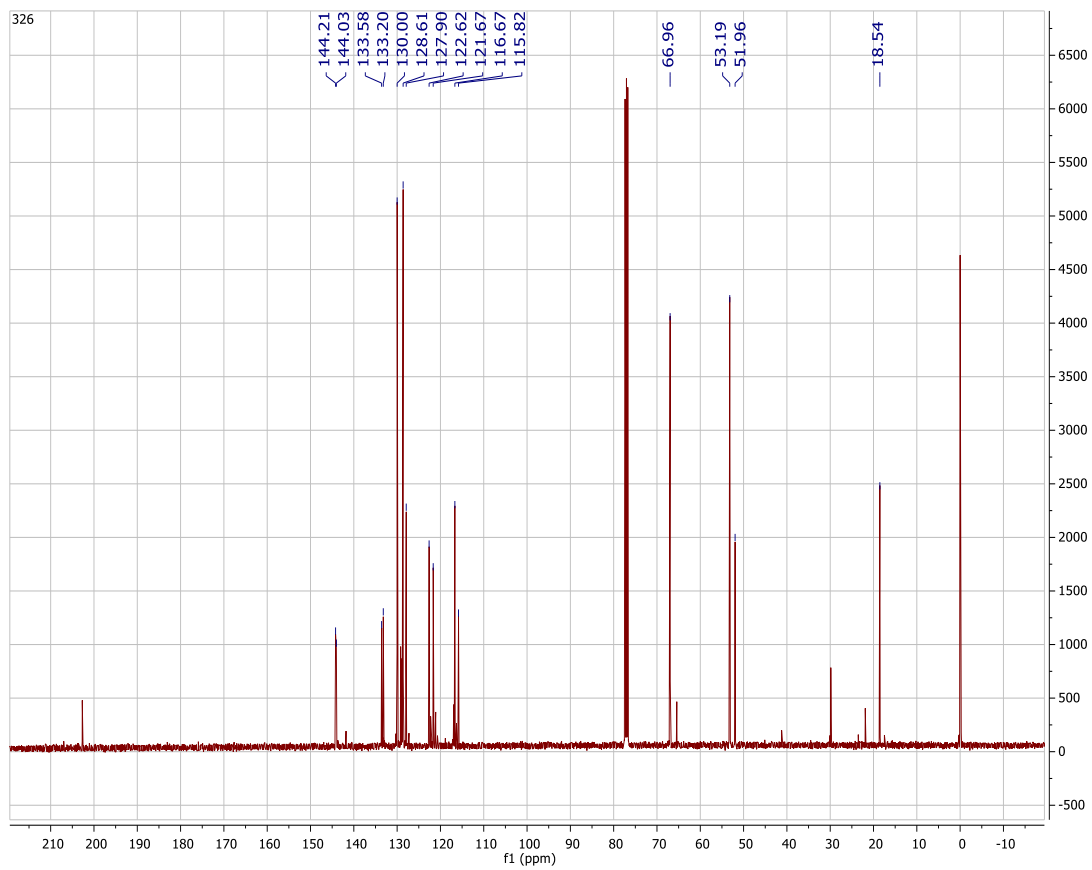


**<sup>1</sup>H NMR (400 MHz, CDCl<sub>3</sub>):**  $\delta$  8.14 (s, 1H), 7.78 – 7.74 (m, 2H), 7.52 (d, J = 9.2 Hz, 1H), 7.43 – 7.38 (m, 2H) 7.07 (dd, J = 9.1, 1.7 Hz, 1H), 3.89 (s, 2H), 3.66 (t, J = 4.6 Hz, 4H), 2.46 (t, J = 4.6 Hz, 4 H), 2.36 (s, 3H)

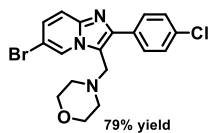
**<sup>13</sup>C NMR (101 MHz, CDCl<sub>3</sub>)**  $\delta$  144.21, 144.03, 133.58, 133.20, 130.00, 128.61, 127.90, 122.62, 121.67, 116.67, 115.82, 66.96, 53.19, 51.96, 18.54.

**LRMS EI (m/z):** [M<sup>+</sup>] calc'd for C<sub>19</sub>H<sub>20</sub>ClN<sub>3</sub>O 341.13, 342.0





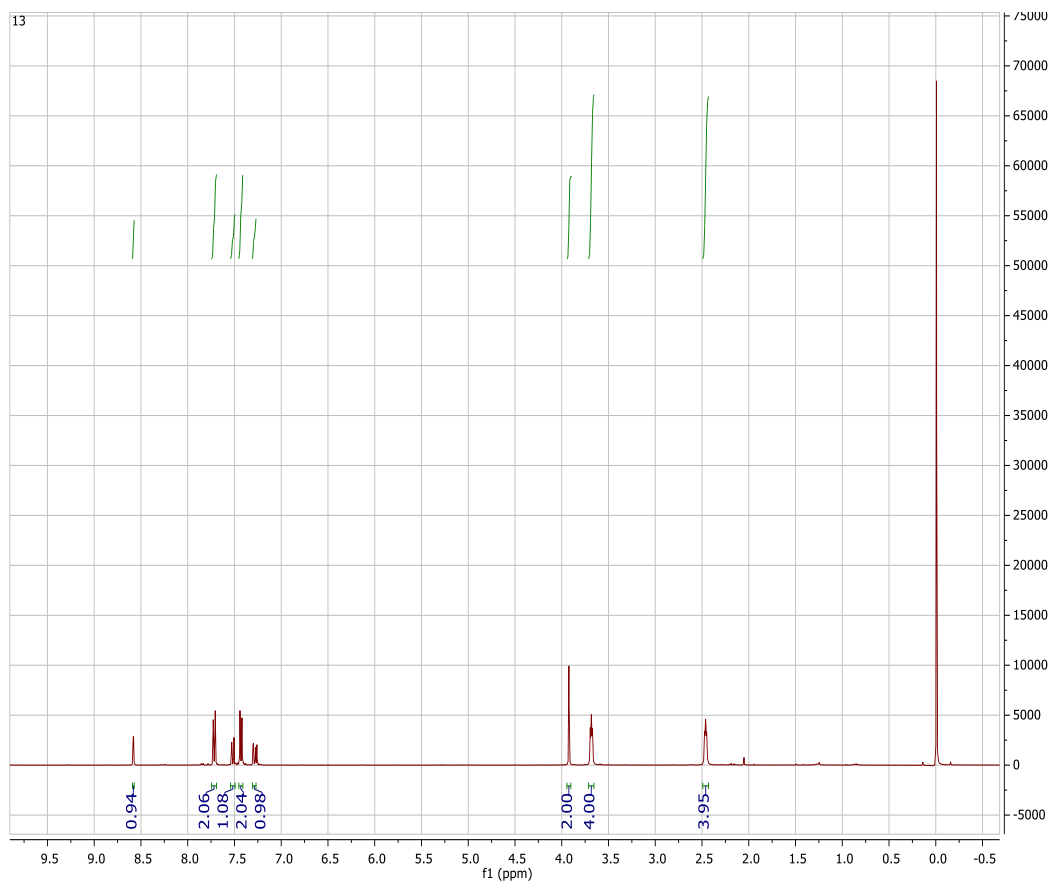
## Characterization of Compound 3.15

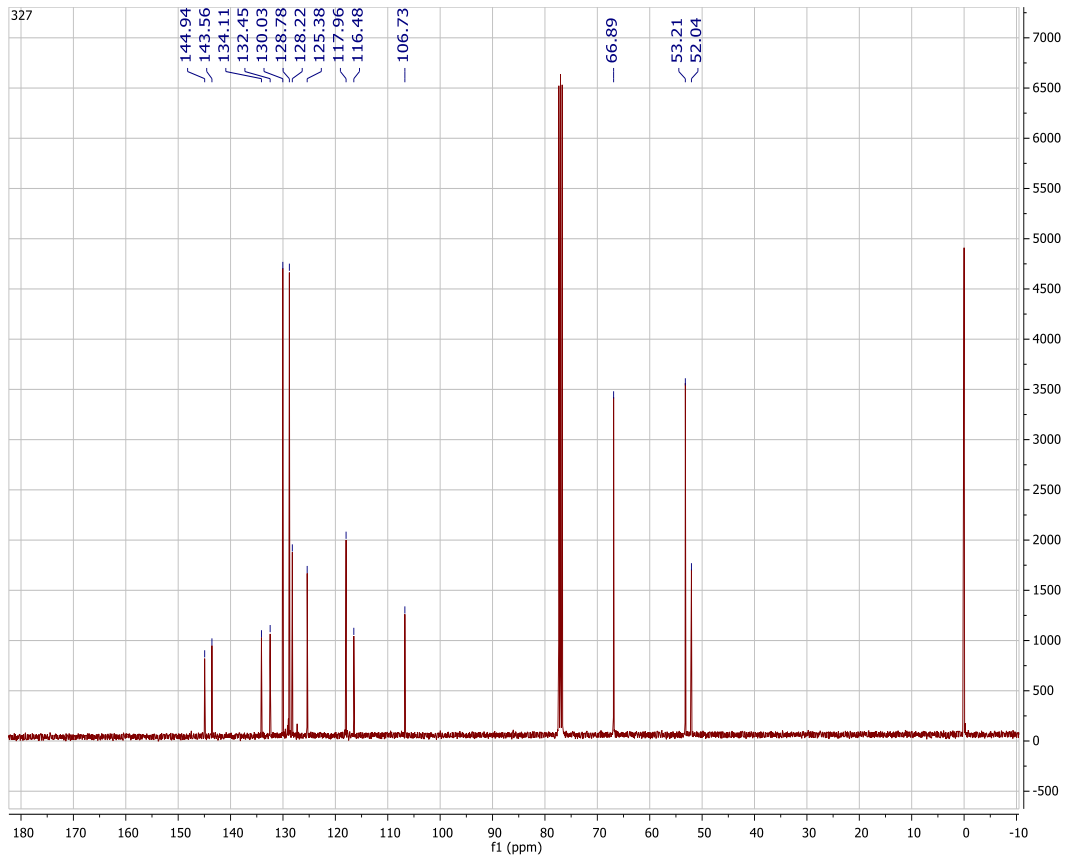


**$^1\text{H}$  NMR (400 MHz,  $\text{CDCl}_3$ ):**  $\delta$  8.58 (s, 1H), 7.74 – 7.69 (m, 2H), 7.52 (d,  $J = 9.5$  Hz, 1H), 7.45 – 7.41 (m, 2H), 7.29 (dd,  $J = 9.5, 1.9$  Hz, 1H), 3.92 (s, 2H), 3.68 (t,  $J = 4.6$  Hz, 4H), 2.46 (t,  $J = 4.6$  Hz, 4H).

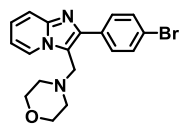
**$^{13}\text{C}$  NMR (101 MHz,  $\text{CDCl}_3$ ):**  $\delta$  144.94, 143.56, 134.11, 132.45, 130.03, 128.78, 128.22, 125.38, 117.96, 116.48, 106.73, 66.89, 53.21, 52.04.

**LRMS EI (m/z):**  $[\text{M}^+]$  calc'd for  $\text{C}_{18}\text{H}_{17}\text{BrClN}_3\text{O}$  405.02, 407.00





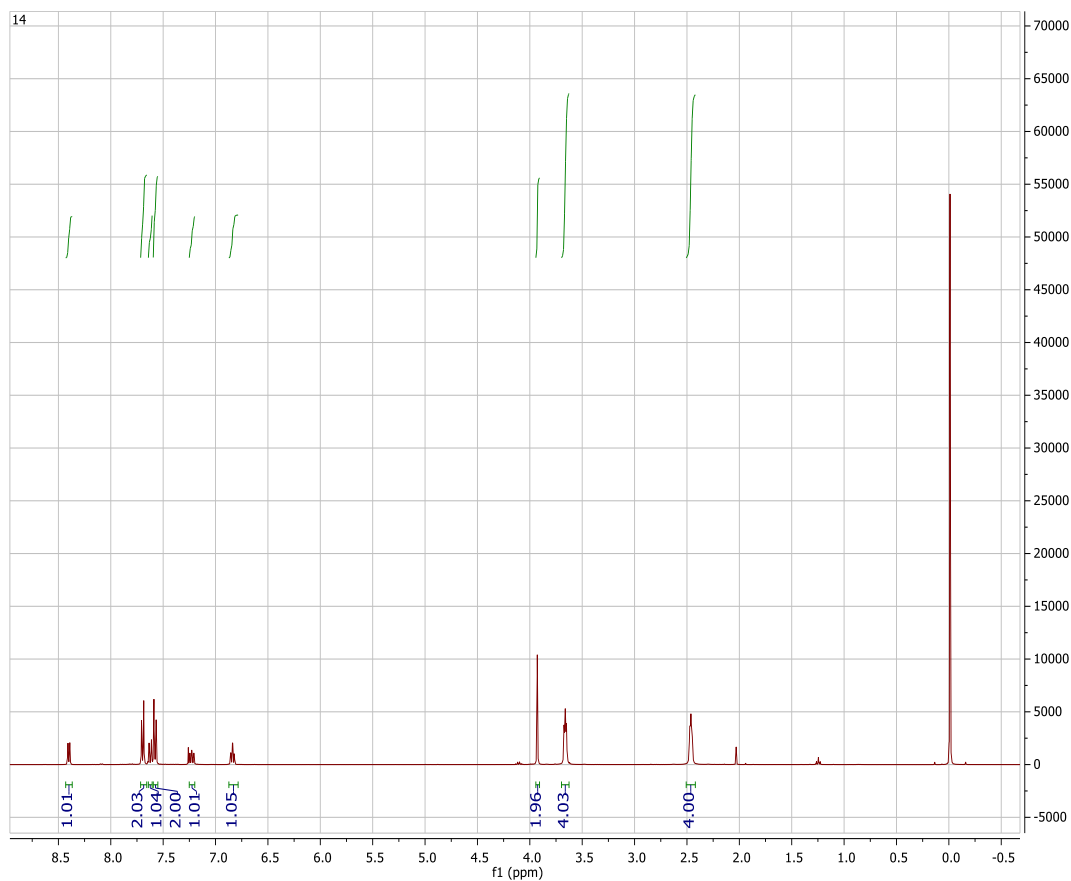
### Characterization of Compound 3.16

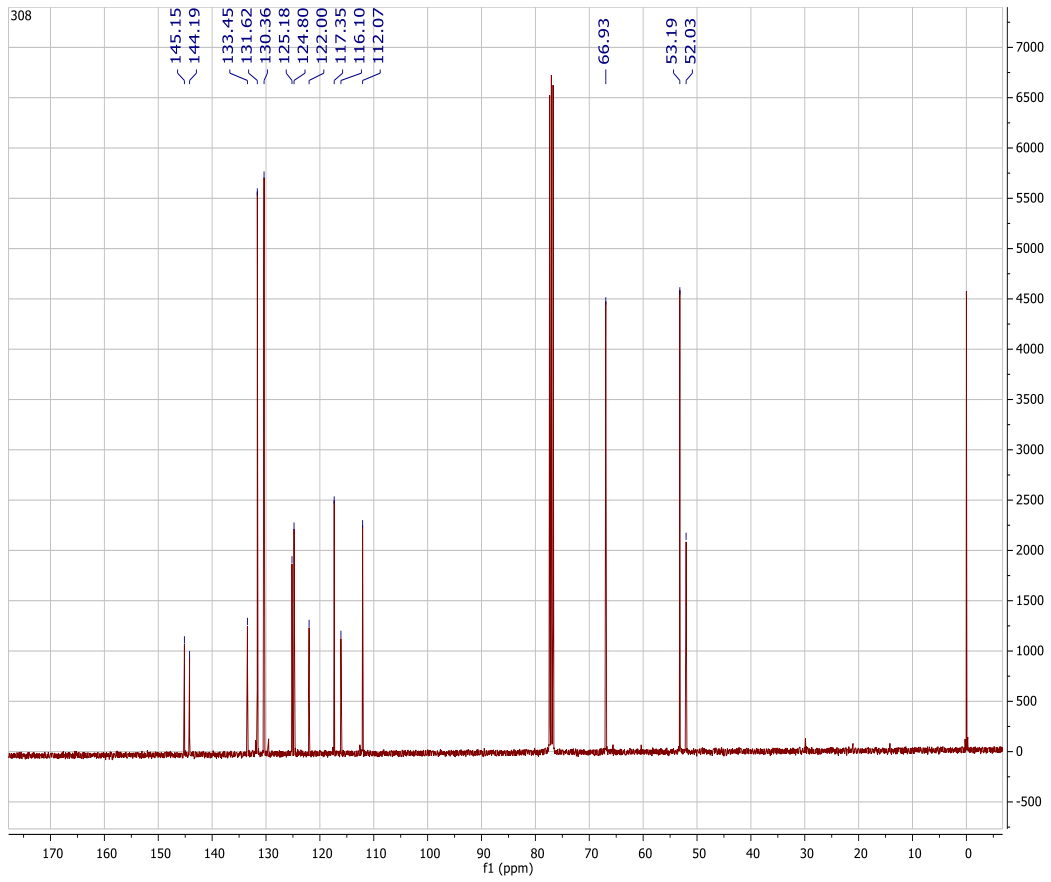


**$^1\text{H}$  NMR (400 MHz,  $\text{CDCl}_3$ ):**  $\delta$  8.40 (d,  $J = 7.0$  Hz, 1H), 7.72 – 7.66 (m, 2H), 7.62 (d,  $J = 9.1$  Hz, 1H), 7.59 – 7.55 (m, 2H), 7.25 – 7.20 (m, 1H), 3.93 (s, 2H), 3.66 (t,  $J = 4.6$  Hz, 4H), 2.46 (t,  $J = 4.6$  Hz, 4H).

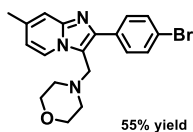
**$^{13}\text{C}$  NMR (101 MHz,  $\text{CDCl}_3$ ):**  $\delta$  145.15, 144.19, 133.45, 131.62, 130.36, 125.18, 124.80, 122.00, 117.35, 116.10, 112.07, 66.93, 53.19, 52.03.

**LRMS EI (m/z):**  $[\text{M}^+]$  calc'd for  $\text{C}_{18}\text{H}_{18}\text{BrN}_3\text{O}$  371.06, observed 371.10





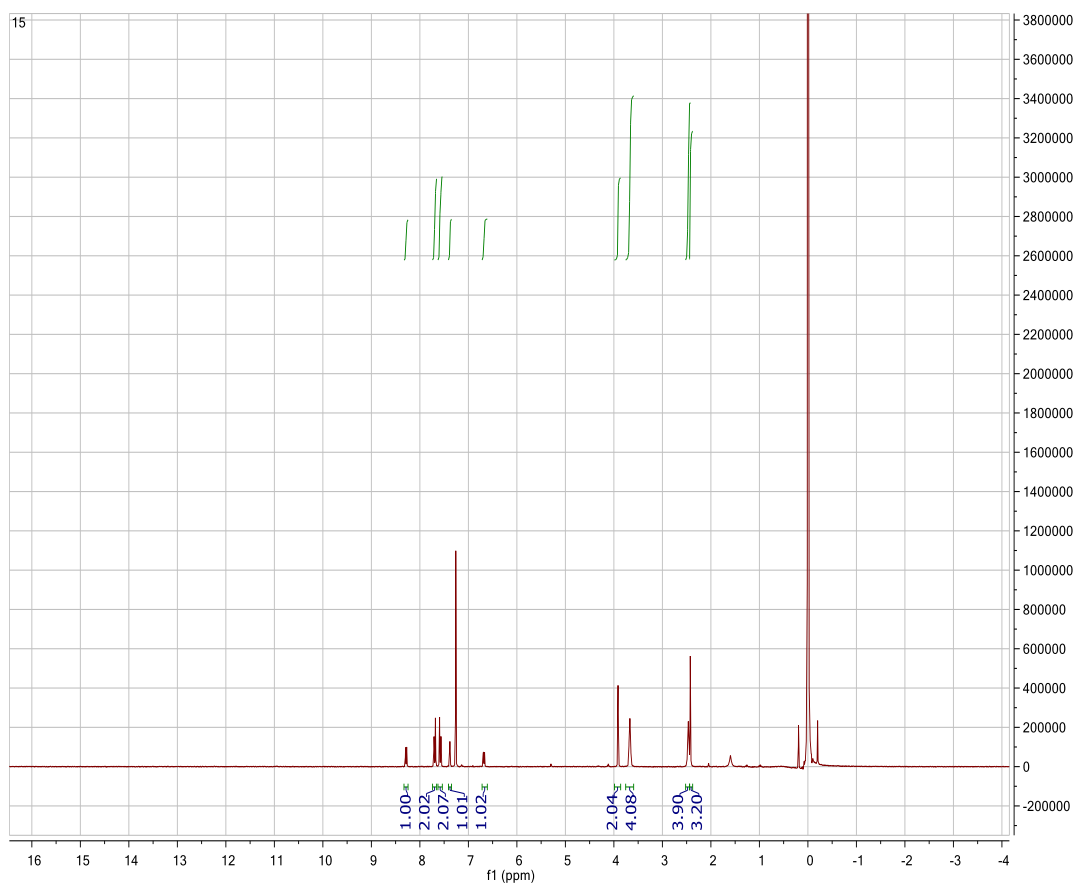
## Characterization of Compound 3.17



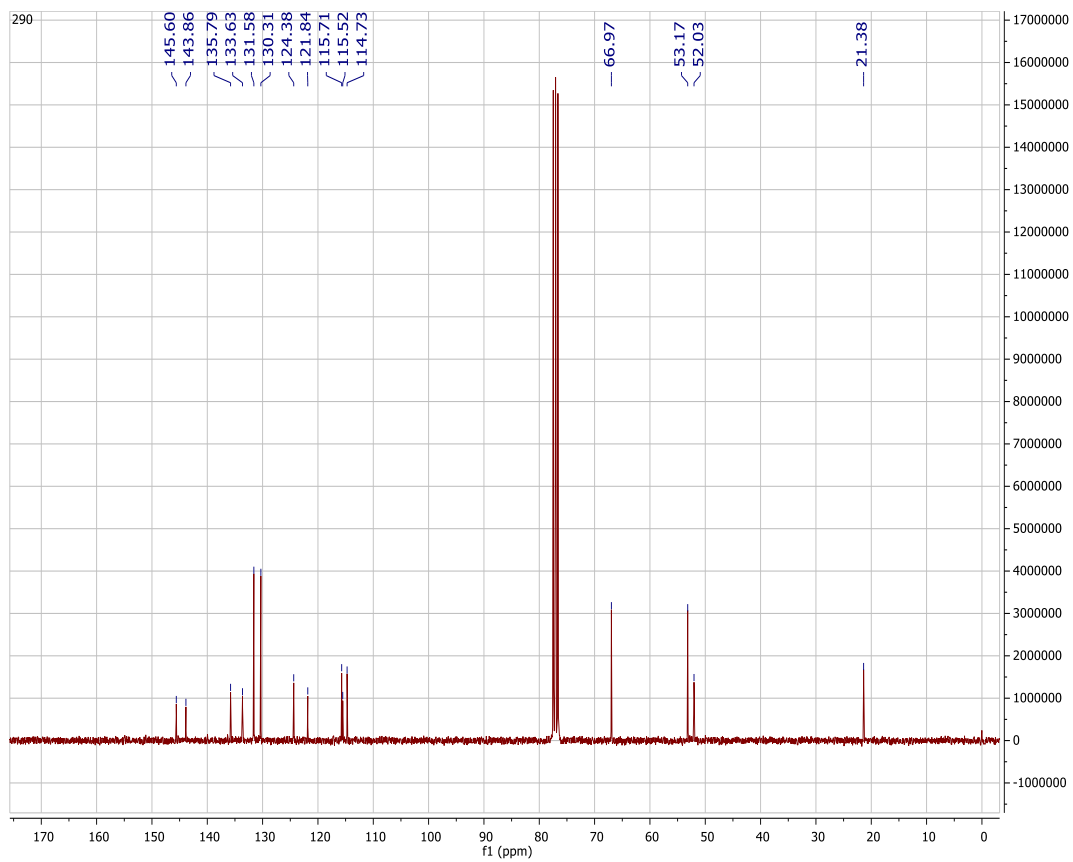
**$^1\text{H}$  NMR (300 MHz,  $\text{CDCl}_3$ ):**  $\delta$  8.28 (d,  $J = 7.1$  Hz, 1H), 7.69 (d,  $J = 8.6$  Hz, 2H), 7.58 (d,  $J = 8.5$  Hz, 2H), 7.38 (s, 1H), 6.68 (d,  $J = 6.7$  Hz, 1H), 3.91 (s, 2H), 3.67 (t,  $J = 4.6$  Hz, 4H), 2.47 (t,  $J = 4.6$  Hz, 4H), 2.43 (s, 3H).

**$^{13}\text{C}$  NMR (101 MHz,  $\text{CDCl}_3$ ):**  $\delta$  145.60, 143.86, 135.79, 133.63, 131.58, 130.31, 124.38, 121.84, 115.71, 115.52, 114.73, 66.97, 53.17, 52.03, 21.38.

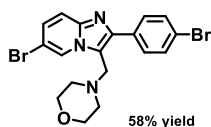
**LRMS EI (m/z):**  $[\text{M}^+]$  calc'd for  $\text{C}_{19}\text{H}_{20}\text{BrN}_3\text{O}$  385.08, observed 385.10







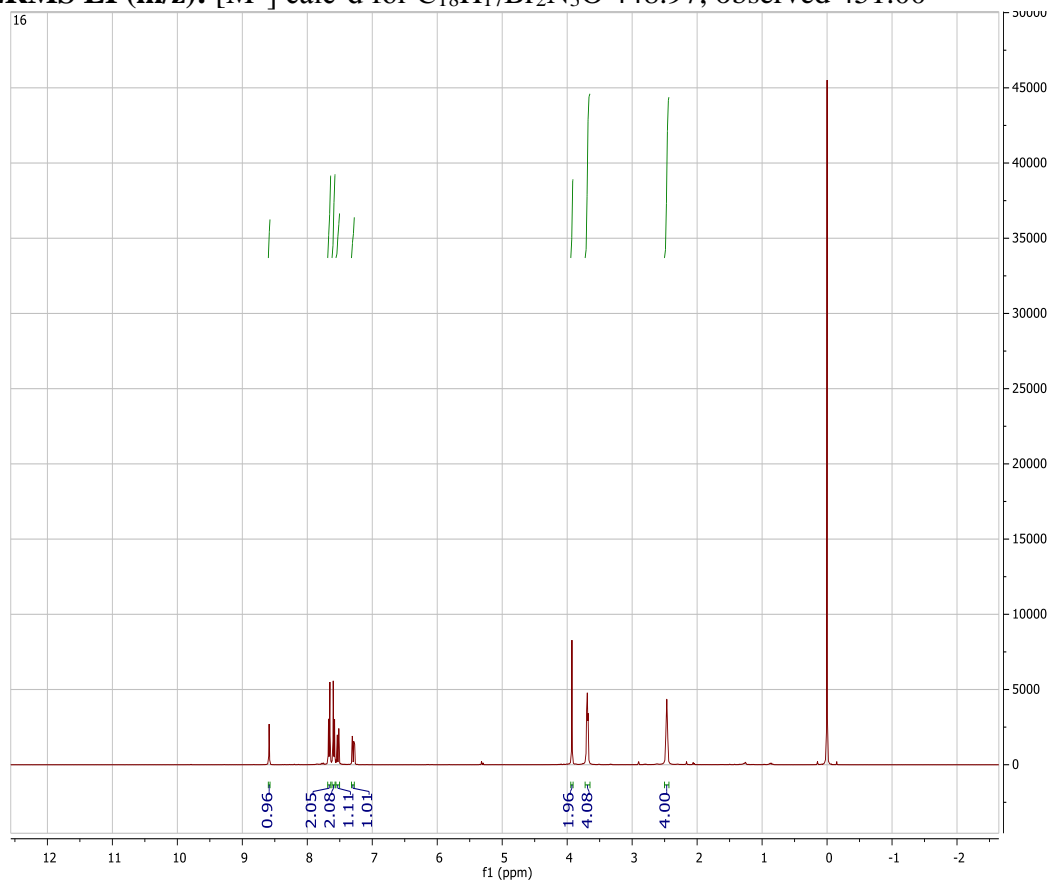
## Characterization of Compound 3.18

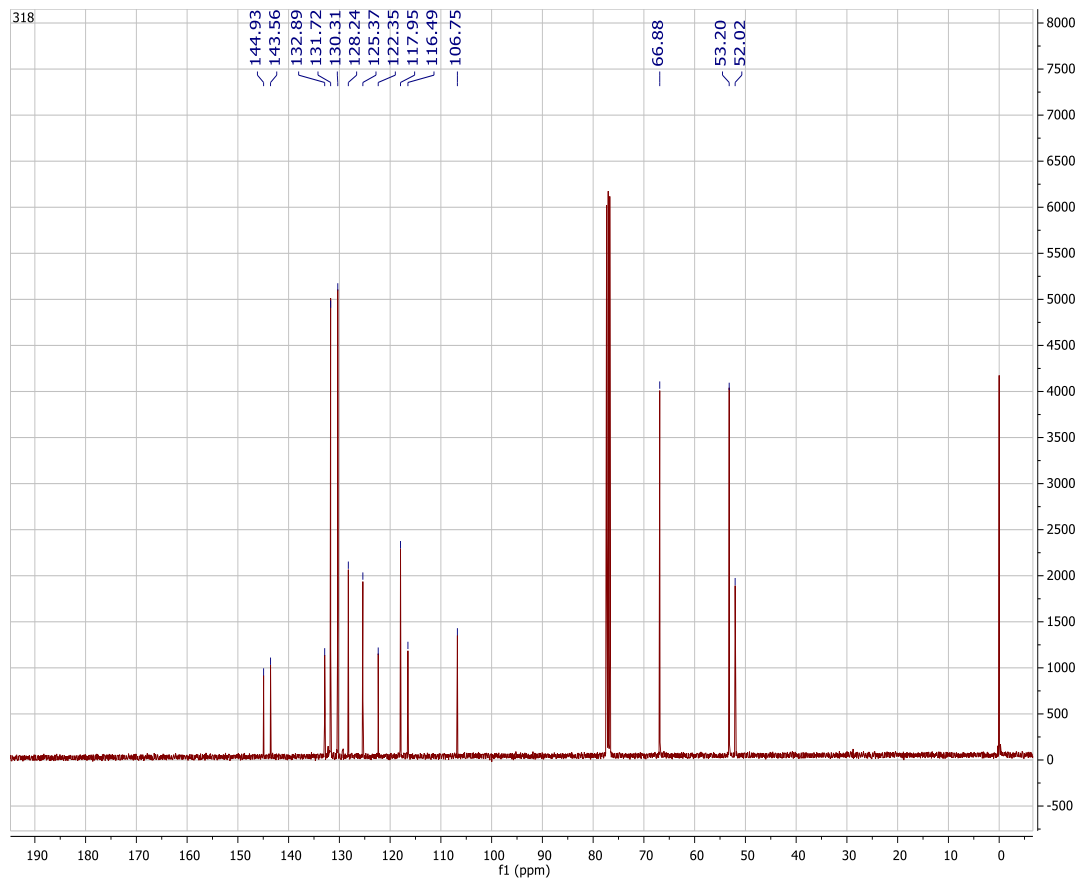


**<sup>1</sup>H NMR (400 MHz, CDCl<sub>3</sub>):**  $\delta$  8.59 (s, 1H), 7.69 – 7.64 (m, 2H), 7.62 – 7.57 (m, 2H), 7.53 (dd,  $J = 9.5, 0.8$  Hz, 1H), 7.29 (dd,  $J = 9.5, 1.9$  Hz, 1H), 3.93 (s, 2H), 3.69 (t,  $J = 4.5$  Hz, 4H), 2.47 (t,  $J = 4.5$  Hz, 4H).

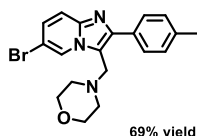
**<sup>13</sup>C NMR (101 MHz, CDCl<sub>3</sub>):**  $\delta$  144.93, 143.56, 132.89, 131.72, 130.31, 128.24, 125.37, 122.35, 117.95, 116.49, 106.75, 66.88, 53.20, 52.02.

**LRMS EI (m/z):** [M<sup>+</sup>] calc'd for C<sub>18</sub>H<sub>17</sub>Br<sub>2</sub>N<sub>3</sub>O 448.97, observed 451.00





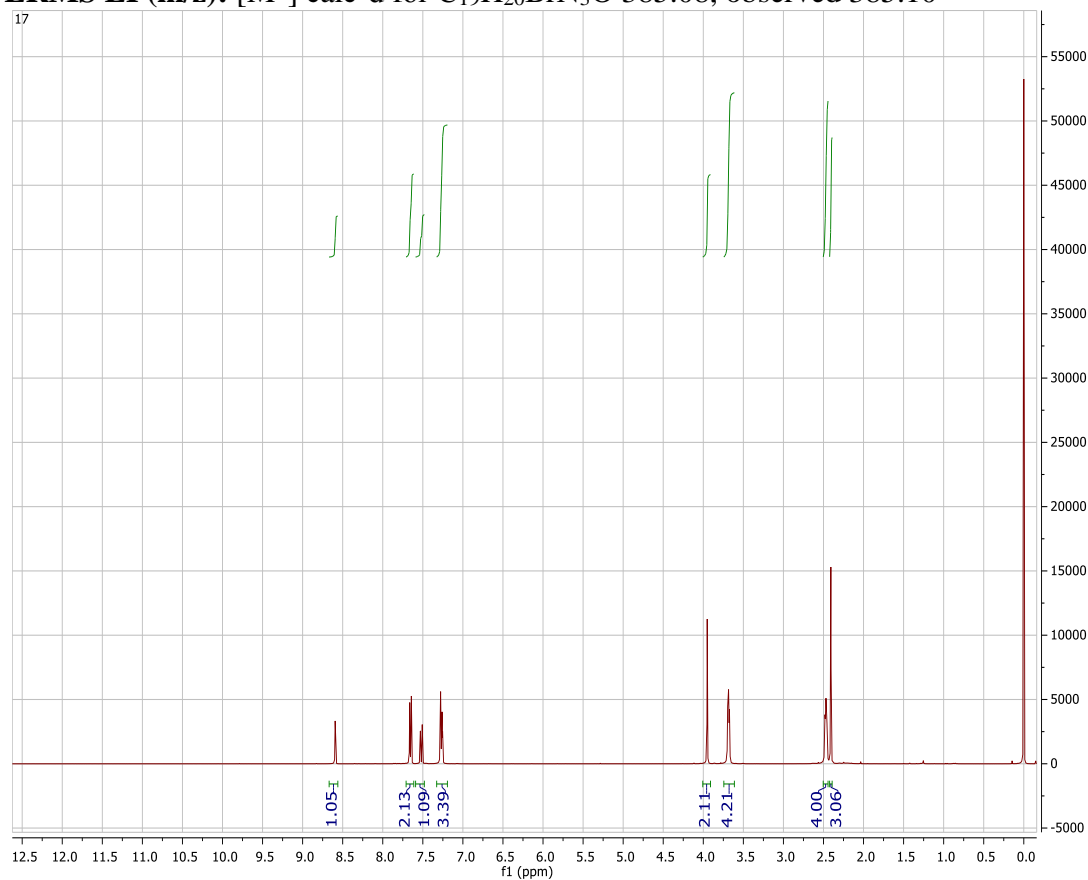
## Characterization of Compound 3.19

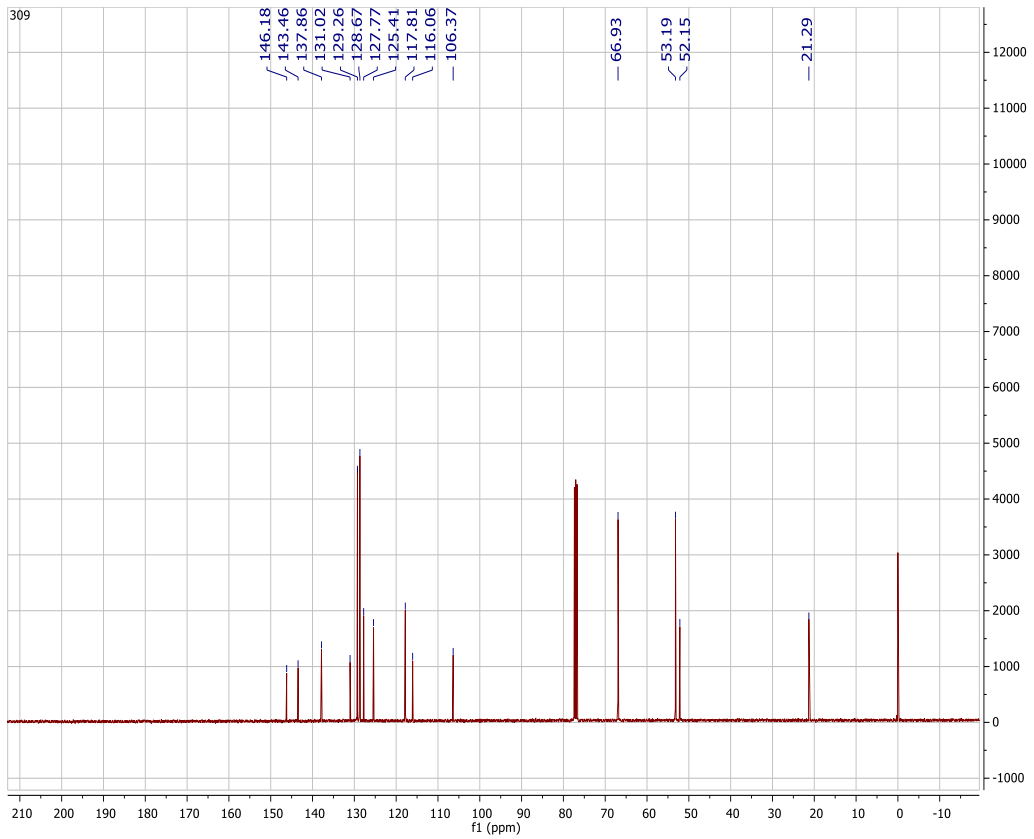


**$^1\text{H}$  NMR (400 MHz,  $\text{CDCl}_3$ ):**  $\delta$  8.59 (s, 1H), 7.71 – 7.61 (m, 2H), 7.52 (d,  $J = 9.5$ , 1H), 7.33 – 7.19 (m, 3H), 3.95 (s, 2H), 3.68 (t,  $J = 4.6$  Hz, 4H), 2.46 (s, 4H), 2.41 (s, 3H).

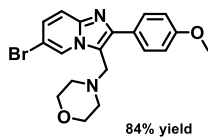
**$^{13}\text{C}$  NMR (101 MHz,  $\text{CDCl}_3$ ):**  $\delta$  146.18, 143.46, 137.86, 131.02, 129.26, 128.67, 127.77, 125.41, 117.81, 116.06, 106.37, 66.93, 53.19, 52.15, 21.29.

**LRMS EI (m/z):**  $[\text{M}^+]$  calc'd for  $\text{C}_{19}\text{H}_{20}\text{BrN}_3\text{O}$  385.08, observed 385.10





## Characterization of Compound 3.21

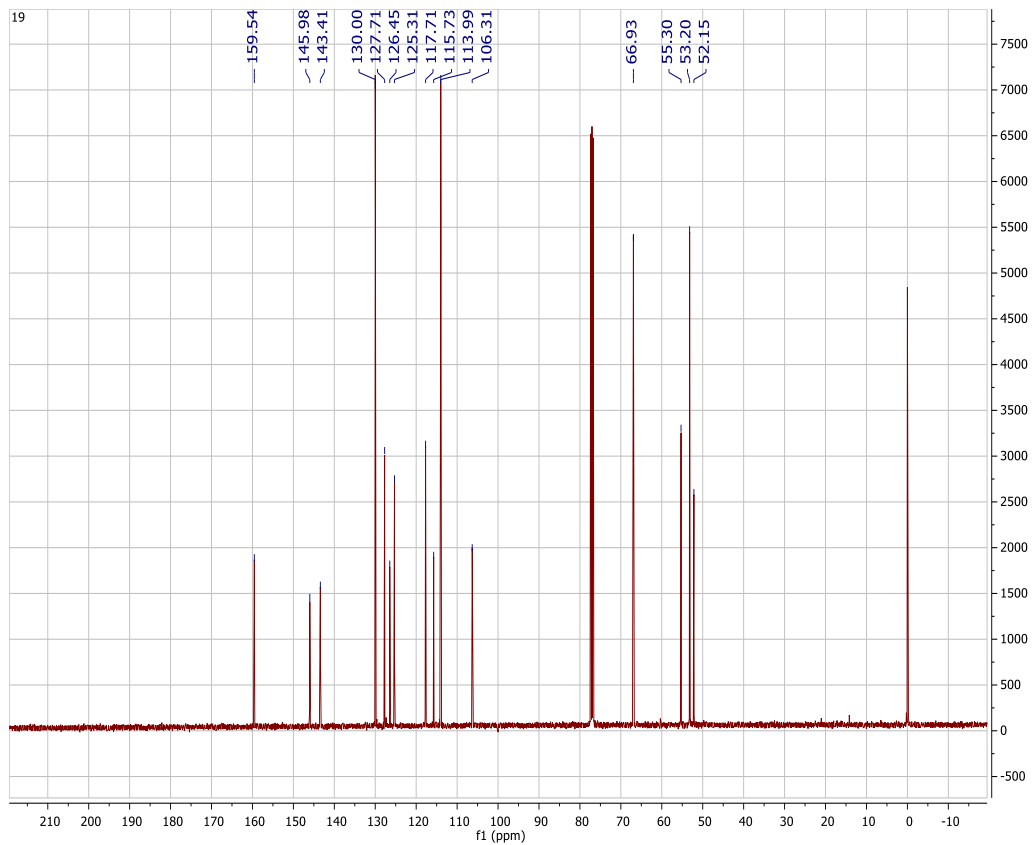


**$^1\text{H}$  NMR (400 MHz,  $\text{CDCl}_3$ ):**  $\delta$  8.57 (s, 1H), 7.73 – 7.67 (m, 2H), 7.51 (d,  $J = 9.4$  Hz, 1H), 7.28 – 7.24 (m, 1H), 7.03 – 6.96 (m, 2H), 3.94 (s, 2H), 3.86 (s, 3H), 3.69 (t,  $J = 4.6$  Hz, 4H), 2.47 (t,  $J = 4.6$  Hz, 4H).

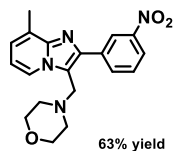
**$^{13}\text{C}$  NMR (101 MHz,  $\text{CDCl}_3$ )**  $\delta$  159.54, 145.98, 143.41, 130.00, 127.71, 126.45, 125.31, 117.71, 115.73, 113.99, 106.31, 66.93, 55.30, 53.20, 52.15.

**LRMS EI (m/z):**  $[\text{M}^+]$  calc'd for  $\text{C}_{19}\text{H}_{20}\text{BrN}_3\text{O}_2$  401.07, observed 403.10





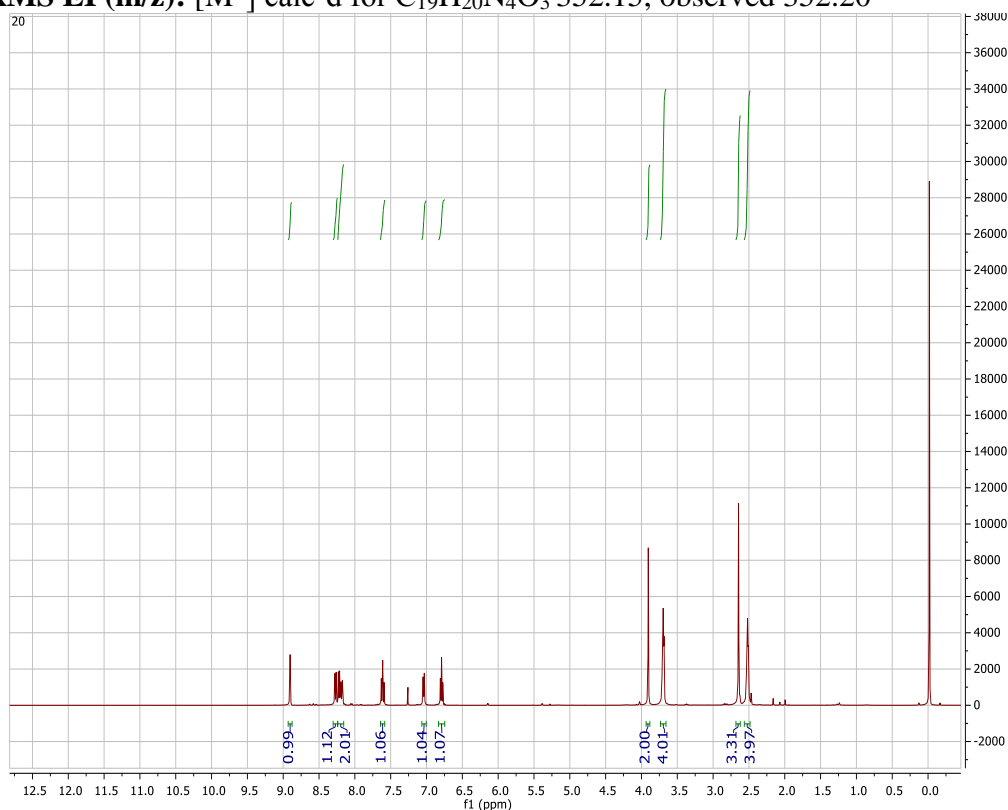
## Characterization of Compound 3.22



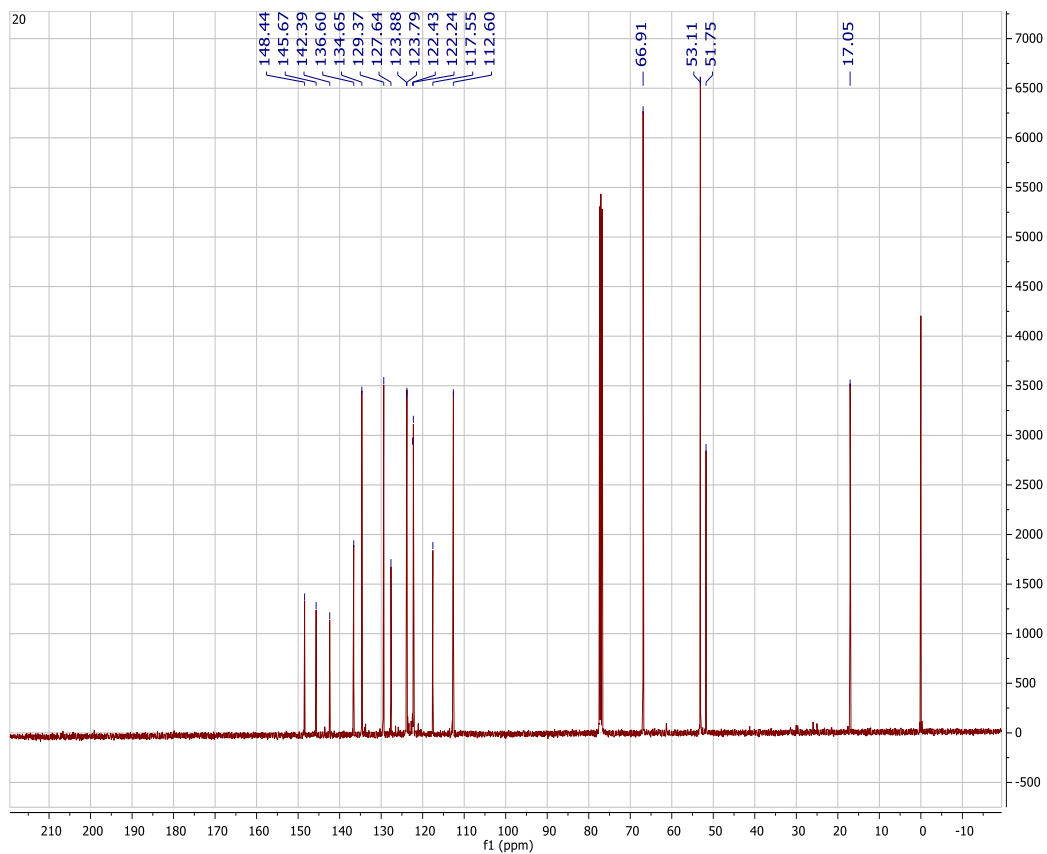
**<sup>1</sup>H NMR (400 MHz, CDCl<sub>3</sub>):**  $\delta$  8.90 (s, 1H), 8.27 (d,  $J$ =7.6 Hz, 1H), 8.22 (d,  $J$ =6.9 Hz, 1H), 8.19 (d,  $J$ =8.39, 1H), 7.61 (t,  $J$ =8.0 Hz, 1H), 7.04 (d,  $J$ =6.8, 1H), 6.79 (t,  $J$ =6.9 Hz, 1H), 3.91 (s, 2H), 3.70 (t,  $J$ =4.6 Hz, 4H), 2.65 (s, 3H), 2.52 (t,  $J$ =4.6 Hz, 4H).

**<sup>13</sup>C NMR (101 MHz, CDCl<sub>3</sub>)**  $\delta$  148.44, 145.67, 142.39, 136.60, 134.65, 129.37, 127.64, 123.88, 123.79, 122.43, 122.24, 117.55, 112.60, 66.91, 53.11, 51.75, 17.05.

**LRMS EI (m/z):** [M<sup>+</sup>] calc'd for C<sub>19</sub>H<sub>20</sub>N<sub>4</sub>O<sub>3</sub> 352.15, observed 352.20







1. Zhu, D.-J.; Chen, J.-X.; Liu, M.-C.; Ding, J.-C.; Wu, H.-Y., Catalyst: and solvent-free synthesis of imidazo[1,2-a]pyridines. *Journal of the Brazilian Chemical Society* **2009**, *20*, 482-487.